A Thesis for the Degree of Doctor of Philosophy

Characterization and Attenuation of Regulatory Network of *Vibrio vulnificus rtxA* Encoding a MARTX Toxin

MARTX 독소를 발현하는 패혈증 비브리오균 *rtxA* 유전자 조절 기전의 특성 규명 및 제어 연구

August, 2020

Zee-Won Lee

Department of Agricultural Biotechnology

The Graduate School

Seoul National University

Characterization and Attenuation of Regulatory Network of *Vibrio vulnificus rtxA* Encoding a MARTX Toxin

MARTX 독소를 발현하는 패혈증 비브리오균 *rtxA* 유전자 조절 기전의 특성 규명 및 제어 연구

지도교수 최 상 호

이 논문을 농학박사학위논문으로 제출함

2020 년 5 월

서울대학교 대학원

농생명공학부

이 지 원

이지원의 박사학위논문을 인준함

2020 년 7 월

위 원 장 _____(인)

부위원장 _____(인)

위 원 _____(인)

위 원 _____(인)

위 원 _____(인)

Abstract

Characterization and Attenuation of Regulatory Network of *Vibrio vulnificus rtxA* Encoding a MARTX Toxin

Zee-Won Lee

Department of Agricultural Biotechnology

The Graduate School

Seoul National University

Bacterial pathogens have evolved the ability to survive and develop diseases in several different environments within the host. The ability requires the production of various virulence factors whose expressions are coordinately controlled by regulatory networks in response to environmental changes. The opportunistic human pathogen *Vibrio vulnificus* can cause food-borne diseases from gastroenteritis to life-threatening septicemia. Among a wide array of virulence factors produced by *V. vulnificus*, a multifunctional-autoprocessing repeats-in-toxin (MARTX) toxin RtxA encoded by the *rtxA* gene plays an essential role in the virulence of the pathogen. It has been previously reported that the expression of *rtxA* is negatively and positively regulated by direct binding of H-NS and HlyU to the *rtxA* promoter, P_{rtxA},

respectively. In the present study, I have further examined additional regulatory proteins as well as environmental signals involved in the *rtxA* expression and identified a small-molecule inhibitor that attenuates the virulence of *V. vulnificus*. As a result, a leucine-responsive regulatory protein (Lrp) was found as a positive regulator of *rtxA*. Electrophoretic mobility shift and DNase I protection assays revealed that Lrp activates the *rtxA* expression by binding directly and specifically to P_{rtxA}. Notably, DNase I cleavage of the P_{rtxA} regulatory region showed phased hypersensitivity, suggesting that Lrp probably induces the DNA bending in P_{rtxA}. Lrp activates *rtxA* in an independent manner with H-NS and HlyU, and leucine inhibits the binding of Lrp to P_{rtxA} and thus decreases the Lrp-mediated activation. Moreover, a cyclic AMP receptor protein (CRP) acts as a negative regulator of the *rtxA* transcription, and exogenous glucose relieves the CRP-mediated repression. Interestingly, biochemical and mutational analyses demonstrated that CRP binds directly and specifically to the upstream regions of P_{rtxA}, which presumably changes the DNA conformation in P_{rtxA} and represses *rtxA*. Furthermore, CRP represses the expressions of *lrp* and *hlyU* by directly binding to their upstream regions, forming coherent feedforward loops with Lrp and HlyU. Taken together, a regulatory network comprising CRP, Lrp, H-NS, and HlyU coordinates the expression of *rtxA* in response to changes in host environmental signals such as leucine and glucose. This collaborative regulation will contribute to the precise expression of *rtxA* during the pathogenesis of *V. vulnificus*.

My next concern was about new approaches called anti-virulence strategies that target virulence of bacterial pathogens in an attempt to control the virulence of *V. vulnificus*. Anti-virulence strategies have the advantage of less selective pressure for inducing resistance than conventional strategies that target viability of the pathogens. Therefore, I performed a high-throughput screening of the small-molecule library containing 8,385 compounds to inhibit HlyU, a transcriptional activator essential for the expression of *V. vulnificus rtxA*. A small molecule [*N*-(4-oxo-4H-thieno[3,4-c]chromen-3-yl)-3-phenylprop-2-ynamide] was identified as an inhibitor of the HlyU activity and named CM14. CM14 reduces HlyU-dependent virulence gene expression in *V. vulnificus*, but does not suppress the bacterial growth or cause host cell death. Treatment of CM14 decreases hemolysis of human erythrocytes and impedes host cell rounding and lysis caused by *V. vulnificus*. Remarkably, co-administration of CM14 improves the survival of mice infected with *V. vulnificus* by alleviating hepatic and renal dysfunction and systemic inflammation. As revealed by biochemical, mass spectrometric, and mutational analyses, CM14 covalently modifies the Cys30 residue of HlyU to prevent the protein from binding to the target DNA. Based on these results, a possible molecular mechanism is proposed for the covalent modification of HlyU by CM14. Because HlyU is a conserved transcriptional activator of virulence genes in *Vibrio* species, CM14 is also capable of reducing the expressions of multiple virulence genes in other *Vibrio* species and attenuating their virulence-related phenotypes. The combined results suggest that

this small-molecule could be an anti-virulence agent against HlyU-harboring pathogenic *Vibrio* species with a low possibility of developing resistance.

Keywords: *Vibrio vulnificus*, MARTX toxin, RtxA, Virulence gene regulation, CRP, Lrp, HlyU, Small-molecule inhibitor, Anti-virulence agent

Student Number: 2016-30488

Contents

List of Figures

List of Tables

Chapter I.

Background

I-1. *Vibrio vulnificus*

Vibrio vulnificus is a gram-negative, motile, and curved-rod shaped bacterium with a single polar flagellum, which belongs to *Vibrio* genus in *Vibrionaceae*. *V. vulnificus* is distinguished from other members of the *Vibrio* genus in its ability to ferment lactose (Baumman et al., 1981; Strom and Paranjpye, 2000). The bacterium inhabits estuarine and marine environments around the world and proliferates in areas or seasons where water temperature exceeds 18°C and salinity is between 15 to 25 parts per thousand (ppt) (Horseman and Surani, 2011). However, it has been reported that salinities greater than 30 ppt negatively affect the survival of *V. vulnificus* regardless of water temperature (Motes et al., 1998). Moreover, at temperatures below 10°C, *V. vulnificus* enters a viable but non-culturable (VBNC) state, in which it becomes dormant and fails to grow even in the rich medium. The bacterium is resuscitated from the VNBC state by a gradual increase in temperature in a nutrient-free medium (Oliver, 2005a).

V. vulnificus can naturally exist in a free-living state or be associated with zooplankton and other aquatic biological flora. When *V. vulnificus* is taken up by filter-feeding mollusks such as oysters, clams, and mussels, the bacterium becomes concentrated in their gut and other tissues. *V. vulnificus* can also be found in the intestines of various fish species that consume the plankton and mollusks probably containing the bacterium. Consequently, these marine organisms such as oysters and

fish may serve as an environmental reservoir or source for the transmission of *V. vulnificus* (DePaola et al., 1994; Strom and Paranjpye, 2000).

I-1-1. Disease caused by *V. vulnificus*

V. vulnificus is an opportunistic human pathogen capable of causing foodborne diseases from gastroenteritis to primary septicemia (Baker-Austin and Oliver, 2018). Consumption of contaminated seafood may result in *V. vulnificus* infection, with the clinical symptoms including fever, chills, nausea, and abdominal pain. *V. vulnificus* infection is characterized by rapid onset of symptoms and can progress to fatal systemic infection within a few days, and the mortality rate has been reported to exceed 50% in primary septicemia. People at high risk of *V. vulnificus* infection involve males, older persons, and individuals with underlying conditions such as chronic liver diseases and compromised immune systems (Jones and Oliver, 2009; Oliver, 2015; Horseman and Surani, 2011). In addition, infection by *V. vulnificus* may also result from exposing open wound to water containing the pathogen during swimming, fishing, or seafood handling. These wound infections develop swelling, erythema, and cellulitis along with fever and chills, which can progress necrotizing fasciitis at the infection site. Compared to septicemia, wound infections result in a lower mortality rate of about 25%, and are restricted to the primary infection site without spreading to other areas of body (Oliver, 2005b; Horseman and Surani, 2011). Furthermore, the underlying conditions that can cause primary septicemia in the

ingestion cases do not appear to be a prerequisite for the wound infections (Gulig et al., 2005; Oliver, 2015).

In South Korea, *V. vulnificus* sepsis is classified as the Group 3 legal infectious disease, which is required to be reported within 24 hours in case of an outbreak for the monitoring. In the last 8 years (from 2011 to 2018), a total number of 418 infections by *V. vulnificus* has been reported, and 203 of them (49%) were dead (Korea Centers for Disease Control and Prevention, KCDC; http://www.cdc.go.kr/npt). In the United States, *V. vulnificus* accounts for over 95% of seafood-related death and has the highest mortality rate among foodborne pathogens (Baker-Austin and Oliver, 2018). Recently, the geographical distribution of *V. vulnificus* has expanded due to global warming and rising seawater temperature, which may increase the incidence of *V. vulnificus* infections (Oliver, 2015; Phillips and Satchell, 2017).

I-1-2. Virulence factors of *V. vulnificus*

In an effort to understand the pathogenesis of *V. vulnificus* infection, considerable works have been conducted to identify and characterize the virulence factors of the pathogen (Jones and Oliver, 2009). For this purpose, various approaches have been developed, including *in vivo*-induced antigen technology (IVIAT), *in vivo* expression technology (IVET), and random transposon mutagenesis (RTM). These studies successfully achieved the list of virulence genes, such as *pyrH*, *hlyU*, *tolC*, *wbpP*,

and *rtxA*, responsible for the cytotoxicity of *V. vulnificus* to host cells (Kim et al., 2003; Park et al., 2006b; Lee et al., 2007a; Lee et al., 2007c). In addition, proteomic analysis has led to identification and characterization of multiple genes, *purH*, *trpD*, *tsaA*, and *groEL2*, which are induced upon exposure to human epithelial INT-407 cells (Oh et al., 2008). Transcriptome analyses, such as microarray and RNA sequencing, have also identified a number of genes, including *vvhA* and *plpA*, which are differentially or preferentially expressed in *in vivo*-like conditions (Kim et al., 2011b; Bisharat et al., 2013; Jang et al., 2017; Choi et al., 2020). More recently, signature-tagged mutagenesis (STM) has been applied to search the *neuC*, *ask*, *flgK*, *vuuA*, and *mukB* genes that are active *in vivo* or are required for the wound infection (Yamamoto et al., 2015; Yamazaki et al., 2019). Among these, the virulence factors that have been well characterized in the pathogenesis of *V. vulnificus* will be further described in the following sections, as classified by capsular polysaccharide, adhesion factors, iron uptake systems, and exotoxins.

Capsular polysaccharide (CPS)

V. vulnificus produces a firmly linked form of extracellular polysaccharide capsule on its cell surface, which is called capsular polysaccharide (CPS) (Strom and Paranjpye, 2000; Chatzidaki-Livanis et al., 2006). The presence of CPS is correlated with colony morphology of *V. vulnificus*; encapsulated strains form opaque colonies, while colonies that undergo phase variation form translucent colonies with reduced

amount of CPS (Wright et al., 1999). Encapsulation by CPS protects *V. vulnificus* by conferring resistance to bactericidal effects of serum and phagocytosis by macrophages (Strom and Paranjpye, 2000; Williams et al., 2014). Therefore, encapsulated *V. vulnificus* cells are more slowly cleared out from the bloodstream and more invasive to subcutaneous tissue than unencapsulated cells in the host (Yoshida et al., 1985). Indeed, a 50% lethal dose (LD_{50}) of the encapsulated cells is lower than that of the unencapsulated cells in a mouse model (Simpson et al., 1987). Inactivation of the *wbpP* and *wza* genes related to the CPS biosynthesis and transport, respectively, reduces CPS expression and attenuates virulence of *V. vulnificus* (Park et al., 2006b; Wright et al., 2001).

Adhesion factors

Adhesion to host cell surfaces is an important step in the early stage of bacterial infection. In addition to CPS, surface structures, such as pili and flagella, and outer membrane proteins assist in the adhesion of *V. vulnificus* to host cells (Strom and Paranjpye, 2000; Srivastava et al., 2009).

Pili. Pili are adhesive hair-like appendages composed of a scaffold-like rod and an adhesin attached upon the scaffold, which protrude from the surface of bacteria (Pizarro-Cerda and Cossart, 2006). In *V. vulnificus*, piliation is correlated with adhesion to human epithelial cells (Gander and LaRocco, 1989), and mutations in

genes encoding pili components decrease attachment to the epithelial cells and virulence in mice (Paranjpye et al., 1998; Paranjpye and Strom, 2005). Recently, thin fimbrial projections from the surface of *V. vulnificus*, called Flp pili encoded by the *tad* operons, are identified as another adhesion factors responsible for invasion of host tissue, survival in the blood, and resistance to complement system (Duong-Nu et al., 2019).

GbpA. Mucins are highly glycosylated large glycoproteins which constitute the mucosal surface of the intestine (McGuckin et al., 2011). *V. vulnificus* secretes a mucin-binding protein GbpA, an adhesin required for adhering to host cells. Accordingly, the *gbpA* mutant of *V. vulnificus* shows impaired binding to mucin and mucin-secreting human colonic cells and attenuated virulence in mice. The amino acid sequence of *V. vulnificus* GbpA (*Vv*GbpA) is 80% identical to that of *V. cholerae* GbpA (*Vc*GbpA). *Vv*GbpA also exhibits a four domain modular structure consisting of two chitin-binding domains and two bacterial surface binding domains as observed in *Vc*GbpA (Jang et al., 2016). These suggest that *Vv*GbpA may bind to *N*-acetyl-D-glucosamine residues of mucin, as *Vc*GbpA does (Kirn et al., 2005; Wong et al., 2012).

Flagellum. A flagellum is a locomotive organelle composed of the basal body, hook, and filament and confers motility to bacteria (Evans et al., 2014; Kim et al., 2014b).

V. vulnificus possesses a single polar flagellum that plays an important role in the pathogenesis. Loss of *flgC* and *flgE*, encoding the flagellar basal body and hook protein, respectively, results in a significant decrease in bacterial motility, adhesion and cytotoxicity to human epithelial cells, and lethality to mice (Kim and Rhee, 2003; Lee et al., 2004). Disruption of the genes encoding the flagellar filament components, flagellins, also reduces motility of *V. vulnificus* as well as its ability to adhere to human epithelial cells and invade the bloodstream of mice (Kim et al., 2014b). Intriguingly, flagellin-homologous proteins FlaE and FlaF are not involved in filament formation and motility, but are related to biofilm formation by directly interacting with exopolysaccharides, the essential constituents for biofilm maturation (Jung et al., 2019).

Outer membrane proteins. *V. vulnificus* produces a membrane-bound lipoprotein IlpA and an outer membrane protein OmpU (Goo et al., 2007; Goo et al., 2006). IlpA directly binds to human epithelial cells and also stimulates the production of pro-inflammatory cytokines in human immune cells (Goo et al., 2007; Lee et al., 2011). OmpU binds to fibronectin, one of the main components comprising extracellular matrix of mammalian cells, thereby helping *V. vulnificus* adhere to host cells (Goo et al., 2006). Both *ilpA* and *ompU* mutants of *V. vulnificus* exhibit decreased adhesion and cytotoxicity to human epithelial cells and reduced lethality to mice (Goo et al., 2007; Lee et al., 2010; Goo et al., 2006).

Iron uptake systems

Iron is an essential nutrient for almost all organisms, including humans and bacterial pathogens. In healthy individuals, most iron in serum is bound to the iron-binding glycoproteins transferrin and lactoferrin, leading to iron-limited conditions to invading bacteria (Weinberg, 1978; Cassat and Skaar, 2013). For acquisition of iron, *V. vulnificus* utilizes multiple iron uptake systems such as siderophores and a heme receptor protein (Simpson and Oliver, 1987; Oh et al., 2009). Siderophores are small secreted iron-chelating compounds that bind to iron with high affinity and reenter the bacterial cell through their specific transporters (Cassat and Skaar, 2013). *V. vulnificus* produces two types of siderophores that use distinct ligands, catechol and hydroxamate, to chelate the iron, respectively (Simpson and Oliver, 1983). It has been reported that the catechol siderophore, called vulnibactin, captures iron from transferrin (Kim et al., 2006), while little is known about the iron uptake mechanism of the hydroxamate siderophore (Alice et al., 2008). Mutations in the *venB*, *vvsA*, *vvsB*, and *vuuA* genes involved in the vulnibactin synthesis and transport result in decreased virulence in mice (Litwin et al., 1996; Kim et al., 2008a; Webster and Litwin, 2000). *V. vulnificus* also produces a heme receptor protein HupA to use heme as an iron source. The *hupA* mutant shows impaired growth during infection of human epithelial cells and reduced virulence in mice, suggesting that HupA is required for survival and multiplication of *V. vulnificus* in the host (Oh et al., 2009).

Interestingly, *V. vulnificus* can obtain iron not only from its own siderophores but also from exogenous siderophores of other bacteria. This ability is attributed to the outer membrane receptor proteins DesA and IutA that bind to a deferoxamine produced by *Streptomyces pilosus* and an aerobactin produced by *Escherichia coli*, respectively (Kim et al., 2007b; Tanabe et al., 2005).

Exotoxins

V. vulnificus secretes a variety of toxins which contribute to invasiveness and tissue damaging ability of the pathogen toward host cells. These exotoxins include cytotoxins such as hemolysin VvhA and a multifunctional-autoprocessing repeats-in-toxin (MARTX) toxin RtxA, and enzymes such as an elastolytic protease VvpE and a phospholipase PlpA (Wright and Morris, 1991; Lee et al., 2007a; Kothary and Kreger, 1987; Jang et al., 2017).

Cytolysin/hemolysin VvhA. VvhA is an extracellular cytolytic hemolysin encoded by *vvhA* and confers powerful hemolytic and cytolytic activities to *V. vulnificus* (Yamamoto et al., 1990; Wright and Morris, 1991). Secreted VvhA monomers are delivered by outer membrane vesicles (OMVs) to target cells (Kim et al., 2010b). The delivered VvhA monomers bind to the target cell membrane, oligomerize into tetramers in a cholesterol-dependent manner, and form small transmembrane pores (Kim et al., 1993; Kim and Kim, 2002a; Park et al., 2005; Yu et al., 2007). A C-

terminal β-trefoil lectin domain of VvhA can facilitate VvhA binding to galactosyl-terminating groups, a common structural motif found on cell-surface glycans, with a wide range of affinity (Kaus et al., 2014).

Purified VvhA lyses erythrocytes of various animal species and causes a variety of pathological manifestations in mice, including extensive extracellular edema, severe tissue damage, and inflammation (Gray and Kreger, 1985; 1987; Qin et al., 2019). VvhA also induces apoptosis by generation of superoxide and elevation of cytosolic Ca^{2+} level (Kwon et al., 2001; Rho et al., 2002; Park et al., 2009; Zhao et al., 2009), and increases vascular permeability and neutrophil sequestration (Park et al., 1996 ; Kim et al., 1998; Kim and Kim, 2002b). In addition, VvhA produces nitric oxide (NO) by increasing inducible NO synthase (iNOS) expression through an interferon-γ signaling pathway (Kang et al., 2002). VvhA triggers NF-κB-dependent mitochondrial and autophagy-related cell death (Lee et al., 2015b; Song et al., 2016). Despite these various effects of the purified VvhA in the pathogenicity of *V. vulnificus*, the *vvhA* mutant shows no significant changes in tissue damage and mortality in mice compared with wild type (Wright and Morris, 1991; Fan et al., 2001). Therefore, this observation suggested that VvhA would exert its effect in combination with other virulence factors, rather than acting alone in the pathogenesis of *V. vulnificus*.

Elastolytic protease VvpE. VvpE is an extracellular zinc metalloprotease with

diverse proteolytic activities (Kothary and Kreger, 1987; Jeong et al., 2000; Chang et al., 2005; Miyoshi, 2006). VvpE contains two functional domains, an N-terminal domain mediating the proteolytic action and a C-terminal domain mediating attachment to the substrate (Miyoshi et al., 1997). Injection of purified VvpE into mice results in many pathological aspects shown in the *V. vulnificus* infection, including hemorrhagic and edematous tissue damage (Miyoshi et al., 1998; Jeong et al., 2000). VvpE enhances vascular permeability in mammalian dorsal skin and forms cutaneous lesions through generation of inflammatory mediators such as bradykinin and histamine (Miyoshi and Shinoda, 1988; 1992; 1997). The production of bradykinin can facilitate the intravascular dissemination of *V. vulnificus* from the peritoneal cavity to the bloodstream in mice (Maruo et al., 1998). Moreover, VvpE degrades fibrin and activates prothrombin and procaspase-3, leading to blood coagulation and apoptosis (Kim et al., 2007c; Kwon et al., 2007; Park et al., 2014). VvpE can also modulate intestinal barrier function by inhibiting mucin 2 expression, stimulating interleukin (IL)-1β production, and disrupting tight junctions (Lee et al., 2015a; Lee et al., 2015c; Lee et al., 2016b). The mutation in *vvpE* impairs swarming ability of *V. vulnificus* on semisolid agars and attenuates the virulence of the pathogen in invertebrates (Kim et al., 2007a; Ha et al., 2014). However, the *vvpE* mutant shows no difference from the wild type with regard to cytotoxicity to human epithelial cells and lethality to mice (Jeong et al., 2000; Shao and Hor, 2000). Furthermore, even the *vvhA vvpE* double mutant remains highly virulent to human epithelial cells and mice

(Fan et al., 2001; Kim et al., 2008b). These results strongly suggested the presence of another toxin(s) that contribute to the virulence of *V. vulnificus*.

MARTX toxin RtxA. The *rtx* gene cluster, encoding RtxA and its associated secretion system, has been identified as a potent virulence factor of *V. vulnificus* from screening of a random transposon mutant library (Lee et al., 2007a; Kim et al., 2008b). RtxA belongs to a multifunctional-autoprocessing repeats-in-toxin (MARTX) toxin produced by various bacterial genera including *Aeromonas*, *Xenorhabdus*, *Photorhabdus*, and *Vibrio* (Satchell, 2007). In *V. vulnificus*, the *rtx* gene cluster consists of *rtxHCA* and *rtxBDE* operons that are divergently transcribed (Park et al., 2012; Lee et al., 2008b). The *rtxHCA* operon encodes the MARTX toxin RtxA, a putative acyl-transferase RtxC, and a conserved hypothetical protein RtxH. The *rtxBDE* operon encodes a trans-membrane linker RtxD and ATPases RtxB and RtxE, which constitute the type I secretion system (T1SS) along with RtxC, for the secretion of RtxA (Boardman and Satchell, 2004; Lee et al., 2008b). Indeed, the mutation in *rtxE* inhibits the secretion of RtxA and reduces cytotoxicity to human epithelial cells and lethality to mice (Lee et al., 2008b).

In general, MARTX toxins are composed of central effector domains and conserved repeat-containing regions at the N- and C-terminus (Satchell, 2011; 2015). Once secreted, the repeat regions are proposed to bind to host cell membrane and form a pore-like structure for translocation of the central effector domains into the host cell

cytoplasm (Satchell, 2007; Kim et al., 2015). Effector domains inside the host cell are first processed by an internal cysteine protease domain (CPD) which is activated upon binding of inositol hexakisphosphate ($InsP_6$), a signal molecule found in eukaryotic cells (Prochazkova and Satchell, 2008; Egerer and Satchell, 2010). Then, the effector domains could be further processed and fully activated by a makes caterpillars floppy-like effector domain (MCF) which functions by interacting with ADP-ribosylation factor (ARF) proteins of the host cells (Lee et al., 2019a; Herrera et al., 2020). Consequently, each of the released effector domains exhibits diverse cytopathic and/or cytotoxic activities to host cells (Gavin and Satchell, 2015; Kim, 2018).

The most remarkable characteristic of RtxA is that this toxin can cause cytolysis of a wide range of eukaryotic cell types, including erythrocytes, epithelial cells, and macrophages (Kim et al., 2008b; Lee et al., 2007a; Lo et al., 2011). In addition to pore formation in host cell membrane, RtxA triggers apoptotic and necrotic cell death by dysregulating host cell functions (Lee et al., 2008a; Kim et al., 2008b; Jeong and Satchell, 2012). These include cytoskeletal rearrangement, bleb formation, generation of excess reactive oxygen species (ROS), and mitochondrial dysfunction of the host cells (Kim et al., 2008b; Chung et al., 2010; Kim et al., 2013b).

RtxA induces intestinal barrier disruption and increases paracellular permeability, promoting rapid growth and dissemination of *V. vulnificus* from the intestine to the other organs in mice (Jeong and Satchell, 2012; Gavin et al., 2017). RtxA also

contributes to the survival of the pathogen by antagonizing and inhibiting the phagocytic activity of host immune cells (Lo et al., 2011; Chen et al., 2017; Gavin and Satchell, 2019). Consistent with this, the *rtxA* mutant exhibits impaired colonization at the infection site, limited systemic spread, and significantly reduced lethality to mice (Lee et al., 2007a; Kim et al., 2008b; Lo et al., 2011; Jeong and Satchell, 2012). Besides, RtxA and VvhA play an additive role in the pathogenesis of *V. vulnificus*, causing intestinal tissue damage and inducing inflammation such as caspase-1 activation, IL-1β production, and Th17 cell responses (Toma et al., 2010; Jeong and Satchell, 2012; Lee et al., 2018).

Phospholipase A_2 PlpA. Phospholipases cleave phospholipids in the host cell membrane and cause the membrane destruction and cell lysis (Schmiel and Miller, 1999; Ghannoum, 2000). Although *V. vulnificus* has been reported to produce extracellular phospholipase(s) that is important for the virulence of the pathogen (Testa et al., 1984; Koo et al., 2007), the corresponding gene had not been yet addressed. Recently, a transcriptome analysis identified the *plpA* gene which is preferentially expressed in *V. vulnificus* exposed to human intestinal cells. A phospholipase PlpA encoded by *plpA* exhibits a phospholipase A_2 activity that hydrolyzes phospholipids at the *sn*-2 position to produce fatty acid and glycerol moiety (Jang et al., 2017). Structural analysis revealed that PlpA consists of an N-terminal domain of unknown function and a C-terminal phospholipase domain,

together with a hydrophobic substrate-binding pocket (Wan et al., 2019). Inactivation of *plpA* results in lower cytotoxicity toward the human epithelial cells than wild type, indicating that PlpA is essential for the lysis and necrotic death of host cells. Consistent with this, the *plpA* mutant shows reduced inflammation, systemic infection, and mortality in mice (Jang et al., 2017).

The virulence factors of *V. vulnificus* discussed above are summarized in Table I-1 with descriptions and references.

Table I-1. List of *V. vulnificus* virulence factors

Virulence factor	Description	Reference
CPS	Extracellular polysaccharide capsule on bacterial cell surface Confers resistance to bactericidal effects of serum and phagocytosis by macrophages	(Strom and Paranjpye, 2000; Chatzidaki-Livanis et al., 2006; Williams et al., 2014)
Adhesion factors		
Pili	Adhesive hair-like appendages protruding from the surface of bacteria Contributes to attachment and adhesion to host cells	(Gander and LaRocco, 1989; Paranjpye and Strom, 2005)
GbpA	Mucin-binding protein required for adhesion to host cells	(Jang et al., 2016)
Flagellum	Locomotive organelle conferring motility to bacteria	(Kim and Rhee, 2003; Lee et al., 2004; Kim et al., 2014b)
Outer membrane proteins	Help adhesion of bacteria to host cells	(Goo et al., 2006; Goo et al., 2007; Lee et al., 2011)
Iron uptake systems		
Siderophores	Small iron-chelating compounds for acquisition of iron from host iron-binding proteins	(Simpson and Oliver, 1983; Kim et al., 2006)
HupA	Heme receptor protein for utilization of heme as an iron source	(Oh et al., 2009)

Exotoxins		
VvhA	Extracellular cytolytic hemolysin Lyses erythrocytes of various animal species Causes edema, tissue damage, inflammation, and cell death by increasing vascular permeability and neutrophil sequestration	(Gray and Kreger, 1985; Wright and Morris, 1991; Park et al., 1996; Lee et al., 2015b; Song et al., 2016)
VvpE	Extracellular zinc metalloprotease with diverse proteolytic activities Triggers enhanced vascular permeability, hemorrhage, and edematous tissue damage Modulates intestinal barrier functions for bacterial invasion and colonization	(Kothary and Kreger, 1987; Jeong et al., 2000; Miyoshi, 2006; Lee et al., 2015a; Lee et al., 2016b)
RtxA	Multifunctional-autoprocessing repeat-in-toxin (MARTX) toxin Causes cytolysis of various eukaryotic cells by pore formation Dysregulates host cell functions such as cytoskeletal rearrangement, bleb formation, generation of excess reactive oxygen species (ROS), and mitochondrial dysfunction Induces intestinal barrier disruption and increases paracellular permeability Contributes to bacterial survival, colonization, and systemic spread	(Lee et al., 2007a; Kim et al., 2008b; Lee et al., 2008a; Lo et al., 2011; Chung et al., 2010; Jeong and Satchell, 2012; Gavin et al., 2017; Chen et al., 2017)
PlpA	Cleaves phospholipids in host cell membrane and causes the membrane destruction and host cell lysis	(Testa et al., 1984; Koo et al., 2007; Jang et al., 2017)

I-1-3. Regulation of virulence genes in *V. vulnificus*

To obtain maximum efficiency during infection, the expressions of many virulence factors are coordinately regulated by common regulatory proteins in pathogens under changing environmental conditions within the host. This coordinate regulation facilitates the cooperation of virulence factors for the successful pathogenesis of invading bacteria, including *V. vulnificus* (Miller et al., 1989; Cotter and DiRita, 2000). Extensive studies have revealed the roles of a lot of regulatory proteins involved in the virulence gene expression in *V. vulnificus*. These include transcriptional regulators such as a cAMP receptor protein (CRP), a leucine-responsive regulatory protein (Lrp), a transcriptional regulator HlyU, an iron-sulfur cluster regulator (IscR), and a quorum-sensing master regulator SmcR (Choi et al., 2002; Ho et al., 2017; Liu et al., 2007; Lim and Choi, 2014; Kim et al., 2013a).

Cyclic AMP receptor protein (CRP). A cyclic AMP (cAMP) receptor protein (CRP) is a global regulator widely found in bacteria. CRP modulates expression of genes associated with carbon and energy metabolism, along with its effector cAMP. CRP consists of an N-terminal region comprising the cAMP-binding domain and a C-terminal region containing a helix-turn-helix DNA-binding domain. Upon binding of cAMP, CRP undergoes a conformational change that allows its binding to DNA and regulation of target genes (Green et al., 2014). In *V. vulnificus*, CRP plays an important role in both virulence and metabolism, leading to the production of

virulence factors such as the hemolysin VvhA, elastolytic protease VvpE, iron-binding protein HupA, mucin-binding protein GbpA, and phospholipase PlpA (Choi et al., 2002; Jeong et al., 2003a; Oh et al., 2009; Jang et al., 2016; Jang et al., 2017). Interestingly, virulence factors whose expressions are negatively regulated by CRP have been rarely reported in *V. vulnificus*, although the expressions of virulence factors such as cholera toxin (CT) and toxin co-regulated pilus (TCP) of *V. cholerae* and type 3 fimbriae of *Klebsiella pneumoniae* are regulated by CRP (Skorupski and Taylor, 1997b; Lin et al., 2016).

Leucine-responsive regulatory protein (Lrp). In addition to CRP, a leucine-responsive regulatory protein (Lrp) is another global regulator that monitors the nutritional state of bacteria and adjusts their metabolism to changing nutritional conditions (Cho et al., 2008). Lrp contains a conserved N-terminal DNA-binding domain and a C-terminal amino acid effector-binding domain (Brinkman et al., 2003). It has been reported that Lrp contributes to the survival of *V. vulnificus* under various stresses such as acidic pH, low temperature, and hyper-osmolarity (Jeong et al., 2003b; Rhee et al., 2008b). Lrp also regulates the expression of the TonB3 transport system that is involved in the invasion of *V. vulnificus* to organs in iron-overloaded mice (Alice and Crosa, 2012). Recent transcriptome study showed that Lrp is required for expression of genes related to chemotaxis, iron-acquisition, and virulence of *V. vulnificus* (Ho et al., 2017).

HlyU. HlyU is a conserved transcriptional regulator that activates various virulence genes in *Vibrio* species, including *V. vulnificus*, *V. cholerae*, *V. anguillarum*, and *V. parahaemolyticus* (Williams et al., 1993; Liu et al., 2007; Li et al., 2011; Getz and Thomas, 2018). HlyU belongs to metal-responding SmtB/ArsR family and forms a dimeric structure similar with that of the proteins in the same family. However, HlyU does not act as a metal-binding protein and lacks the metal binding site(s) (Nishi et al., 2010). In *V. vulnificus*, HlyU induces the expressions of *rtxA*, *vvhA*, and *plpA*, encoding the MARTX toxin RtxA, hemolysin VvhA, and phospholipase A_2 PlpA, respectively, by directly binding to their promoter regions (Liu et al., 2009; Choi et al., 2020; Jang et al., 2017). In the case of *rtxA* and *vvhA*, the binding of HlyU to each promoter region relieves the repression by H-NS, a histone-like nucleoid-structuring protein that silences the expression of a variety of genes in gram-negative bacteria (Liu et al., 2009; Choi et al., 2020). Accordingly, the mutation in *hlyU* significantly attenuates the virulence of *V. vulnificus* against human epithelial cells and mice (Kim et al., 2003; Liu et al., 2007).

Iron-sulfur cluster regulator (IscR). An iron-sulfur (Fe-S) cluster-containing transcription factor IscR senses the cellular Fe-S cluster status and adjusts the Fe-S cluster biogenesis (Schwartz et al., 2001; Giel et al., 2013). Under conditions such as anaerobic growth, the amount of the Fe-S cluster is sufficient to occupy IscR,

which results in the [2Fe-2S]-IscR (holo-IscR). This holo-form of IscR represses the *isc* operon encoding IscR along with the proteins required for Fe-S cluster biogenesis. In contrast, under conditions such as oxidative stress or iron starvation, the [2Fe-2S] cluster in IscR is disrupted. As a result, the clusterless IscR (apo-IscR) relieves the repression of the *isc* operon and increases the cellular level of IscR, which most likely exists in its apo-form. Consequently, the increased level of IscR promotes Fe-S cluster biogenesis (Giel et al., 2013; Imlay, 2006; Outten et al., 2004; Schwartz et al., 2001; Zheng et al., 2001). In *V. vulnificus*, IscR activates the expression of *gbpA* and *vvhA*, encoding the mucin-binding protein GbpA and hemolysin VvhA, in response to oxidative or nitrosative stress, respectively (Jang et al., 2016; Choi et al., 2020). IscR also regulates various genes whose products are involved in motility, methyl-accepting chemotaxis, and survival under oxidative stress (Lim and Choi, 2014; Lim et al., 2014a). The *iscR* mutant exhibits reduced cytotoxicity to human epithelial cells and mortality in mice, indicating that IscR is essential for the virulence of *V. vulnificus* (Lim and Choi, 2014).

SmcR. Quorum sensing (QS) is a bacterial cell-to-cell communication process in which bacteria secretes and detects diffusible signaling molecules called autoinducers (Ng and Bassler, 2009). In addition to monitoring the cell population density, this communication process also acts as a global regulatory system which controls the expression of numerous virulence factors in pathogens, including *V.*

vulnificus (Antunes et al., 2010; Rutherford and Bassler, 2012). *V. vulnificus* possesses a QS master regulator SmcR, a homologue of *V. harveyi* LuxR that regulates diverse bacterial phenotypes (Rutherford and Bassler, 2012). SmcR directly controls the expressions of *vvpE* and *flhF* encoding the elastolytic protease VvpE and flagellar regulator FlhF (Jeong et al., 2003a; Kim et al., 2012). Furthermore, SmcR also appears to regulate a lot of genes related to the virulence, biofilm development, and survival of the pathogen under acidic pH and hyper-osmolarity conditions (Lee et al., 2007b; Lee et al., 2008c; Kim et al., 2013a; Jang et al., 2016).

OxyR1 and OxyR2. OxyR, a member of LysR-type transcriptional regulator family, recognizes hydrogen peroxide (H_2O_2) above a certain threshold concentration and regulates the expression of antioxidant genes, including catalase-peroxidase *katG* and peroxiredoxin (*prx*) genes (Aslund et al., 1999; Jo et al., 2017). *V. vulnificus* has two OxyR proteins, OxyR1 and OxyR2, which induce the expressions of *prx*1 and *prx*2, respectively, in response to oxidative stress (Bang et al., 2012; Kim et al., 2014a). Prx1 decomposes large amounts of H_2O_2 rapidly with high turnover rate (Baek et al., 2009b). In contrast, Prx2 scavenges small amounts of H_2O_2 effectively with high affinity (Bang et al., 2012). Consistent with this, OxyR1 activates *prx*1 upon exposure to exogenous H_2O_2, while OxyR2 activates *prx*2 during aerobic growth, suggesting that OxyR2 recognizes relatively lower levels of H_2O_2 compared

to OxyR1 (Bang et al., 2016). Employing two OxyRs and two Prxs may provide *V. vulnificus* with the ability to cope with various ranges of oxidative stress that the pathogen might encounter during infection (Kim et al., 2014a).

In summary, Figure I-1 shows the regulation of virulence genes in *V. vulnificus* discussed above.

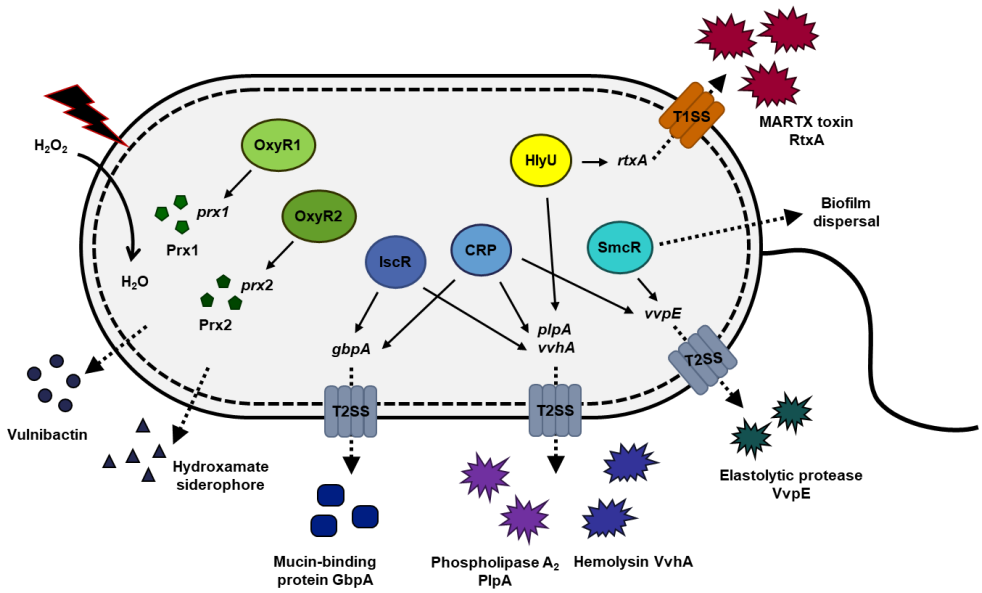

Figure I-1. Regulation of virulence genes in *V. vulnificus*. Details of the regulatory proteins are described in the following references: OxyR1 and OxyR2 (Kim et al., 2014a), IscR (Lim and Choi, 2014; Jang et al., 2016; Choi et al., 2020), CRP (Choi et al., 2002; Jeong et al., 2003a; Jang et al., 2016; Jang et al., 2017), HlyU (Liu et al., 2007; Jang et al., 2017 ; Choi et al., 2020), and SmcR (Jeong et al., 2003a; Lee et al., 2008c; Kim et al., 2013a; Jang et al., 2016). T1SS, type 1 secretion system; T2SS, type 2 secretion system.

I-2. Objective of this study

The pathogenicity of *V. vulnificus* comes from the production of numerous virulence factors during host infection. Many of these virulence factors are coordinately expressed by a common global regulatory network in response to various environmental signals. This coordinate regulation facilitates cooperation of the virulence factors for the overall success of *V. vulnificus* within the host. Therefore, it is necessary to elucidate the regulatory mechanisms of virulence gene expression for understanding the molecular pathogenesis of *V. vulnificus*. This will contribute to the development of advanced treatment and prevention of *V. vulnificus*, as well as the discovery of novel approaches for the control of the pathogen. Considerable works have been conducted to investigate the virulence gene regulation in *V. vulnificus*, including the *rtxA* gene encoding an essential virulence factor MARTX toxin RtxA. However, studies focusing on regulatory proteins and environmental signals involved in the expression of *rtxA* are still limited. In the present study, I identified a regulatory network coordinating the *rtxA* expression in response to environmental signals that *V. vulnificus* may encounter within the host during infection. These findings led to the development of the anti-virulence strategy that controls the virulence of *V. vulnificus* by targeting HlyU, a transcriptional activator of *rtxA*. Compared to strategies that impede viability, this anti-virulence strategy may exert less selective pressure for the emergence of resistant strains. Accordingly, a small-

molecule inhibitor of HlyU was found from a high-throughput screening of 8,385 compounds using the *Escherichia coli* reporter strain. Effects of the HlyU inhibitor on the virulence of *V. vulnificus* were assessed and evaluated *in vitro*, *ex vivo*, and *in vivo*. The possible molecular mechanism of the HlyU inhibitor was proposed by biochemical, mass spectrometric, and crystallographic analyses.

Chapter II.

Regulatory Network of *Vibrio vulnificus rtxA* Encoding a MARTX Toxin

Part of this work in Chapter II was published in *mBio* in 2020, as an article entitled "A MARTX toxin *rtxA* gene is controlled by host environmental signals through a CRP-coordinated regulatory network in *Vibrio vulnificus*".

II-1. Introduction

For establishing a successful infection, bacterial pathogens recognize environmental changes and produce virulence factors appropriately to survive and multiply within the host (Cotter and DiRita, 2000). These environmental signals that the pathogens may encounter in the host include pH, temperature, osmolarity, iron levels, types and levels of nutrients, and concentrations of various ions (Mekalanos, 1992). Accordingly, the pathogens have evolved mechanisms to regulate the expression of virulence genes in response to the various environmental signals (Miller et al., 1989; Fang et al., 2016). Numerous transcriptional regulatory proteins have been identified and characterized in an effort to understand the virulence gene regulation (Cotter and DiRita, 2000; Fang et al., 2016). Integration of the signals by the multiple transcriptional regulators may allow the pathogens to fine-tune the expression of virulence factors during all stages of infection (Miller et al., 1989; Skorupski and Taylor, 1997a). The different types of global regulatory proteins cooperate to regulate the expression of many virulence genes, resulting in the coordinated production of virulence factors for the overall success of the pathogens during host infection (Cotter and DiRita, 2000; Miller et al., 1989).

A leucine-responsive regulatory protein (Lrp) is a global regulator which participates in the regulation of a large number of genes, including the genes involved in amino acid biosynthesis and degradation, small molecule transport, pili synthesis, and stress

tolerance (Cho et al., 2008; Ho et al., 2017). Lrp also regulates the expression of virulence factors in pathogens such as *Salmonella enterica* Serovar Typhimurium, *X. nematophila*, and *V. cholerae* (Baek et al., 2009a; Cowles et al., 2007; Lin et al., 2007). As a small nucleoid-structuring protein, Lrp binds DNA and induces the bending or wrapping of DNA (Rhee et al., 2005; Pul et al., 2007). The transcriptional regulatory action of Lrp on target genes may be modulated by binding of leucine, a small effector molecule known to affect the multimeric state of the protein (Cho et al., 2008; Deng et al., 2011). Upon addition of leucine, the regulatory activity of Lrp can be enhanced, reversed, or unaffected, as represented in different regulatory modes of Lrp for individual genes (Cho et al., 2008). As a result, Lrp regulates a variety of genes in response to changing conditions such as nutritional state of the bacteria and host environments, and coordinates the gene expression in cooperation with other regulatory proteins (Baek et al., 2009a; Lin et al., 2007; Cho et al., 2008). A cyclic AMP receptor protein (CRP) is a central regulator of carbon and energy metabolism which makes the expression of virulence factors metabolically coordinated (Skorupski and Taylor, 1997a; Jeong et al., 2003a). The availability of carbon and energy sources in the environment is sensed by the carbohydrate phosphotransferase system (PTS). In the absence of glucose, the enzyme IIA^{glu} of PTS remains phosphorylated and activates the adenylate cyclase which synthesizes cAMP, resulting in the increase of intracellular cAMP levels (Skorupski and Taylor, 1997a). CRP forms a complex with cAMP and then binds DNA to control the gene

expression. Therefore, the genes regulated by cAMP-CRP signaling pathway are expressed in response to nutrient availability (Manneh-Roussel et al., 2018). In this way, CRP coordinates the expression of genes involved in metabolism and virulence, and thus assures optimal growth and virulence factor production in bacteria under changing environmental conditions. Accordingly, the expressions of virulence factors, such as cholera toxin (CT) and toxin co-regulated pilus (TCP) of *V. cholerae*, type 3 fimbriae of *Klebsiella pneumoniae*, and plasminogen activator protease of *Yersinia pestis*, are regulated by CRP and affected by exogenous glucose (Kühn et al., 2014; Lin et al., 2016; Kim et al., 2007d).

The opportunistic human pathogen, *Vibrio vulnificus*, is a causative agent of foodborne diseases from mild gastroenteritis to primary septicemia (Baker-Austin and Oliver, 2018; Jones and Oliver, 2009). Infection by *V. vulnificus* is characterized by rapid dissemination and severe tissue destruction, leading to high mortality rates. The pathogenicity of *V. vulnificus* results from numerous virulence factors produced by the bacteria. The virulence factors include a carbohydrate capsule, a lipopolysaccharide, a metalloprotease, a cytolysin/hemolysin, and a large pore-forming toxin RtxA which is also referred to as a multifunctional-autoprocessing repeats-in-toxin (MARTX) toxin (Baker-Austin and Oliver, 2018; Jang et al., 2017). Notably, the ability of *V. vulnificus* to cause diseases is strongly linked to the production of RtxA, encoded by the *rtxA* gene in the *rtxHCA* operon (Park et al., 2012). RtxA is composed of the effector domains that exhibit cytopathic effects to

host cells and the N-terminal and C-terminal repeat-containing regions that form a pore in the host cell membrane for the translocation of effector domains (Kim et al., 2015; Satchell, 2015). Consequently, RtxA triggers cytoskeletal rearrangement, bleb formation, and actin aggregation of host cells (Kim et al., 2008b). Such changes result in apoptotic and necrotic cell death and enable *V. vulnificus* to invade the host bloodstream (Kim et al., 2008b; Lee et al., 2008a; Jeong and Satchell, 2012). Furthermore, RtxA contributes to the survival of the pathogen during infection by antagonizing phagocytic activity of host immune cells (Lo et al., 2011; Gavin and Satchell, 2019).

A histone-like nucleoid-structuring protein (H-NS) represses the expression of *rtxA* by directly binding to multiple AT-rich regions in the *rtxA* promoter, P_{rtxA}. HlyU directly binds to P_{rtxA} and induces the *rtxA* expression by relieving the binding of H-NS (Liu et al., 2009). Although those two regulatory proteins have been reported to control the *rtxA* transcription, very little is known about the environmental signals involved in the *rtxA* expression. In the present study, Lrp was identified as a positive regulator of the *rtxA* transcription that directly binds to the specific sequences in the P_{rtxA} regulatory region. Molecular genetic analyses revealed that Lrp activates *rtxA* in an independent manner with H-NS and HlyU. The effect of leucine on the regulatory mode of Lrp was investigated, and leucine acts as an antagonist of the P_{rtxA} activation by Lrp. Furthermore, CRP represses the *rtxA* expression, and glucose alleviates the repression of *rtxA* caused by CRP. Biochemical and mutational

analyses demonstrated that CRP directly and specifically binds to upstream regions in the P_{rtxA} regulatory region, which results in the repression of *rtxA*. Interestingly, CRP also represses both *lrp* and *hlyU* by directly binding to their upstream regions, forming coherent feedforward loops with Lrp and HlyU to regulate *rtxA*. Taken together, this study suggested that CRP coordinately regulates the expression of *rtxA* in an elaborate regulatory network comprising Lrp and HlyU for the overall success of *V. vulnificus* during infection.

II-2. Materials and Methods

II-2-1. Strains, plasmids, and culture conditions

The strains and plasmids used in this study are listed in Table II-1. Unless stated otherwise, the *V. vulnificus* and *Escherichia coli* strains were grown at 30°C in Heart Infusion (HI) medium supplemented with 2.5% (w/v) NaCl and at 37°C in Luria-Bertani (LB) medium, respectively. Growth of the *V. vulnificus* strains was monitored spectrophotometrically at 600 nm (A_{600}). When necessary, antibiotics were added to the medium at the following concentrations: 3 μg/mL chloramphenicol and 2 μg/mL tetracycline for *V. vulnificus*, and 20 μg/mL chloramphenicol and 10 μg/mL tetracycline for *E. coli*.

Table II-1. Bacterial strains and plasmids used in this study

Strain or plasmid	Relevant characteristics[a]	Reference or source
Bacterial strains		
V. vulnificus		
MO6-24/O	Wild type; clinical isolate; virulent	Laboratory collection
ZW181	MO6-24/O with Δ*lrp*	This study
EJ151	MO6-24/O with Δ*hns*	(Choi et al., 2020)
ZW141	MO6-24/O with Δ*hlyU*	(Jang et al., 2017)
MO6Δ*lacZ*	MO6-24/O with Δ*lacZ*	(Baek and Kim, 2003)
DI0201	MO6-24/O with Δ*crp*	(Choi et al., 2002)
ZW191	MO6-24/O with Δ*hns* Δ*lrp*	This study
ZW192	MO6-24/O with Δ*hlyU* Δ*lrp*	This study
ZW193	MO6-24/O with Δ*lrp* Δ*lacZ*	This study
ZW194	MO6-24/O with Δ*crp* Δ*lacZ*	This study
GR192	MO6-24/O with Δ*toxR*	This study
JK093	MO6-24/O with Δ*iscR*	(Lim and Choi, 2014)
JK131	MO6-24/O with Δ*aphA*	(Lim et al., 2014b)
JR312	MO6-24/O with Δ*aphB*	(Jeong and Choi, 2008)
MO6_rpoS	MO6-24/O with Δ*rpoS*	(Kim et al., 2018b)
HS03	MO6-24/O with Δ*smcR::nptI*; Km^r	(Kim et al., 2018a)
V. parahaemolyticus		
FORC_008	Wild type; clinical isolate; virulent	(Kim et al., 2016)
V. alginolyticus		
ATCC17749	Wild type; virulent	Korean Collection for Type Cultures
V. cholerae		
El Tor N16961	Wild type; clinical isolate; virulent	(Fullner and Mekalanos, 1999)

E. coli		
DH5α	*supE44 ΔlacU169* (*Φ80 lacZ ΔM15*) *hsdR17 recA1 endA1 gyrA96 thi-1 relAI*	Laboratory collection
BL21 (DE3)	*F*$^-$, *ompT*, *hsdS* (r_B^-, m_B^-), *gal dcm* (DE3)	Laboratory collection
C43 (DE3)	*F*$^-$, *ompT*, *hsdS* (r_B^-, m_B^-), *gal dcm* (DE3)	(Dumon-Seignovert et al., 2004)
S17-1 λ *pir*	Tc::Mu-Km::Tn7;Tp^r Sm^r; host for π-requiring plasmids	(Simon et al., 1983)
Plasmids		
pDM4	Suicide vector; R6K γ ori *sacB*; *oriT* of RP4; Cm^r	(Milton et al., 1996)
pBS0907	pDM4 with Δ*crp*; Cm^r	(Kim et al., 2011a)
pZW1817	pDM4 with Δ*lrp*; Cm^r	This study
pGR1907	pDM4 with Δ*toxR*; Cm^r	This study
pJH0311	0.3-kb MCS of pUC19 cloned into pCOS5; Ap^r, Cm^r	(Goo et al., 2006)
pKK1502	pJH0311 with *crp*; Ap^r, Cm^r	(Jang et al., 2017)
pZW1818	pJH0311 with *lrp*; Ap^r, Cm^r	This study
pHK0201	pRSET A with *crp*; Ap^r	(Choi et al., 2002)
pET-28a(+)	His_6-tag fusion protein expression vector; Km^r	Novagen
pKK1636	pET-28a(+) with *hns*; Km^r	(Choi et al., 2020)
pZW1903	pET-28a(+) with *lrp*; Km^r	This study
pRKΩlacZ	pRK415 derivative containing promoterless *lacZ*; Tc^r	(Park et al., 2006a)
pZW1517	pRKΩlacZ with P_{rtxA}; Tc^r	This study
pZW1930	pRKΩlacZ with P_{rtxA} carrying mutated CRP-binding sequence 1; Tc^r	This study
pZW1931	pRKΩlacZ with P_{rtxA} carrying mutated CRP-binding sequence 2; Tc^r	This study
pZW1936	pRKΩlacZ with P_{rtxA} carrying	This study

	mutated CRP-binding sequence 3; Tc^r	
pBBR_lux	Broad host range vector with promoterless *luxCDABE*; Cm^r	(Lenz et al., 2004)
pZW1608	pBBR_lux with P_{VVMO6_00539}; Cm^r	This study
pZW1609	pBBR_lux with P_{rtxA}; Cm^r	This study
pBAD24	Expression vector with the P_{BAD} promoter; Ap^r	(Guzman et al., 1995)
pKK1306	pBAD24 with *hlyU*; Ap^r	This study
pProEX-HTa	His_6-tag fusion protein expression vector; Ap^r	Invitrogen
pZW1610	pProEX-HTa with *hlyU*; Ap^r	This study
pZW1611	pProEX-HTa with mutant *hlyU* encoding HlyU-C30S; Ap^r	This study
pZW1612	pProEX-HTa with mutant *hlyU* encoding HlyU-C96S; Ap^r	This study
pZW1510	pJH0311 with *hlyU*; Ap^r, Cm^r	(Jang et al., 2017)
pZW1511	pJH0311 with mutant *hlyU* encoding HlyU-C30S; Ap^r, Cm^r	This study
pZW1512	pJH0311 with mutant *hlyU* encoding HlyU-C96S; Ap^r, Cm^r	This study

[a] Km^r, kanamycin-resistant; Tp^r, trimethoprim resistant; Sm^r, streptomycin resistant; Cm^r, chloramphenicol-resistant; Ap^r, ampicillin-resistant; Tc^r, tetracycline-resistant.

II-2-2. Generation and complementation of deletion mutants

The isogenic *hns* mutant EJ151, *hlyU* mutant ZW141, *lacZ* mutant MO6Δ*lacZ*, and *crp* mutant DI0201 were constructed previously (Choi et al., 2020; Jang et al., 2017; Baek and Kim, 2003; Choi et al., 2002) and used in this study (Table II-1). For construction of an isogenic *lrp* mutant, the *lrp* gene was inactivated *in vitro* by deletion of the ORF of *lrp* (324 of 495 bp) using the PCR-mediated linker-scanning method as described previously (Jang et al., 2016). Briefly, pairs of primers, LRPD-F1 and -R1 or LRPD-F2 and -R2, were used for amplification of the 5' amplicon and 3' amplicon, respectively (Table II-2). The 324-bp deleted *lrp* was amplified by PCR using the mixture of both amplicons as the templates and LRPD-F1 and -R2 as primers. The resulting Δ*lrp* was ligated into SpeI-SphI-digested pDM4 (Milton et al., 1996) to create pZW1817 (Table II-1). Similarly, pGR1907 carrying the 501-bp deleted *toxR* on pDM4 was constructed using the primers TOXRD-F1 and -R1 or TOXRD-F2 and -R2 (Table II-2). *E. coli* S17-1 λ*pir* strain (Simon et al., 1983) containing pZW1817 was used as a conjugal donor to the *V. vulnificus* MO6-24/O wild type and to the *hns*, *hlyU*, or *lacZ* mutant to generate the *lrp* mutant ZW181, *hns lrp* double mutant ZW191, *hlyU lrp* double mutant ZW192, or *lrp lacZ* double mutant ZW193, respectively (Table II-1). Similarly, *E. coli* S17-1 λ*pir* strain containing pGR1907 or pBS0907, which was constructed previously to carry a mutant allele of *V. vulnificus crp* on pDM4 (Kim et al., 2011a), was used as a conjugal donor to the wild type or the *lacZ* mutant to generate the *toxR* mutant GR192, or *crp*

lacZ double mutant ZW194 (Table II-1). The conjugation and isolation of the transconjugants were conducted using the method as described previously (Bang et al., 2016).

To complement the mutations, pKK1502 carrying the *crp* gene on the broad-host-range vector pJH0311 (Goo et al., 2006) was used in this study (Table II-1) (Jang et al., 2017). Similarly, the *lrp* gene was amplified by PCR using a pair of specific primers LRPC-F and -R listed in Table II-2 and cloned into pJH0311 to create pZW1818 (Table II-1). The plasmids were transferred into the appropriate mutants by conjugation as described above.

Table II-2. Oligonucleotides used in this study

Name	Oligonucleotide sequence, 5' →3'[a, b]	Use
For mutant construction		
LRPD-F1	AGCTCAGGTTACCCGCATGCCAGCTTGAGGTTCTTTTACC	Deletion of *lrp* ORF
LRPD-R1	CAACGTAGGATCCCACGCGCTTAGAGAGTTC	
LRPD-F2	GCGCGTGGGATCCTACGTTGTAATGGAAGAAG	
LRPD-R2	CTCGAGTACGCGTCACTAGTATATCTCCACCCCATGAGG	
TOXRD-F1	GAGCTCAGGTTACCCGCATGGAGATGTTGGTCTAAGCG	Deletion of *toxR* ORF
TOXRD-R1	ATCCGGATCCCGTTACGAGTTAACACCTC	
TOXRD-F2	ACTCGTAACGGGATCCGGATGCCTTCTATTAGGC	
TOXRD-R2	CGACCCTCGAGTACGCGTCAGTGATGACTGTCACCATATAG	
For mutant complementation		
LRPC-F	GAGGATCCCCGGGTACCTTGGTGACCATGTGAGATA	Amplification of *lrp* ORF
LRPC-R	CATGATTACGAATTCGAGCTCAGTAACTGAAACATTCCGAG	
For protein overexpression		
LRPP-F	GTTTAACTTTAAGAAGGAGATATACCATGGTAGATAACTACAAAAAG CC	Amplification of *lrp* ORF
LRPP-R	CAGTGGTGGTGGTGGTGGTGACGTGTTTTAATCACAAGTTG	
HLYUP-F	GGTGGATCCAATGAACTTAAAAGATATGG	Amplification of *hlyU* ORF
HLYUP-R	GGTCTCGAGTTATTCTTCGCAATAAAG	

For EMSA and DNase I protection assay		
PrtxA_P1-F	GTTAAGTTCGTGATAAGAGACCAC	Amplification of P_{rtxA} regulatory
PrtxA_P1-R	CACACAATGAAGACCAATAAACG	region, Probe 1
PrtxA_P2-F	CGTTTATTGGTCTTCATTGTGTG	Amplification of P_{rtxA} regulatory
PrtxA_P2-R	TTTCAGCCATTACGCCATT	region, Probe 2
Plrp-F	AATGAGCTCTGAAAAACCGATGCCT	Amplification of P_{lrp} regulatory
Plrp-R	TTTACTAGTTGGAGAAAGCCCCACG	region
PhlyU-F	CAAGAGCTCGACTCGACACAAAGT	Amplification of P_{hlyU} regulatory
PhlyU-R	AGACTAGTTCATGTGTTGGTCCTCTAG	region
PrtxA-EMSA-F	TCAAATAAAATGGCGGGTGT	Amplification of 264-bp P_{rtxA}
PrtxA-EMSA-R	CCTTCAAAAACGCTGCAAT	regulatory region
For *rtxA-lacZ* reporter construction		
PrtxAZ-F	CTGCAGGAATCAAATAAAATGGCGG	Amplification of P_{rtxA} regulatory
PrtxAZ-R	GGATCCATTTTTTTGATCCTGGCCTAC	region
For site-directed mutagenesis		
CRPB1_mt-F	AATACAAAACCGCGTCAAGCGTTCATTGCCGTCCATAATGAAATTA	Site-directed mutagenesis of
CRPB1_mt-R	TAATTTCATTATGGACGGCAATGAACGCTTGACGCGGTTTTGTATT	CRP-binding sequence 1
CRPB2_mt-F	CAAATGAATGATGCAGCATTCGTTAAGATGTAATCAAGGT	Site-directed mutagenesis of
CRPB2_mt-R	ACCTTGATTACATCTTAACGAATGCTGCATCATTCATTTG	CRP-binding sequence 2
CRPB3_mt-F	TCAAGGGCCTACGTCCATGAAGATGGAATTGAG	Site-directed mutagenesis of
CRPB3_mt-R	CTCAATTCCATCTTCATGGACGTAGGCCCTTGA	CRP-binding sequence 3

HLYUC30S-F	GACGCCTGCAAATCTTATCCATGCTACACAATCAAGAG	Construction of HlyU-C30S mutant
HLYUC30S-R	CTCTTGATTGTGTAGCATGGATAAGATTTGCAGGCGTC	
HLYUC96S-F	GCACAGTCTTTATTCCGAAGAATAATGCTTTTGCGTGCC	Construction of HlyU-C96S mutant
HLYUC96S-R	GGCACGCAAAAGCATTATTCTTCGGAATAAAGACTGTGC	
For *E. coli* reporter strain construction		
HLYUS-F	GCTAGCTAGAGGACCAACACATG	Amplification of *hlyU* ORF for reporter strain construction
HLYUS-R	GGTACCTTATTCTTCGCAATAAAG	
00539S-F	GAGCTCATTTGTTTAAGCGTGTAAAGC	Amplification of VVMO6_00539 upstream region
00539S-R	ACTAGTTTTTCGTAGCTGCTCAATTTGTAAT	
03281S-F	GGCCAAGTAATTTTATCGTTTTCATGATAC	Amplification of VVMO6_03281 upstream region
03281S-R	ACTAGTAAAGGGGTTGTGAGTCGATAATCA	
PrtxA-F	GAGCTCGAATCAAATAAAATGGC	Amplification of P_{rtxA}
PrtxA-R	ACTAGTTATTTTTTTGATCCTGGCCTAC	
For qRT-PCR analysis		
RTXA_qRT-F	TAGCGGCGACAATGAAACCT	
RTXA_qRT-R	CCCATCACCGCAAGGGTATT	
LRP_qRT-F	GGGGCTTTCTCCAACTCCAT	
LRP_qRT-R	GCAACGAGGCGTCTAGGTAT	
HLYU_qRT-F	CATGGCCAATGAAAGACGCC	
HLYU_qRT-R	ACCATGCCAGATGCTGAGAC	
VVHA-qRT-F	ACAGCTGGTTCCAGAGTTGG	

VVHA-qRT-R	AACGGGTTTCACCCAAAGGT
PLPA-qRT-F	TTGTTGGTATCGAACGGGCA
PLPA-qRT-R	CGAGCTCCACCAATAACCGT
00539-qRT-F	CAGGCGGGTTATTACGGTGT
00539-qRT-R	TTTCTTGCTCGCTCTTTGCG
01210-qRT-F	AAAACCACCTTGCTCAACGC
01210-qRT-R	ATCCAATGTGGCTGGGTCAG
03281-qRT-F	GGCATCAGTTTGGCGAAGTC
03281-qRT-R	TATACGCTACGTTGGACAGGC
03824-qRT-F	ATCTTCGATTTGGCCGTTGC
03824-qRT-R	CTCGCGGTATGGACGTAGAC
VPEXSA-qRT-F	TTTCCGGCATGAAAACGCTG
VPEXSA-qRT-R	GGTTCGGTTAGTTTGCTGCG
VP1668-qRT-F	ACCAATTTCGCTTGGCGTTC
VP1668-qRT-R	AACGGTTACGTCTACGTCCG
VPVOPQ-qRT-F	CGCCGATAGCAAAAGAAGCC
VPVOPQ-qRT-R	TGGCCCTTGTTTGAGTTGGT
VPVOPS-qRT-F	TAGAACGCGATTACCGTGGG
VPVOPS-qRT-R	TTACCGAGGTCTTTGTCCGC
VPVOPR-qRT-F	CAAAACGTGCTCAATGGCGA
VPVOPR-qRT-R	TTTGGAAGACGAGGTGTCGG

VALEXSA-qRT-F	TGGTGCCAGCTTAACCACTT
VALEXSA-qRT-R	ACGATGCTCATCTTGCTCGT
VAL1668-qRT-F	TTAGCGGAAGTGGTTGGCTT
VAL1668-qRT-R	GTACCTAACAGGTGGTCGCC
VALVOPQ-qRT-F	CACCGATAGCAAAAGAGGCA
VALVOPQ-qRT-R	CTCACCTTGCATGAGTTGTT
VALVOPS-qRT-F	TACCAAATCAACGCAGCGAC
VALVOPS-qRT-R	ACCGATTGTGGGCTACCTTC
VALVOPR-qRT-F	ACAAACGGCAGCCTCTTCTT
VALVOPR-qRT-R	TGACCCCTTAACACCGAACG
HLYA-qRT-F	CGTCAACAATACGCGACAGC
HLYA-qRT-R	CTCAGCGGGCTAATACGGTT
TLH-qRT-F	GTCAACCACGATTTTGCCGA
TLH-qRT-R	GATGCGGTTGGACTGAACCT
RTXAVC-qRT-F	AAAGCCAACGTCGTGACTCATG
RTXAVC-qRT-R	ATCGGAAATCAACAACCCTACCGT

[a] The oligonucleotides were designed using the *V. vulnificus* MO6-24/O genomic sequence (GenBank™ accession number CP002469 and CP002470, www.ncbi.nlm.nih.gov).

[b] Regions of oligonucleotides not complementary to the corresponding genes are underlined.

II-2-3. RNA purification and transcript analysis

Total RNAs from the *V. vulnificus* strains were isolated and quantified using an RNeasy® Mini Kit (Qiagen, Valencia, CA). For quantitative reverse transcription-PCR (qRT-PCR), the concentrations of total RNAs were measured by using a NanoDrop™ One^{C} spectrophotometer (Thermo Scientific, Waltham, MA), and cDNA was synthesized from 1 μg of the total RNAs by using an iScript™ cDNA synthesis kit (Bio-Rad, Hercules, CA). Real-time PCR amplification of the cDNA was performed by using a CFX96 real-time PCR detection system (Bio-Rad) with pairs of specific primers (Table II-2), as described previously (Lee et al., 2019b). Relative expression levels of the transcripts were calculated by using the 16S rRNA expression level as an internal reference for normalization (Lee et al., 2019b).

II-2-4. Western blot analysis

The *V. vulnificus* strains were harvested and fractionated into cells and supernatants by centrifugation. The supernatants were concentrated using Amicon Ultra-15 (cut-off 30 kDa; Millipore, Burlington, MA). RtxA and OmpU in the supernatant concentrates were detected by Western blot analysis using mouse anti-*V. vulnificus* RtxA monoclonal antibody (Lee et al., 2014) and rabbit anti-*V. vulnificus* OmpU antibody (Choi et al., 2020). The cells were lysed using B-PER™ Bacterial Protein Extraction Reagent with Enzymes (Thermo Fisher Scientific), and residual cell debris was removed by centrifugation to obtain clear cell lysates. Lrp, H-NS, HlyU, CRP, and DnaK in the clear cell lysates were detected by Western blot analysis using rabbit anti-*V. vulnificus* Lrp antibody (Rhee et al., 2008a), rabbit anti-*V. vulnificus* H-NS antibody (Choi et al., 2020), rabbit anti-*V. vulnificus* HlyU antibody (Lee et al., 2019b), rabbit anti-*V. vulnificus* CRP antibody (Jang et al., 2017), and mouse anti-*E. coli* DnaK antibody (Enzo lifescience, Farmingdale, NY) as described previously (Jang et al., 2017; Lee et al., 2019b).

II-2-5. Protein purification

To overexpress H-NS, HlyU, and CRP, pKK1636 carrying the *hns* gene on pET-28a(+) (Novagen, Madison, WI) (Choi et al., 2020), pZW1610 carrying the *hlyU* gene on pProEX-HTa (Invitrogen, Carlsbad, CA) (Lee et al., 2019b), and pHK0201 carrying the *crp* gene on pRSET A (Invitrogen) (Choi et al., 2020) were constructed

previously and used in this study (Table II-1). Similarly, the *lrp* gene was subcloned into pET-28a(+) using a pair of specific primers LRPP-F and -R listed in Table II-2 to create pZW1903 (Table II-1). The resulting His_6-tagged Lrp, H-NS, HlyU, and CRP were expressed in *E. coli* BL21 (DE3) and purified by affinity chromatography according to the manufacturer's procedure (Qiagen).

II-2-6. EMSA and DNase I protection assay

For EMSA, the 881-bp *rtxBDE-rtxHCA* intergenic region containing P_{rtxA} was divided into two 452-bp regions [-629 to -178 for Probe 1 and -200 to +252 for Probe 2 from the transcription start site of *rtxHCA* (Liu et al., 2009)]. Each 452-bp DNA probe was amplified by PCR using unlabeled PrtxA_P1-F and [γ-^{32}P]ATP-labeled PrtxA_P1-R or unlabeled PrtxA_P2-F and [γ-^{32}P]ATP-labeled PrtxA_P2-R as primers, respectively (Table II-2). Similarly, the 424-bp *lrp* upstream region and the 572-bp *hlyU* upstream region were amplified by PCR using unlabeled Plrp-F and [γ-^{32}P]ATP-labeled Plrp-R or unlabeled PhlyU-F and [γ-^{32}P]ATP-labeled PhlyU-R as primers, respectively (Table II-2).

The radiolabeled DNA probes were incubated with the purified Lrp, H-NS, or HlyU for 0.5 h at 25°C in a 20-μl reaction mixture containing 1× Lrp binding buffer [50 mM Tris-Cl (pH 8.0), 20 mM KCl, 100 μg BSA, 1 mM DTT, and 10% glycerol] and 0.1 μg of poly(dI-dC) (Sigma-Aldrich, St. Louis, MO) as described previously (Lin et al., 2007). Similarly, the DNA probes were incubated with the purified CRP for

0.5 h at 37°C in a 20-μl reaction mixture containing 1× CRP binding buffer [10 mM Tris-Cl (pH 7.9), 50 mM NaCl, 1 mM DTT, and 1 mM cAMP] and 0.1 μg of poly(dI-dC) as described previously (Kim et al., 2011a). For competition analysis, the same but unlabeled DNA fragment was used as a self-competitor DNA. Electrophoretic analysis of the DNA-protein complexes was performed as described previously (Lee et al., 2019b). When necessary, various concentrations of L-leucine were added to the reaction mixture before incubation.

For DNase I protection assay, the same DNA probes of each 452-bp P_{rtxA} regulatory region were amplified by PCR using unlabeled PrtxA_P1-F and 6-carboxyfluorescein (FAM)-labeled PrtxA_P1-R or unlabeled PrtxA_P2-F and 6-FAM-labeled PrtxA_P2-R as primers, respectively (Table II-2). The binding of purified Lrp or CRP to the labeled DNA was performed as described above. DNase I digestion of the DNA-protein complexes was performed as described previously (Hwang et al., 2019). The digested DNA products were precipitated with ethanol and eluted in sterilized H_2O, and then analyzed using an ABI 3730xl DNA analyzer (Applied Biosystems, Foster City, CA) with Peak Scanner™ Software v1.0 (Applied Biosystems).

II-2-7. Construction of an *rtxA-lacZ* transcriptional fusion reporter and β-galactosidase activity assay

The 753-bp promoter region of *rtxA*, P_{rtxA}, was amplified using a pair of primers PrtxAZ-F and -R (Table II-2) and then fused to promoterless *lacZ* of pRKΩlacZ (Park et al., 2006a) to create pZW1517 (Table II-1). *E. coli* S17-1 λ*pir* strain containing pZW1517 was used as a conjugal donor to the *lacZ* mutant, *lrp lacZ* double mutant, or *crp lacZ* double mutant as described previously (Bang et al., 2016). The P_{rtxA} activity of the *V. vulnificus* strains was determined by measuring the β-galactosidase activity. The β-galactosidase activity was determined by the chloroform/SDS method described previously by Miller (Miller, 1972).

II-2-8. Site-directed mutagenesis of CRP-binding sequences

The sequences of the CRP-binding sites (wtCRPB) determined by the DNase I protection assay were mutagenized using the PCR-mediated linker-scanning method with the mutagenic primers carrying the substituted nucleotides (Table II-2) (Lee et al., 2008c). For site-directed mutagenesis, pairs of primers, PrtxA_P1-F and CRPB1_mt-R or CRPB1_mt-F and PrtxA_P2-R, were used for amplification of the 5' amplicon and 3' amplicon of the mutated CRP-binding sequence 1 (mtCRPB1), respectively. Then, the mtCRPB1 was amplified by PCR using the mixture of both amplicons as the templates, and PrtxA_P1-F and PrtxA_P2-R as primers. Similarly, the mutated CRP-binding sequence 2 and 3 (mtCRPB2 and mtCRPB3) were created

using the mutagenic primers listed in Table II-2, respectively. All the mutations in the mtCRPBs were confirmed by DNA sequencing. The DNA probes of the P_{rtxA} regulatory region carrying wt or mt CRPB were amplified using unlabeled and [γ-^{32}P]ATP-labeled primers as described above and then used for EMSA.

For β-galactosidase activity assay, the reporter plasmid pZW1930 with promoterless *lacZ* fused to P_{rtxA} carrying mtCRPB1 was constructed as described above (Table II-1). Similarly, the reporter plasmids pZW1931 and pZW1936 with promoterless *lacZ* fused to P_{rtxA} carrying either mtCRPB2 or mtCRPB3, respectively, were constructed (Table II-1). *E. coli* S17-1 λ*pir* strain containing pZW1517, pZW1930, pZW1931, or pZW1936 was used as a conjugal donor to the *lacZ* or *crp lacZ* mutant as described above. The activity of P_{rtxA} carrying wt or mt CRPB in the *V. vulnificus* strains was determined by measuring the β-galactosidase activity as described above.

II-2-9. Data analyses

Averages and standard deviations (SD) were calculated from at least three independent experiments. Statistical analyses were performed by the Student's *t*-test or one-way analysis of variance (ANOVA) as indicated in the figure legends using GraphPad Prism 7.0 (GraphPad Software, San Diego, CA).

II-3. Results

II-3-1. Lrp and CRP affect the *rtxA* transcription

It has been reported that H-NS represses but HlyU derepresses the *rtxA* transcription in *V. vulnificus*, respectively (Liu et al., 2009). In an effort to identify other transcription factor(s) associated with the *rtxA* regulation, the *rtxA* transcript levels were compared in the wild type and various isogenic mutants lacking transcription factors that are known to affect the virulence gene expression in *V. vulnificus* (Ho et al., 2017; Jeong et al., 2003a; Lee et al., 2000; Lim and Choi, 2014; Lim et al., 2014b; Jeong and Choi, 2008; Choi et al., 2002; Kim et al., 2018a). The *rtxA* transcript level in the *lrp* mutant was significantly lower than that in the wild type (Fig. II-1), indicating that Lrp may act as a positive regulator of the *rtxA* expression. In contrast, the *rtxA* transcript level in the *crp* mutant was substantially higher than that in the wild type (Fig. II-1), indicating that CRP may act as a negative regulator of the *rtxA* expression. Expression of *rtxA* did not differ in the wild type and the mutants lacking ToxR, IscR, AphA, AphB, an alternative sigma factor RpoS (Choi et al., 2002), or a quorum-sensing master regulator SmcR (Kim et al., 2018a) (Fig. II-1), suggesting that *rtxA* may not be regulated by those transcriptional regulators under the conditions tested. This observation led to the further analysis on the roles of Lrp and CRP in the transcription of *rtxA* at the molecular levels.

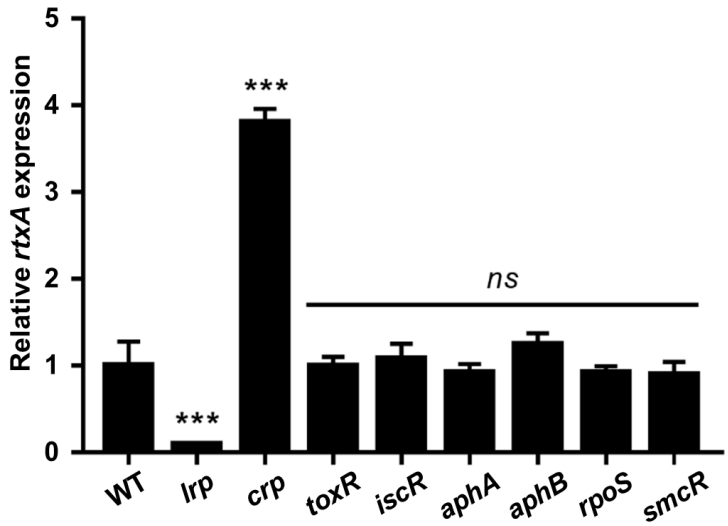

Figure II-1. Expression of *rtxA* in *V. vulnificus* with different genetic background. Total RNAs were isolated from the wild type (WT) and isogenic mutants grown to A_{600} of 0.5 and used to determine the *rtxA* transcript levels. The *rtxA* transcript levels were determined by qRT-PCR analyses, and the *rtxA* transcript level in the wild type was set as 1. Error bars represent the SD. Statistical significance was determined by the multiple comparisons after one-way ANOVA (***, $p < 0.0005$; *ns*, not significant relative to the wild type). *lrp*, *lrp* mutant; *crp*, *crp* mutant; *toxR*, *toxR* mutant; *iscR*, *iscR* mutant; *aphA*, *aphA* mutant; *aphB*, *aphB* mutant; *rpoS*, *rpoS* mutant; *smcR*, *smcR* mutant.

II-3-2. Lrp activates the *rtxA* expression by directly binding to P_{rtxA}

The *rtxA* transcript and RtxA protein levels were decreased in the *lrp* mutant and restored to the levels comparable to those in the wild type by introducing pZW1818 carrying a recombinant Lrp (Fig. II-2). These results confirmed that Lrp is a positive regulator of the *rtxA* transcription. To examine whether Lrp directly binds to the *rtxA* promoter, P_{rtxA}, EMSAs were performed. For this purpose, the 881-bp *rtxBDE-rtxHCA* intergenic region was divided into two 452-bp regions [referred to as Probe 1 (-629 to -178) and Probe 2 (-200 to +252) from the transcription start site of *rtxHCA* (Liu et al., 2009); see Materials and Methods]. The addition of Lrp to the radiolabeled DNA Probe 1 and Probe 2 resulted in a single retarded band of a DNA-Lrp complex in an Lrp concentration-dependent manner, respectively (Fig. II-3A and B). Interestingly, Lrp at 720 nM was required for the full retardation of Probe 1, while Lrp at 180 nM was sufficient for that of Probe 2 (Fig. II-3A and B). The results indicated that at least two binding sites of Lrp with different DNA-binding affinities are present in the P_{rtxA} regulatory region. The same but unlabeled DNA fragment, which was used as a self-competitor, showed the competition for Lrp binding in a dose-dependent manner (Fig. II-3A and B), confirming the specific binding of Lrp to P_{rtxA}.

To determine the binding sequences for Lrp in the P_{rtxA} regulatory region, DNase I protection assays were performed using the same DNA probes but labeled with 6-FAM. When Lrp was added to the DNA probes, Lrp largely protected three regions

extending from -453 to -387 (LRPB1, centered at -420), -298 to -219 (LRPB2, centered at -258.5), and -63 to -10 (LRPB3, centered at -36.5), respectively, from the DNase I digestion (Fig. II-3C to E). Combined with the EMSA results (Fig. II-3A and B), these results suggested that Lrp directly binds to LRPB1 and LRPB2 with similar binding affinities but binds to LRPB3 relatively strongly. Notably, within the regions protected by Lrp, a periodic pattern of reduced cleavage followed by short regions of enhanced cleavage was observed (Fig. II-3C to E). This pattern is known as phased hypersensitivity which is consistent with the DNA bending by Lrp (Pul et al., 2007), suggesting that Lrp induces the DNA bending in the P_{rtxA} regulatory region. Together, these results indicated that Lrp activates the *rtxA* transcription by binding directly and specifically to P_{rtxA}.

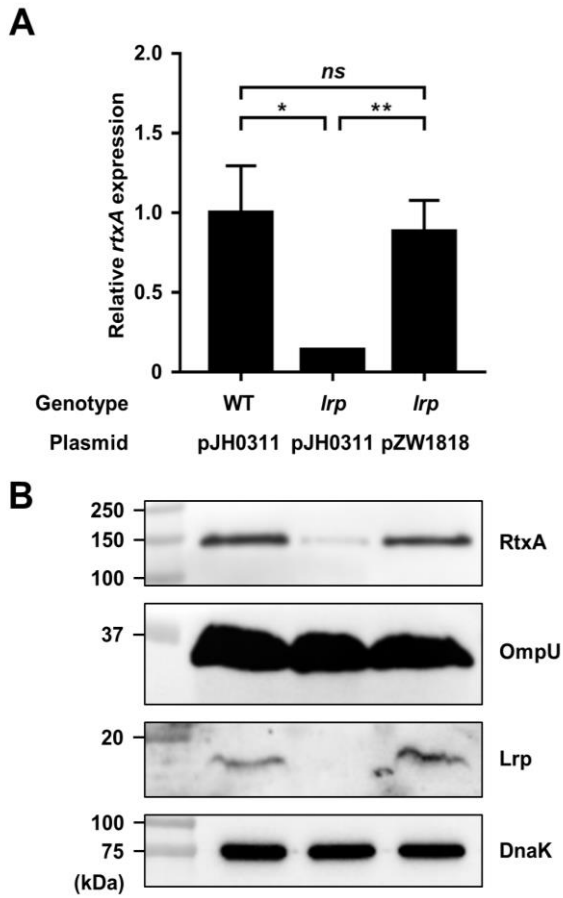

Figure II-2. Effect of the *lrp* mutation on the *rtxA* expression. Total RNAs and proteins were isolated from the *V. vulnificus* strains grown to A_{600} of 0.5 and used to determine the *rtxA* transcript and RtxA, OmpU, Lrp, and DnaK protein levels. (A) The *rtxA* transcript levels were determined by qRT-PCR analyses, and the *rtxA* transcript level in the wild type was set as 1. Error bars represent the SD. Statistical significance was determined by the Student's *t*-test (**, $p < 0.005$; *, $p < 0.05$; *ns*, not significant). (B) The secreted RtxA and OmpU (as an internal control), and cellular Lrp and DnaK (as an internal control) levels were determined by Western

blot analysis. Molecular size markers (Bio-Rad) are shown in kDa. WT (pJH0311), wild type; *lrp* (pJH0311), *lrp* mutant; *lrp* (pZW1818), *lrp* complemented strain.

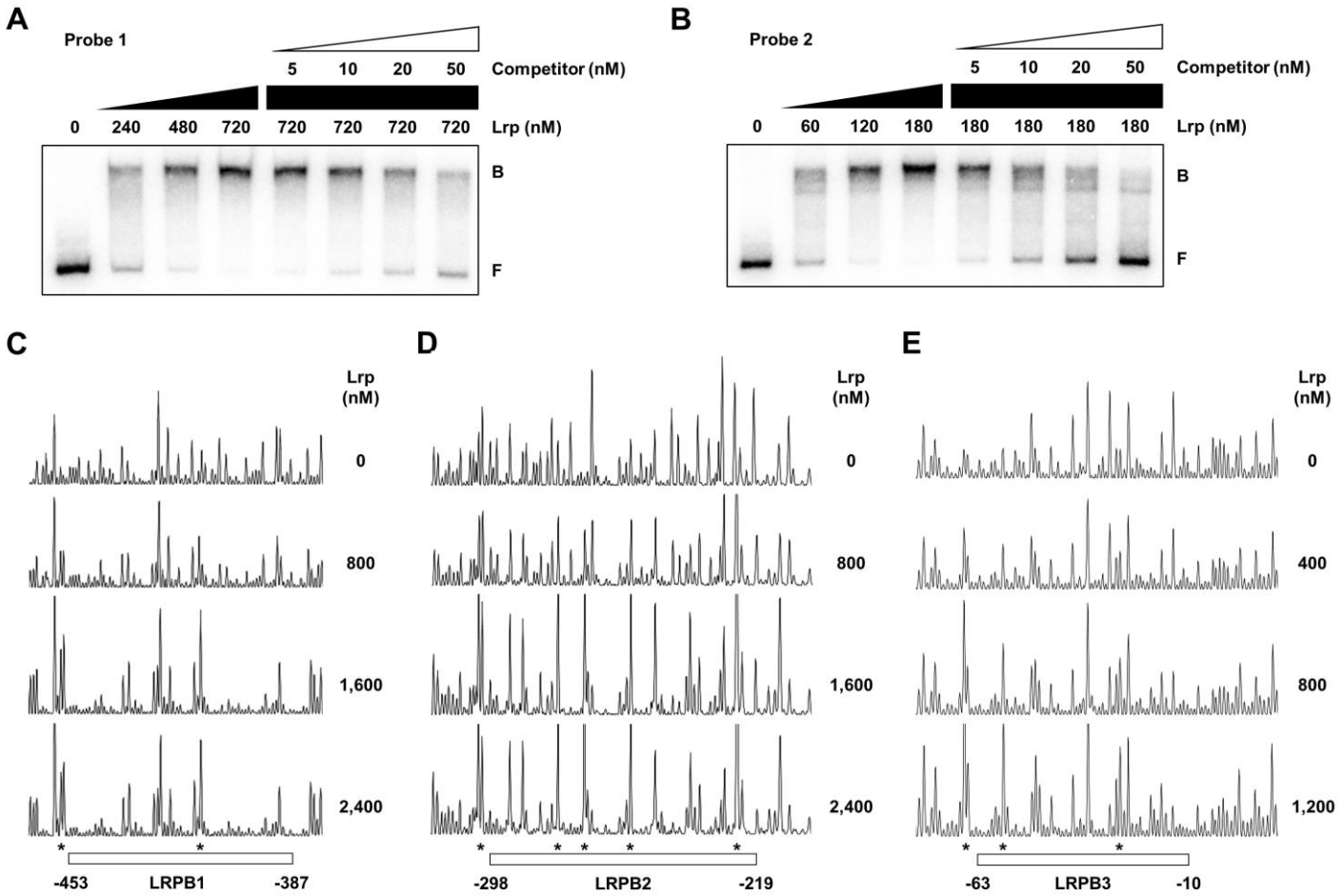
A
Probe 1
5 10 20 50 Competitor (nM)
0 240 480 720 720 720 720 720 Lrp (nM)
B
F
B
Probe 2
5 10 20 50 Competitor (nM)
0 60 120 180 180 180 180 180 Lrp (nM)
B
F
C
Lrp (nM)
0
800
1,600
2,400
-453 LRPB1 -387
D
Lrp (nM)
0
800
1,600
2,400
-298 LRPB2 -219
E
Lrp (nM)
0
400
800
1,200
-63 LRPB3 -10

Figure II-3. Specific binding of Lrp to the P_{rtxA} regulatory region. (A and B) Each 452-bp DNA probe of the P_{rtxA} regulatory region [Probe 1 for (A) and Probe 2 for (B); 5 nM] was radioactively labeled and then incubated with increasing amounts of Lrp as indicated. For competition analysis, various amounts of the same but unlabeled each DNA fragment were used as a self-competitor and added to the reaction mixture containing the 5 nM labeled DNA before the addition of 720 nM (A) or 180 nM (B) Lrp. The DNA-protein complexes were separated by electrophoresis. B, bound DNA; F, free DNA. (C to E) The same DNA probes of each P_{rtxA} regulatory region (40 nM) were labeled with 6-FAM, incubated with increasing amounts of Lrp as indicated, and then digested with DNase I. The regions protected by Lrp are indicated by white boxes (LRPB1, LRPB2, and LRPB3), respectively. The nucleotides showing enhanced cleavage are indicated by asterisks. Nucleotide numbers shown are relative to the transcription start site of *rtxA*.

II-3-3. Lrp activates *rtxA* in an independent manner with H-NS and HlyU

It was observed that the binding sites of Lrp in the P_{rtxA} regulatory region (LRPB1 and LRPB2) overlapped with those of H-NS and HlyU (Liu et al., 2009) (Fig. II-4). To understand how Lrp activates the *rtxA* expression in the presence of H-NS or HlyU, it was investigated whether Lrp interacts with H-NS or HlyU in the P_{rtxA} regulatory region. To this end, EMSAs were performed using reaction mixtures containing the radiolabeled DNA Probe 1 and a fixed concentration of either H-NS or HlyU with various amounts of Lrp. As the concentrations of Lrp increased, the band representing the DNA-H-NS complex (B1) was gradually retarded, generating the band representing the DNA-H-NS-Lrp complex (B4) (Fig. II-5A). This result suggested that Lrp binds to the P_{rtxA} regulatory region simultaneously with H-NS, rather than displaces H-NS. Similarly, EMSA with a fixed concentration of HlyU and increasing amounts of Lrp revealed that Lrp binds to the P_{rtxA} regulatory region simultaneously with HlyU (Fig. II-5B).

Fig. II-5C to F confirmed that H-NS negatively but HlyU positively regulate the *rtxA* expression at the translational as well as transcriptional levels. The relationship of Lrp with either H-NS or HlyU in the *rtxA* regulation was further investigated. As shown in Fig. II-5C and D, the *rtxA* transcript and RtxA protein levels in the *hns lrp* double mutant decreased compared with those in the *hns* mutant. Furthermore, the extent of the decrease in the *rtxA* transcript and RtxA protein levels caused by the *lrp* mutation was similar in the wild type and *hns* mutant (Fig. II-5C and D). These

results indicated that Lrp activates the *rtxA* expression in an independent manner with H-NS. Similarly, the *rtxA* transcript and RtxA protein levels in the *hlyU lrp* double mutant decreased compared with those in the *hlyU* mutant (Fig. II-5E and F). The presence of HlyU did not affect the extent of the decrease in the *rtxA* transcript and RtxA protein levels carried by the *lrp* mutation (Fig. II-5E and F), indicating that Lrp activates the *rtxA* expression in an independent manner with HlyU. Western blot analysis also revealed that the cellular levels of Lrp, H-NS, and HlyU were not significantly affected by one another (Fig. II-5D and F), suggesting that these transcriptional regulators function cooperatively to regulate *rtxA* rather than sequentially in a regulatory cascade. Taken together, the results indicated that Lrp binds to the P_{rtxA} regulatory region simultaneously with H-NS or HlyU and activates *rtxA* independently of H-NS and HlyU.

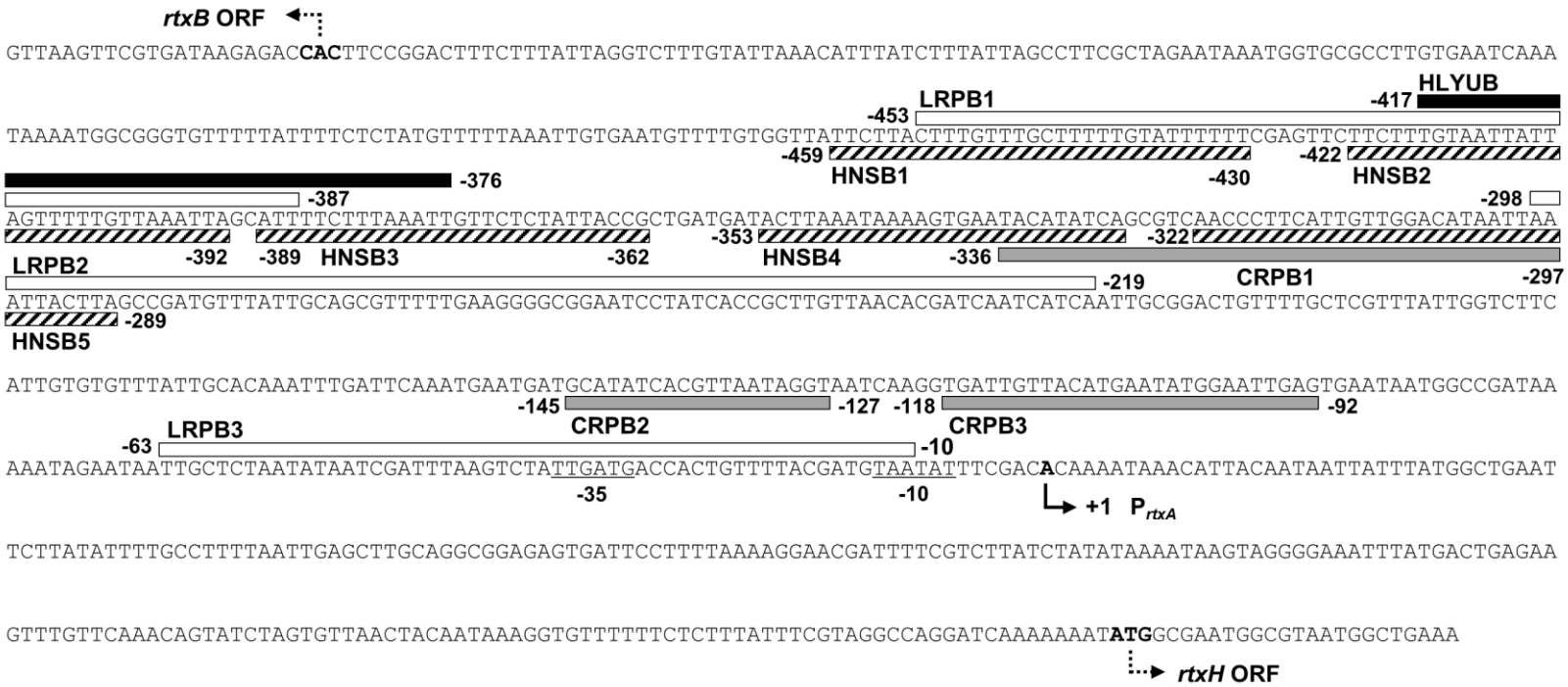

Figure II-4. Sequence analysis of the P_{rtxA} regulatory region. The DNA sequence between *rtxBDE* and *rtxHCA* is shown. The transcription start site of the *rtxHCA* operon is indicated in boldface and by solid bent arrow, and the positions of the putative -10 and -35 regions are underlined. The putative translational initiation codons of *rtxB* and *rtxH* are indicated in boldface and by dashed bent arrow, respectively. The

sequences for the binding of Lrp (LRPB1, LRPB2, and LRPB3; white boxes) and CRP (CRPB1, CRPB2, and CRPB3; gray boxes) were determined in this study. The sequences for the binding of HlyU (HLYUB) and H-NS (HNSB1, HNSB2, HNSB3, HNSB4, and HNSB5) are indicated by black box and dashed boxes, respectively.

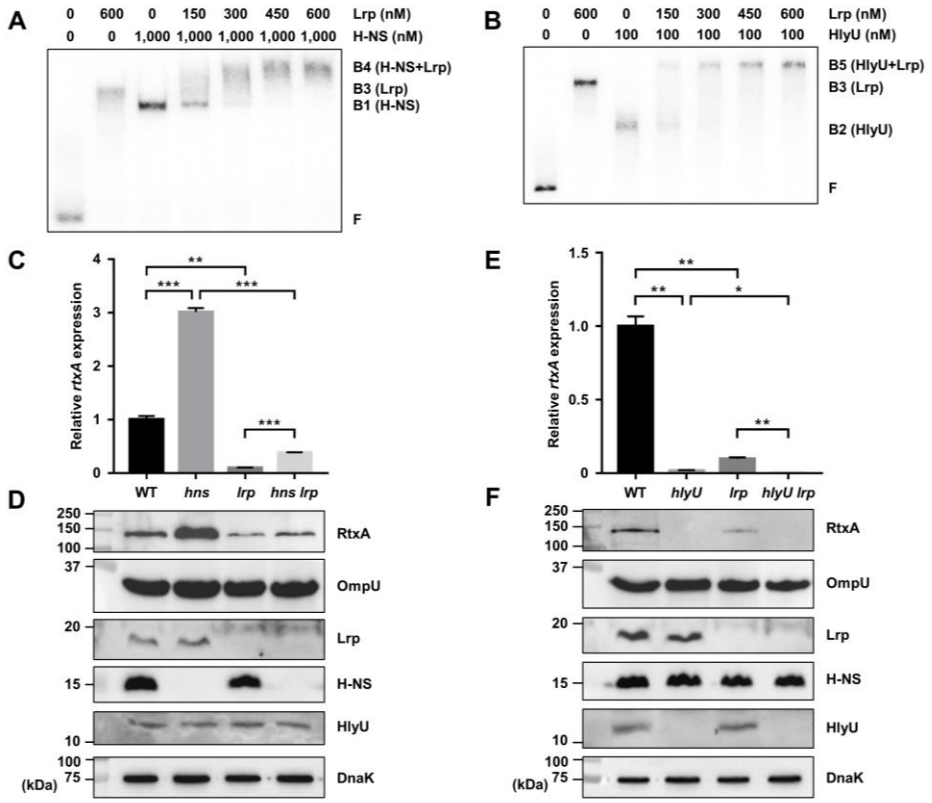

Figure II-5. Lrp activates the *rtxA* expression independently of H-NS and HlyU.

(A and B) Interaction of Lrp with either H-NS (A) or HlyU (B) in the binding to P_{rtxA}. A 452-bp DNA probe of the P_{rtxA} regulatory region (Probe 1; 5 nM) was radioactively labeled and then incubated with increasing amounts of Lrp in the presence of 1,000 nM H-NS (A) or 100 nM HlyU (B). The DNA-protein complexes were separated by electrophoresis. B1, DNA-H-NS complex; B2, DNA-HlyU complex; B3, DNA-Lrp complex; B4, DNA-H-NS-Lrp complex; B5, DNA-HlyU-Lrp complex; F, free DNA. (C to F) Total RNAs and proteins were isolated from the *V. vulnificus* strains grown to A_{600} of 0.5 and used to determine the *rtxA* transcript and RtxA, OmpU, Lrp, H-NS, HlyU, and DnaK protein levels. (C and E) The *rtxA* transcript levels were determined

by qRT-PCR analyses, and the *rtxA* transcript level in the wild type was set as 1. Error bars represent the SD. Statistical significance was determined by the Student's *t*-test (***, $p < 0.0005$; **, $p < 0.005$; *, $p < 0.05$). (D and F) The secreted RtxA and OmpU (as an internal control), and cellular Lrp, H-NS, HlyU, and DnaK (as an internal control) levels were determined by Western blot analysis. Molecular size markers (Bio-Rad) are shown in kDa. WT, wild type; *hns*, *hns* mutant; *lrp*, *lrp* mutant; *hns lrp*, *hns lrp* double mutant; *hlyU*, *hlyU* mutant; *hlyU lrp*, *hlyU lrp* double mutant.

II-3-4. Leucine inhibits Lrp binding to P_{rtxA} and activation of *rtxA*

To investigate the effect of leucine on the regulatory mode of Lrp, it was first examined whether leucine affects the DNA-binding activity of Lrp. EMSAs revealed that the addition of increasing amounts of leucine to the radiolabeled DNA Probe 1 and Probe 2 resulted in a concentration-dependent decrease of Lrp binding to DNA (Fig. II-6A and B). Next, the P_{rtxA} activity of *V. vulnificus* cells grown with or without leucine was determined *in vivo*. The presence of exogenous leucine significantly reduced the P_{rtxA} activity in the wild-type strain but had no effect on the P_{rtxA} activity in the *lrp* mutant (Fig. II-6C). The effects of different amino acids on the DNA-binding activity of Lrp were also examined. The addition of various amino acids decreased the binding of Lrp in the order of leucine, methionine, isoleucine, and phenylalanine (Fig. II-7). In contrast, the addition of tryptophan and histidine did not alter the DNA-binding activity of Lrp (Fig. II-7). The combined results indicated that leucine exhibits an antagonistic effect on the P_{rtxA} activity, and the effect is mediated by Lrp. Together, the results suggested that leucine inhibits the Lrp binding to P_{rtxA} and reduces the P_{rtxA} activation.

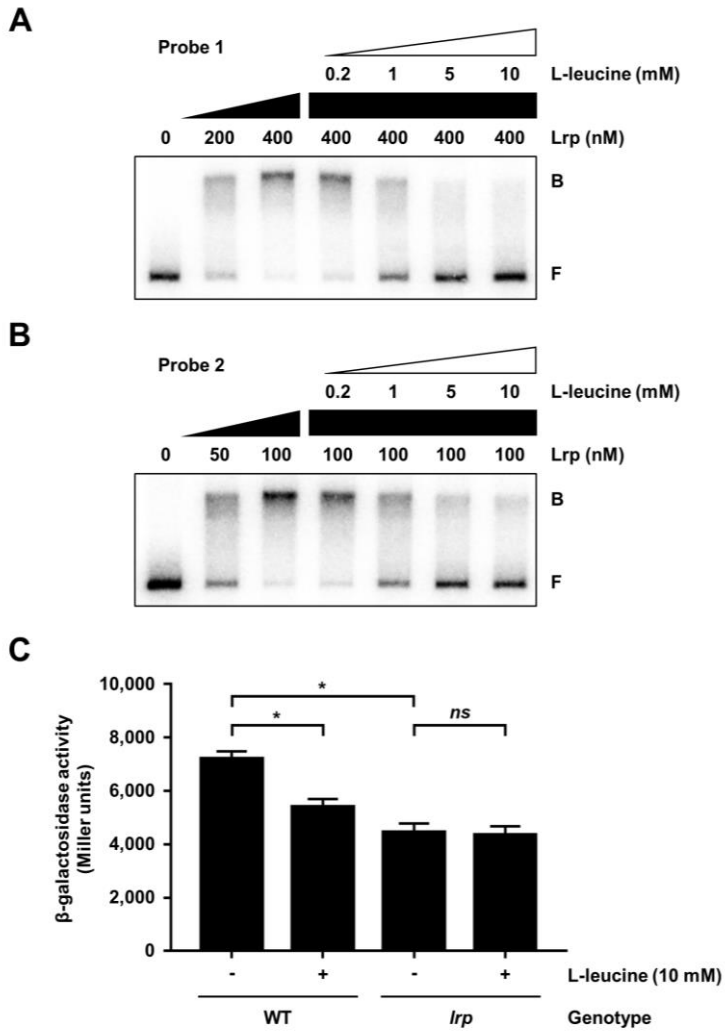

Figure II-6. Effects of L-leucine on Lrp binding to and activation of P_{rtxA}. (A and B) Each 452-bp DNA probe of the P_{rtxA} regulatory region [Probe 1 for (A) and Probe 2 for (B); 5 nM] was radioactively labeled and then incubated with increasing amounts of Lrp as indicated. Increasing amounts of L-leucine were added to the reaction mixture containing the 5 nM labeled DNA and 400 nM (A) or 100 nM (B) Lrp as indicated. The DNA-protein complexes were separated by electrophoresis. B, bound DNA; F, free DNA. (C) The *V. vulnificus* strains harboring the reporter

plasmid with promoterless *lacZ* fused to P_{rtxA} were grown to A_{600} of 0.5 with or without 10 mM L-leucine. The β-galactosidase activities of the *V. vulnificus* strains were measured and expressed in Miller units. Error bars represent the SD. Statistical significance was determined by the Student's *t*-test (*, $p < 0.05$; *ns*, not significant). WT, *lacZ* mutant harboring the reporter plasmid; *lrp*, *lrp lacZ* double mutant harboring the reporter plasmid.

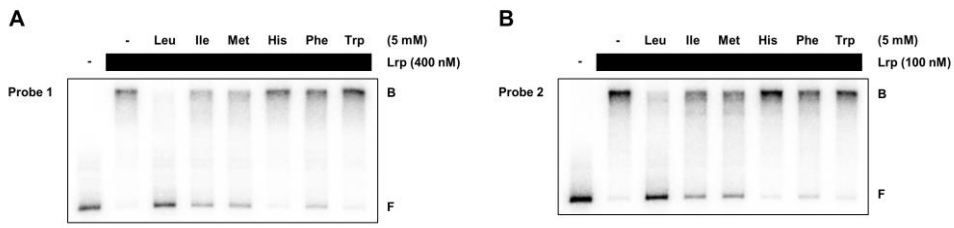

Figure II-7. Effects of various amino acids on Lrp binding to P_{rtxA}. (A and B) Each 452-bp DNA probe of the P_{rtxA} regulatory region [Probe 1 for (A) and Probe 2 for (B); 5 nM] was radioactively labeled and then incubated with 400 nM (A) or 100 nM (B) Lrp. L-leucine (Leu), L-isoleucine (Ile), L-methionine (Met), L-histidine (His), L-phenylalanine (Phe), or L-tryptophan (Trp) at 5 mM were added to the reaction mixture containing the 5 nM labeled DNA and Lrp as indicated. The DNA-protein complexes were separated by electrophoresis. B, bound DNA; F, free DNA.

II-3-5. CRP represses but glucose derepresses the *rtxA* expression

Because the *crp* mutant showed significantly higher *rtxA* transcript level than wild type (Fig. II-1), it was investigated whether CRP negatively regulates the expression of *rtxA*. Consistent with the result, the *rtxA* transcript and RtxA protein levels were increased in the *crp* mutant and restored to the levels comparable to those in the wild type by introducing pKK1502 carrying a recombinant CRP (Fig. II-8A and B). These results indicated that the *rtxA* expression is negatively regulated by CRP at the transcriptional level. Furthermore, it was also examined whether the *rtxA* expression is increased by exogenous glucose. Indeed, in both exponential and stationary phases, the P_{rtxA} activity was higher in the *V. vulnificus* cells grown with 0.5% glucose than that in the cells grown without glucose (Fig. II-8C), indicating that the P_{rtxA} activity is induced in the presence of exogenous glucose. It was further investigated whether the production of RtxA is also increased upon the addition of exogenous glucose. As shown in Fig. II-8D, the RtxA level was elevated in wild-type *V. vulnificus* cells grown with 0.5% glucose compared with that in the cells grown without glucose. Moreover, the addition of exogenous glucose did not affect the production of RtxA in the *crp* mutant (Fig. II-8D), confirming that the induction of *rtxA* in the presence of exogenous glucose is mediated by CRP. These results indicated that the *rtxA* expression is repressed by CRP but derepressed by exogenous glucose.

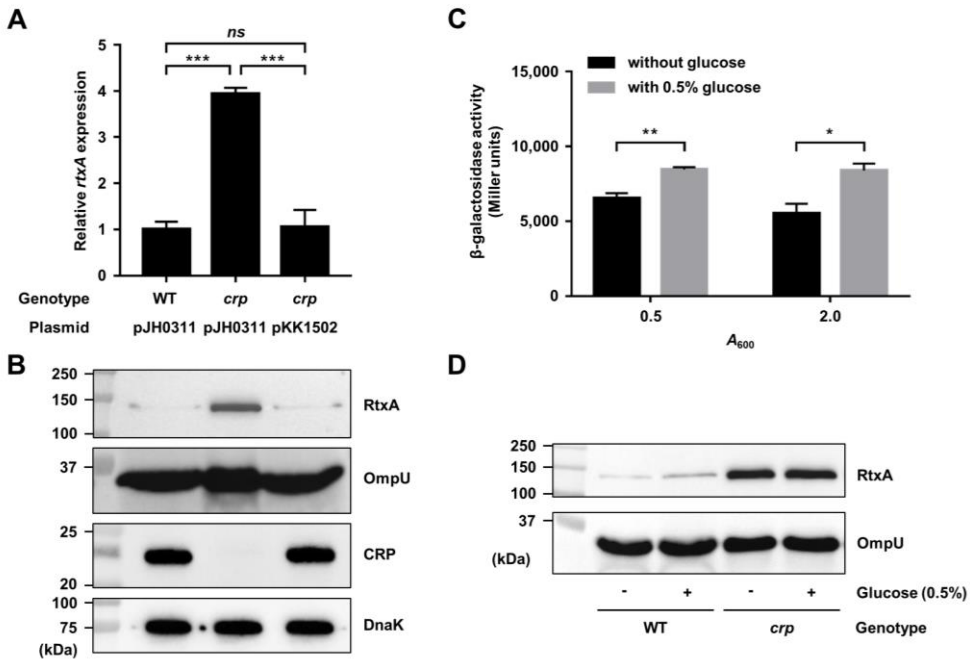

Figure II-8. Effects of the *crp* mutation and glucose on the *rtxA* expression. (A and B) Total RNAs and proteins were isolated from the *V. vulnificus* strains grown to A_{600} of 0.5 and used to determine the *rtxA* transcript and RtxA, OmpU, CRP, and DnaK protein levels. (A) The *rtxA* transcript levels were determined by qRT-PCR analyses, and the *rtxA* transcript level in the wild type was set as 1. Error bars represent the SD. Statistical significance was determined by the Student's *t*-test (***, $p < 0.0005$; *ns*, not significant). (B) The secreted RtxA and OmpU (as an internal control), and cellular CRP and DnaK (as an internal control) levels were determined by Western blot analysis. WT (pJH0311), wild type; *crp* (pJH0311), *crp* mutant; *crp* (pKK1502), *crp* complemented strain. (C) *V. vulnificus lacZ* mutant harboring the reporter plasmid with promoterless *lacZ* fused to P_{rtxA} was grown to A_{600} of 0.5 (for exponential phase) and 2.0 (for stationary phase) with or without 0.5% glucose. The

β-galactosidase activities of the *V. vulnificus* strains were measured and expressed in Miller units. Error bars represent the SD. Statistical significance was determined by the Student's *t*-test (**, $p < 0.005$; *, $p < 0.05$). (D) The *V. vulnificus* strains were grown to A_{600} of 0.5 with or without 0.5% glucose and used to determine RtxA and OmpU protein levels. The secreted RtxA and OmpU levels were determined by Western blot analysis. WT, wild type; *crp*, *crp* mutant. Molecular size markers (Bio-Rad) are shown in kDa in (B) and (D).

II-3-6. CRP represses *rtxA* by directly binding to the upstream regions of P_{rtxA}

To examine whether CRP directly regulates *rtxA* by binding to P_{rtxA}, EMSA was performed. The addition of CRP to the radiolabeled DNA Probe 1 resulted in a single retarded band of a DNA-CRP complex in a CRP concentration-dependent manner (Fig. II-9A). In contrast, the addition of CRP to the radiolabeled DNA Probe 2 resulted in two retarded bands (Fig. II-9B), indicating that CRP binds to at least two binding sites in Probe 2. The combined results suggested that at least three binding sites of CRP are present in the P_{rtxA} regulatory region. The same but unlabeled DNA fragment, which was used as a self-competitor, showed the competition for CRP binding in a dose-dependent manner (Fig. II-9A and B), confirming the specific binding of CRP to the P_{rtxA} regulatory region. DNase I protection assays revealed that CRP protected two regions extending from -336 to -297 (CRPB1, centered at -316.5) and -145 to -127 (CRPB2, centered at -136), respectively, from the DNase I digestion (Fig. II-9C and D). Upon an increase in the CRP concentrations, another additional region extending from -118 to -92 (CRPB3, centered at -105) was protected from the DNase I digestion (Fig. II-9D). Several nucleotides showed enhanced cleavage, which is frequently observed in the DNase I protection assay of CRP-binding sites (Jeong et al., 2003a; Jang et al., 2016), indicating that CRP binding alters the DNA conformation in P_{rtxA} (Fig. II-9C and D). Combined with the EMSA results (Fig. II-9A and B), these results suggested that CRP represses the *rtxA* expression by directly binding to specific regions within P_{rtxA}. It is noteworthy that

all three binding sites of CRP are located in the upstream regions of P_{rtxA}, which is unusual for a negative regulator.

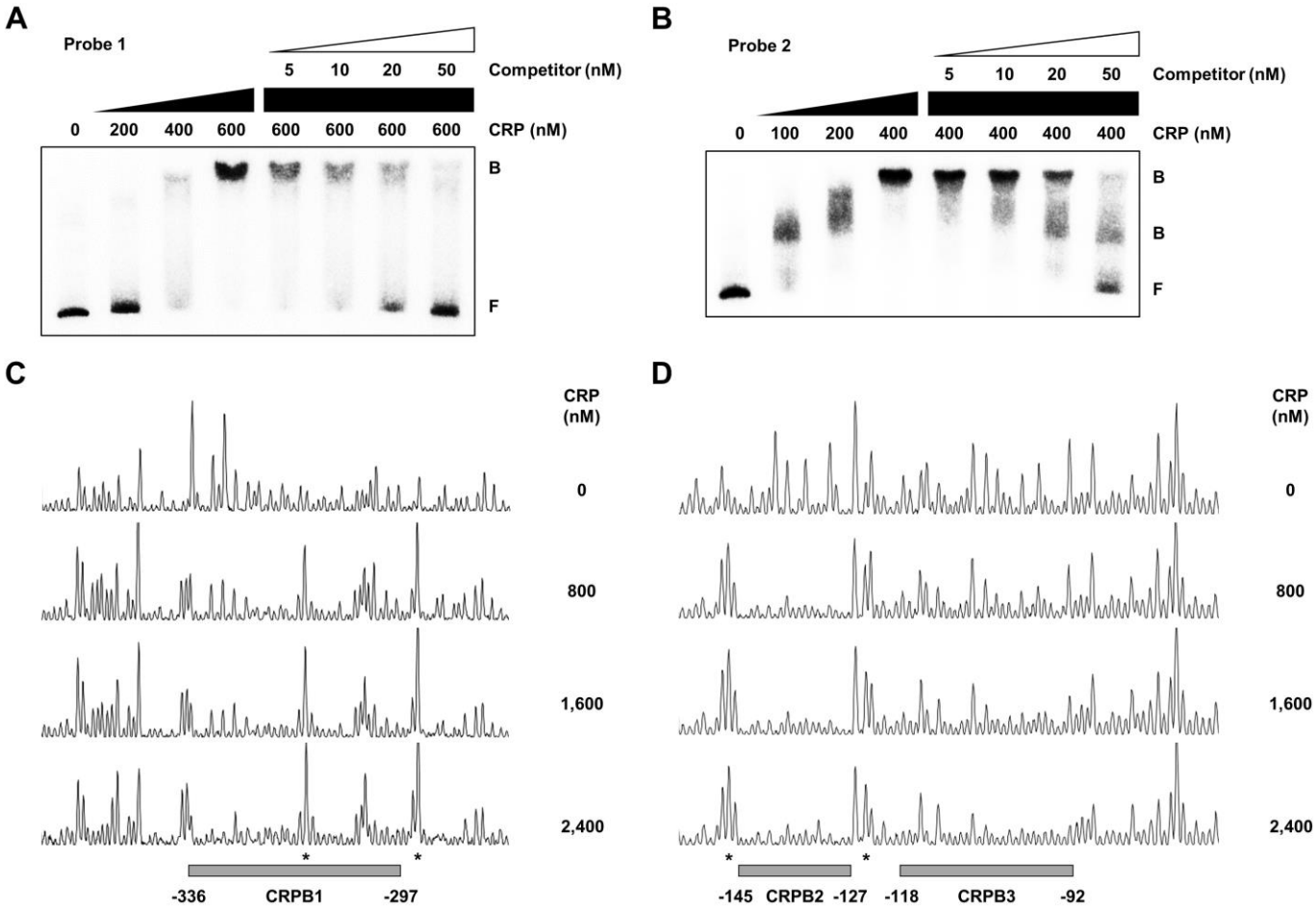
A
Probe 1
5 10 20 50
Competitor (nM)
0 200 400 600 600 600 600 600
CRP (nM)
B
F
B
Probe 2
5 10 20 50
Competitor (nM)
0 100 200 400 400 400 400 400
CRP (nM)
B
B
F
C
CRP (nM)
0
800
1,600
2,400
-336 CRPB1 -297
D
CRP (nM)
0
800
1,600
2,400
-145 CRPB2 -127 -118 CRPB3 -92

Figure II-9. Specific binding of CRP to the P_{rtxA} regulatory region. (A and B) Each 452-bp DNA probe of the P_{rtxA} regulatory region [Probe 1 for (A) and Probe 2 for (B); 5 nM] was radioactively labeled and then incubated with increasing amounts of CRP as indicated. For competition analysis, various amounts of the same but unlabeled each DNA fragment were used as a self-competitor and added to the reaction mixture containing the 5 nM labeled DNA before the addition of 600 nM (A) or 400 nM (B) CRP. The DNA-protein complexes were separated by electrophoresis. B, bound DNA; F, free DNA. (C and D) The same DNA probes of each P_{rtxA} regulatory region (40 nM) were labeled with 6-FAM, incubated with increasing amounts of CRP as indicated, and then digested with DNase I. The regions protected by CRP are indicated by gray boxes (CRPB1, CRPB2, and CRPB3), respectively. The nucleotides showing enhanced cleavage are indicated by asterisks. Nucleotide numbers shown are relative to the transcription start site of *rtxA*.

II-3-7. Mutational analyses of the CRP-binding sequences of P_{rtxA}

To investigate whether the CRP-binding sites located upstream of P_{rtxA} are effective for CRP binding, mutations were introduced in the CRP-binding sequences as shown in Fig. II-10A to C. First, the CRP binding to P_{rtxA} carrying the wild-type or each mutated CRP-binding sequence was examined. CRP bound to the radiolabeled DNA Probe 1 carrying the wild-type CRP-binding sequence 1, resulting in a single retarded band of the DNA-CRP complex in a CRP concentration-dependent manner (Fig. II-10A; wtCRPB1). When the DNA probe carrying the mutated CRP-binding sequence 1 was used, however, the binding of CRP to DNA decreased, as a reduced amount of retarded bands was detected compared to the DNA probe with the wild-type CRP-binding sequence (Fig. II-10A; mtCRPB1). Similar results were obtained with the DNA Probe 2 carrying the wild-type or mutated CRP-binding sequence 2 (Fig. II-10B; wtCRPB2 and mtCRPB2). The results indicated that the CRP-binding sites located upstream of P_{rtxA} are effective for CRP binding. In contrast, the CRP binding to the mutated CRP-binding sequence 3 was not significantly altered compared with that to the wild-type CRP-binding sequence (Fig. II-10C; wtCRPB3 and mtCRPB3), suggesting that the binding of CRP to CRPB3 is less sequence-specific than CRPB1 or CRPB2.

Next, the activity of P_{rtxA} carrying the wild-type or each mutated CRP-binding sequence was assessed *in vivo* using the *rtxA-lacZ* transcriptional fusion reporters. Consistent with the EMSA results, the P_{rtxA} activity in wild-type *V. vulnificus* cells

was increased when either CRPB1 or CRPB2 was mutated but not altered when CRPB3 was mutated (Fig. II-10D). These results indicated that the CRP binding to CRPB1 and CRPB2 is really responsible for the repression of *rtxA in vivo*. Furthermore, the presence of exogenous glucose induced the P_{rtxA} activity in the wild-type strain, while it had no effect on the P_{rtxA} activity in the *crp* mutant (Fig. II-10D). This result was consistent with the observation that the induction of *rtxA* by exogenous glucose is mediated by CRP (Fig. II-8D). The combined results demonstrated that CRP represses P_{rtxA} by directly binding to its upstream regions but derepresses in the presence of exogenous glucose.

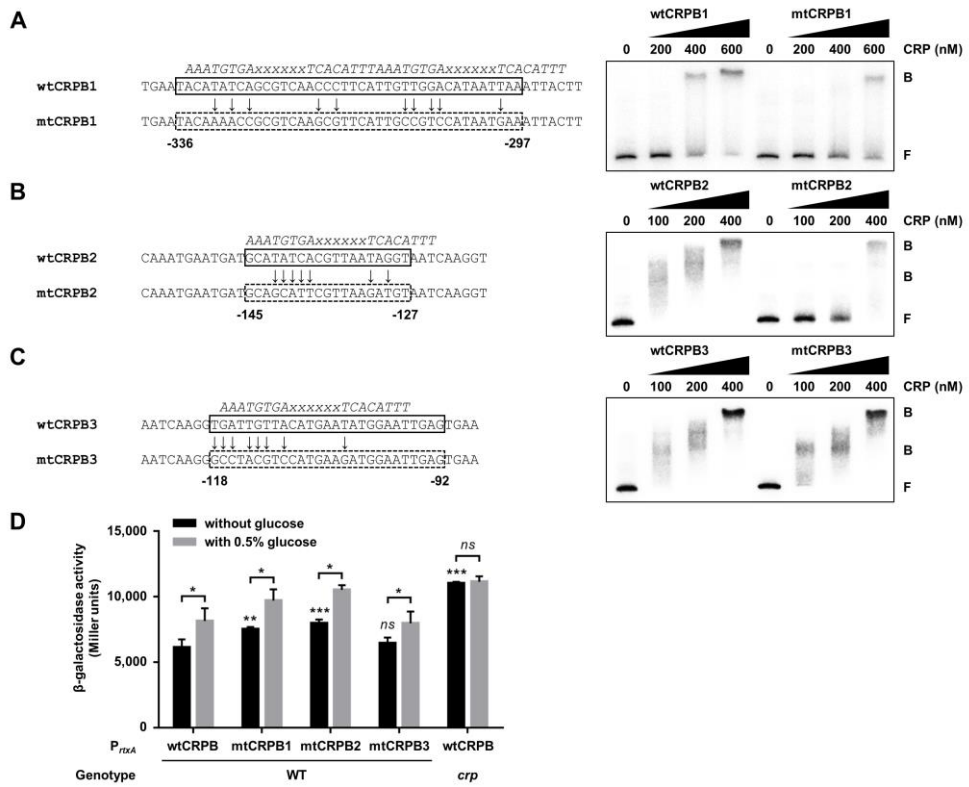

Figure II-10. Mutations in the CRP-binding sequences affect the binding of CRP to and activity of P_{rtxA}. (A to C) The CRP-binding sequences wtCRPB1 (A), wtCRPB2 (B), and wtCRPB3 (C) in the P_{rtxA} regulatory region are indicated by solid boxes. The mutated CRPBs (mtCRPBs) are indicated by dashed boxes, respectively, with the site-directed mutagenized nucleotides marked by arrows. The consensus sequences for the CRP binding are indicated by italicized letters above the wtCRPBs. x, any nucleotide. Nucleotide numbers shown are relative to the transcription start site of *rtxA*. For EMSAs, each radiolabeled DNA probe of wt or mt CRPB (5 nM) was incubated with increasing amounts of CRP as indicated. The DNA-protein complexes were separated by electrophoresis. B, bound DNA; F, free DNA. (D) The *V. vulnificus* strains harboring reporter plasmids with promoterless *lacZ* fused to P_{rtxA}

carrying either wild-type or mutated CRPB as described in (A to C) were grown to A_{600} of 0.5 with or without 0.5% glucose. The β-galactosidase activities of the *V. vulnificus* strains were measured and expressed in Miller units. Error bars represent the SD. Statistical significance was determined by the multiple comparisons after one-way ANOVA among the strains grown without glucose (***, $p < 0.0005$; **, $p < 0.005$; *ns*, not significant relative to the wild-type strain with P_{rtxA} carrying wtCRPB) and by the Student's *t*-test between the single strains grown with or without glucose (*, $p < 0.05$; *ns*, not significant). WT, *lacZ* mutant harboring the reporter plasmid with promoterless *lacZ* fused to P_{rtxA} carrying wt or mt CRPB, respectively; *crp*, *crp lacZ* double mutant harboring the reporter plasmid with promoterless *lacZ* fused to P_{rtxA} carrying wtCRPB.

II-3-8. CRP directly represses the *lrp* and *hlyU* expression

It is still possible that CRP indirectly regulates the *rtxA* expression by modulating the cellular level of other transcription factors. For example, CRP can negatively regulate the *rtxA* expression by repressing the expressions of Lrp or HlyU, the positive regulators of *rtxA*. Surprisingly, the *lrp* transcript and Lrp protein levels were significantly increased in the *crp* mutant and restored to the levels comparable to those in the wild type by complementation of the *crp* gene (Fig. II-11A and B), indicating that CRP represses the *lrp* expression. To examine whether CRP represses *lrp* by directly binding to its upstream region, EMSA was performed. The addition of CRP to the radiolabeled DNA resulted in a single retarded band of the DNA-CRP complex in a CRP concentration-dependent manner (Fig. II-11C). The same but unlabeled DNA fragment, which was used as a self-competitor, showed the competition for CRP binding in a dose-dependent manner (Fig. II-11C), confirming the specific binding of CRP to the upstream region of *lrp*. This result suggested that CRP directly represses the *lrp* expression.

In a similar way, the *hlyU* transcript and HlyU protein levels were substantially increased in the *crp* mutant and restored to the levels comparable to those in the wild type by complementation of the *crp* gene (Fig. II-12A and B), indicating that CRP also represses the *hlyU* expression. Furthermore, EMSA revealed that CRP binds directly and specifically to the upstream region of *hlyU* (Fig. II-12C). The combined results suggested that CRP directly represses the expression of both *lrp* and *hlyU*,

resulting in the *rtxA* repression. Moreover, the cellular level of CRP was not altered by the mutation in *hns*, *lrp*, or *hlyU* (Fig. II-13), suggesting that the expression of *crp* is not controlled by H-NS, Lrp, or HlyU. These results implied that CRP also indirectly represses *rtxA* by forming coherent feedforward loops with Lrp and HlyU, respectively. In conclusion, H-NS, HlyU, Lrp, and CRP constitute a regulatory network for the *rtxA* transcription in *V. vulnificus*. CRP elaborately controls *rtxA* not only by directly binding to P_{rtxA} but also by coordinating the components of the *rtxA* regulatory network through the repression of *lrp* and *hlyU*. This collaborative regulation probably contributes to the precise expression of *rtxA* in response to environmental signals such as leucine and glucose during host infection.

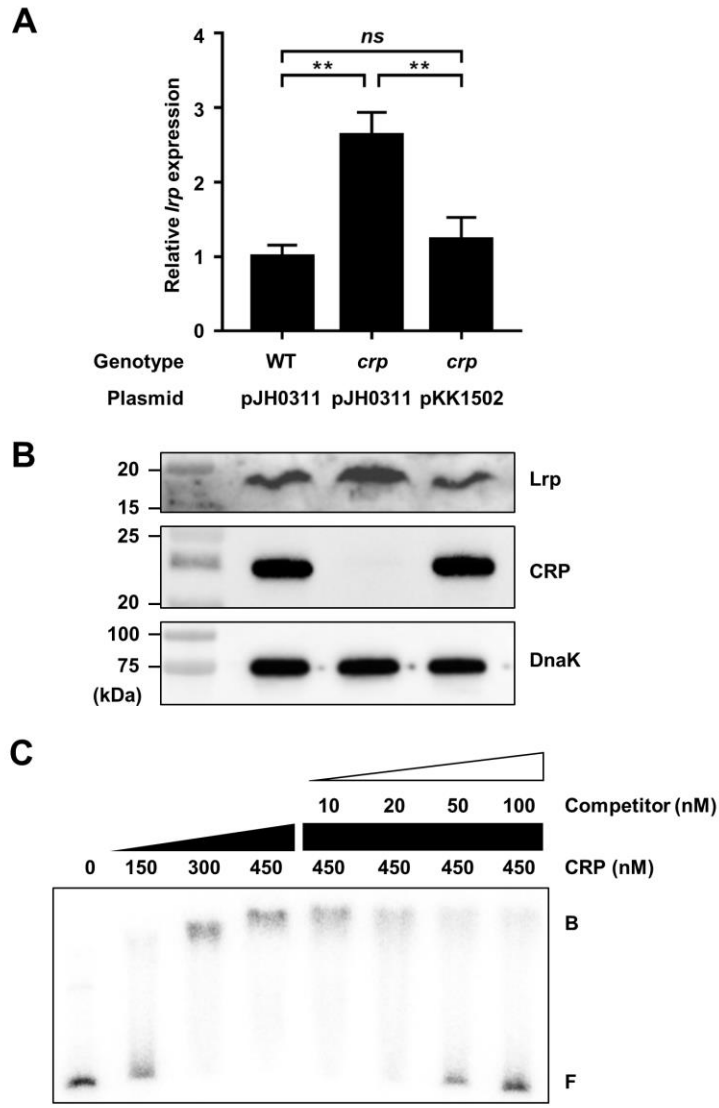

Figure II-11. CRP represses the *lrp* expression by directly binding to the upstream region. (A and B) Total RNAs and proteins were isolated from the *V. vulnificus* strains grown to A_{600} of 0.5 and used to determine the *lrp* transcript and Lrp, CRP, and DnaK protein levels. (A) The *lrp* transcript levels were determined by qRT-PCR analyses, and the *lrp* transcript level in the wild type was set as 1. Error bars represent the SD. Statistical significance was determined by the Student's *t*-test (**, $p < 0.005$; *ns*, not significant). (B) The cellular Lrp, CRP, and DnaK (as an

internal control) levels were determined by Western blot analysis. Molecular size markers (Bio-Rad) are shown in kDa. WT (pJH0311), wild type; *crp* (pJH0311), *crp* mutant; *crp* (pKK1502), *crp* complemented strain. (C) A 424-bp DNA probe of the *lrp* upstream region was radioactively labeled and then incubated with increasing amounts of CRP as indicated. For competition analysis, various amounts of the same but unlabeled DNA fragment were used as a self-competitor and added to the reaction mixture containing the 5 nM labeled DNA before the addition of 450 nM CRP. The DNA-protein complexes were separated by electrophoresis. B, bound DNA; F, free DNA.

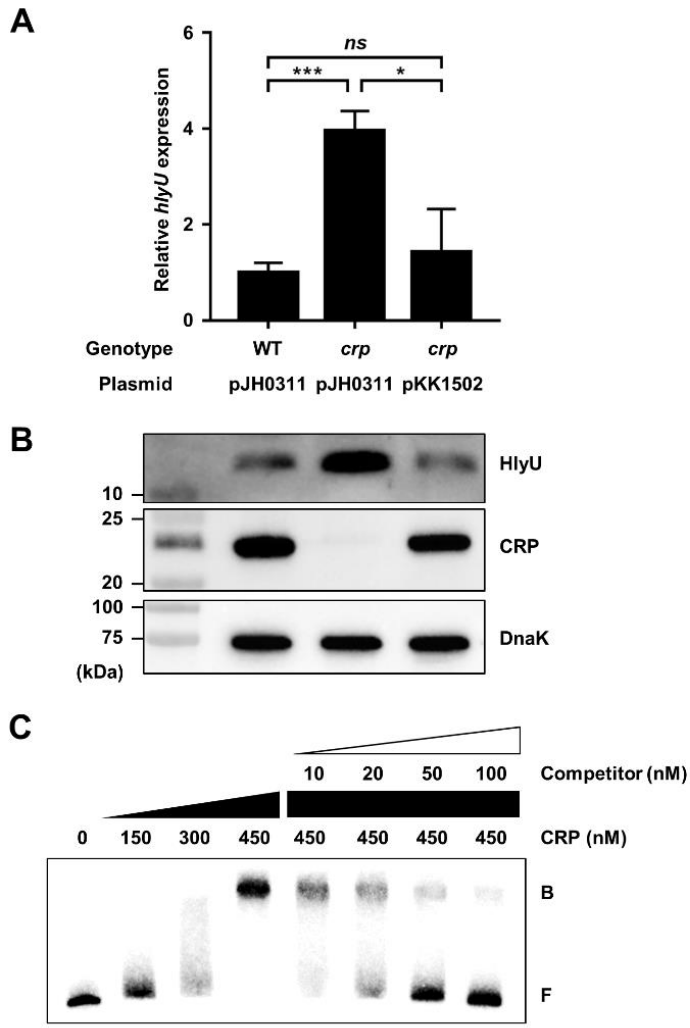

Figure II-12. CRP represses the *hlyU* expression by directly binding to the upstream region. (A and B) Total RNAs and proteins were isolated from the *V. vulnificus* strains grown to A_{600} of 0.5 and used to determine the *hlyU* transcript and HlyU, CRP, and DnaK protein levels. (A) The *hlyU* transcript levels were determined by qRT-PCR analyses, and the *hlyU* transcript level in the wild type was set as 1. Error bars represent the SD. Statistical significance was determined by the Student's *t*-test (***, $p < 0.0005$; *, $p < 0.05$; *ns*, not significant). (B) The cellular

HlyU, CRP, and DnaK (as an internal control) levels were determined by Western blot analysis. Molecular size markers (Bio-Rad) are shown in kDa. WT (pJH0311), wild type; *crp* (pJH0311), *crp* mutant; *crp* (pKK1502), *crp* complemented strain. (C) A 572-bp DNA probe of the *hlyU* upstream region was radioactively labeled and then incubated with increasing amounts of CRP as indicated. For competition analysis, various amounts of the same but unlabeled DNA fragment were used as a self-competitor and added to the reaction mixture containing the 5 nM labeled DNA before the addition of 450 nM CRP. The DNA-protein complexes were separated by electrophoresis. B, bound DNA; F, free DNA.

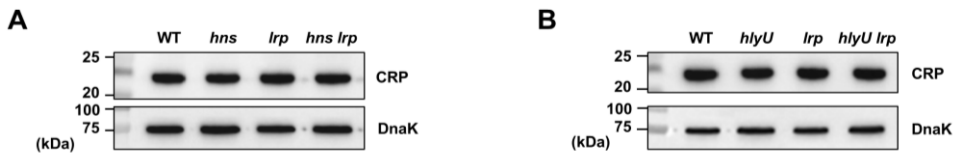

Figure II-13. Expression of *crp* is not affected by *hns, lrp,* or *hlyU* mutations. (A and B) Total proteins were isolated from the *V. vulnificus* strains grown to A_{600} of 0.5 as described in Fig. II-5C to F and used to determine the CRP and DnaK protein levels. The cellular CRP and DnaK (as an internal control) levels were determined by Western blot analysis. Molecular size markers (Bio-Rad) are shown in kDa. WT, wild type; *hns*, *hns* mutant; *lrp*, *lrp* mutant; *hns lrp*, *hns lrp* double mutant; *hlyU*, *hlyU* mutant; *hlyU lrp*, *hlyU lrp* double mutant.

II-4. Discussion

In the present study, Lrp was newly identified as a positive regulator of the *rtxA* transcription in *V. vulnificus* (Figs. II-1 and 2). Although the binding sites of Lrp in the P_{rtxA} regulatory region overlapped with those of H-NS and HlyU (Figs. II-3 and 4), Lrp binds to P_{rtxA} simultaneously with H-NS and HlyU (Fig. II-5A and B). Consistent with this, Lrp activates the *rtxA* expression independently of H-NS and HlyU (Fig. II-5C to F). When acting as a sole transcriptional activator, Lrp can stimulate the promoter activity by remodeling DNA structure and/or mediating protein-protein interactions (Peeters et al., 2009). Based on these findings, one possible explanation for how Lrp activates *rtxA* is that the Lrp-induced DNA bending stores elastic energy that could facilitate the transcription activation of RNA polymerase (RNAP) (Wang and Calvo, 1993). Because the Lrp binding to P_{rtxA} is reduced in the presence of leucine (Fig. II-6A and B), it is reasonable to hypothesize that exogenous leucine would inhibit the Lrp-induced DNA bending and thus the transcription of *rtxA*. Indeed, exogenous leucine significantly reduced the P_{rtxA} activity only when Lrp was present (Fig. II-6C). Accordingly, the regulatory mode of Lrp for *rtxA* in response to exogenous leucine is found to be the reciprocal mode, in which leucine inhibits the regulatory activity of Lrp (Cho et al., 2008).

Among a wide variety of environmental signals, nutrient availability is an important factor that pathogens monitor for the modulation of virulence gene expression

(Miller et al., 1989; Fang et al., 2016). In *V. cholerae*, the production of CT and TCP is negatively regulated by CRP, suggesting that intra-intestinal glucose levels could affect the ability of the pathogen to colonize and cause diarrhea in the host (Skorupski and Taylor, 1997a). In enterotoxigenic *E. coli*, the differential regulation of heat-labile toxin (LT) and heat-stable toxin (ST) by CRP also suggests that the glucose levels in the lumen of the small intestine might determine where and when each enterotoxin is expressed maximally (Bodero and Munson, 2009). In this study, the expression of *rtxA* in *V. vulnificus* was found to be repressed by CRP and induced by exogenous glucose (Fig. II-8). It has been suggested that RtxA promotes the growth of *V. vulnificus* in the early stage of infection and thus dissemination of the bacteria from the small intestine to other organs in mice (Jeong and Satchell, 2012; Gavin et al., 2017). Therefore, it is tempting to speculate that, for successful pathogenesis, the *rtxA* expression is favored in glucose-rich environments such as duodenum and jejunum where carbohydrates are digested to monosaccharides, rather than in glucose-poor environments such as ileum (Wright et al., 2003; Bodero and Munson, 2009). Induction of *rtxA* in the early stage of infection could provide the pathogen with the benefit of surviving from phagocytosis during infection (Lo et al., 2011; Gavin and Satchell, 2019). Moreover, these findings are consistent with the observation that people whose glucose levels are higher because of diabetes or chronic liver disease are at high risk of infection by *V. vulnificus* (Jones and Oliver, 2009).

EMSAs and DNase I protection assays revealed that CRP directly binds to specific sequences in the upstream regions of P_{rtxA} (Fig. II-9), which is unusual as a negative regulator. Nevertheless, several transcription factors including CRP have been reported to bind upstream of promoters and repress transcription (Manneh-Roussel et al., 2018; Lee and Busby, 2012). In *V. cholerae*, CRP negatively regulates the *rtxBDE* operon, encoding the components of the secretion system for RtxA, by directly binding to the upstream region of the promoter (Manneh-Roussel et al., 2018). Similarly, in enterotoxigenic *E. coli*, CRP directly represses the *eltA* gene encoding LT by binding to the upstream region of the promoter (Bodero and Munson, 2009). *V. vulnificus* CRP also binds to the upstream regions and represses P_{rtxA}, and thus, it was further examined whether the CRP-binding sites determined by the DNase I protection assay are effective for CRP binding (Fig. II-10). Because H-NS binds to the sequences overlapped with the CRP-binding sites in the upstream region of P_{rtxA} (Fig. II-4), a deletion assay of the CRP-binding sites without deletion of the H-NS binding sites was not possible. Therefore, site-directed mutational analyses of the CRP-binding sequences were performed to define whether the CRP-binding sites are effective for CRP binding. The results demonstrate that CRP directly binds to the upstream regions of P_{rtxA} to repress the *rtxA* expression (Fig. II-10). One possible hypothesis for this unusual repression is that the upstream-bound CRP interacts with the C-terminal domains of the RNAP α subunit, thereby restraining RNAP from escaping from the initiation complex in P_{rtxA} (Lee and Busby, 2012). This hypothesis

can be supported by the enhanced cleavage suggesting the conformational changes in P_{rtxA} DNA by the CRP binding, as shown in the DNase I protection assay results (Fig. II-9C and D). In addition, CRP represses the expressions of *lrp* and *hlyU* by directly binding to their upstream regions (Figs. II-11 and 12), resulting in the negative regulation of *rtxA*. Taken together, these results indicated that CRP, along with Lrp and HlyU, forms complex coherent feedforward loops for the coordinated regulation of *rtxA* (Alon, 2007).

CRP, Lrp, H-NS, and HlyU constitute a complex regulatory network for the *rtxA* transcription as depicted in Fig. II-14A. H-NS represses *rtxA* by directly binding to multiple sites in the P_{rtxA} regulatory region, while HlyU directly binds to P_{rtxA} and relieves the repression by H-NS (Liu et al., 2009). Lrp directly activates *rtxA*, whereas CRP represses *rtxA* directly and indirectly through the repression of *lrp* and *hlyU* (Fig. II-14A). Intriguingly, while CRP negatively regulates the expression of RtxA, CRP positively regulates the expression of other exotoxins, VvhA, VvpE, and PlpA, in *V. vulnificus* (Choi et al., 2002; Jeong et al., 2003a; Jang et al., 2017). As shown in Fig. II-14B, this differential regulation is likely to determine which exotoxin is expressed spatially and temporally in *V. vulnificus* during the course of infection. For example, the expression of RtxA is predicted to be high in the early stage of infection such as in the upper small intestine and upon invasion into the bloodstream where glucose levels are relatively high. Produced RtxA could have an essential role in the invasion of *V. vulnificus* from the intestine into the bloodstream

(Kim et al., 2008b; Gavin et al., 2017), as well as in the survival of the pathogen from immune clearance (Lo et al., 2011). The expression of *rtxA* will decrease in the later stage of infection where glucose levels are relatively low due to the absorption by the enterocytes in the upper and mid small intestine (Wright et al., 2003), or the consumption by the invading *V. vulnificus* in the blood. The decreased expression of *rtxA* may be facilitated by responding to other signals such as leucine at any rate. Furthermore, the production of VvhA, VvpE, and PlpA in the later stage of infection might cause cell damage and accelerate the cell death process (Kim et al., 2008b; Jang et al., 2017; Lee et al., 2016b). Altogether, this spatiotemporal expression of virulence factors regulated by CRP will enhance the *in vivo* fitness of *V. vulnificus*. Coordinated regulation of *rtxA* by multiple transcription factors including CRP and Lrp enables the elaborate expression of *rtxA* in response to environmental and metabolic stimuli, further contributing to the successful infection of *V. vulnificus* within the host.

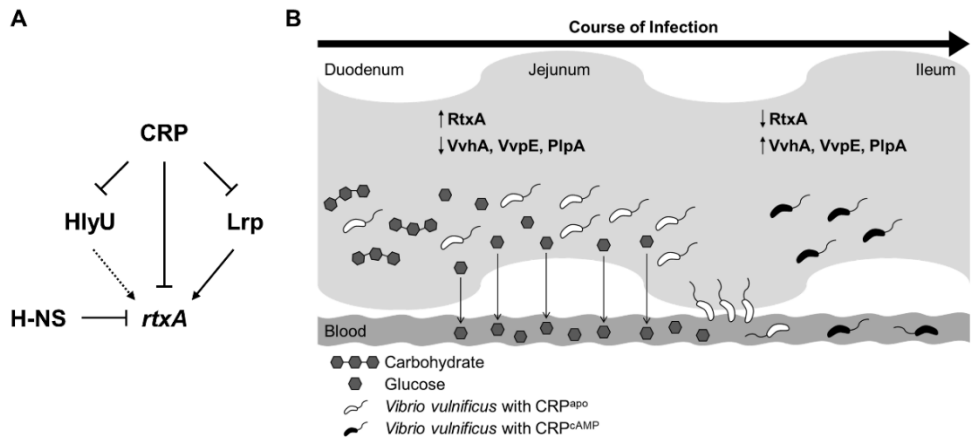

Figure II-14. A regulatory network controlling the *rtxA* expression and a spatiotemporally differential expression of exotoxins in *V. vulnificus*. (A) A regulatory network comprising transcriptional regulators CRP, Lrp, HlyU, and H-NS controls the *rtxA* expression. H-NS represses *rtxA*, and HlyU relieves the repression of H-NS. Lrp activates *rtxA*, while CRP represses *rtxA* directly and indirectly through the repression of *lrp* and *hlyU* in coherent feedforward loops. (B) The *V. vulnificus* exotoxins may be expressed spatially and temporally as the bacteria moves through the small intestine during the course of infection. In the early stage of infection, relatively high glucose levels in the duodenum and jejunum lead to the inactive form of CRP (CRP^{apo}) and thereby prevent the CRP-mediated repression of *rtxA*. Thus, the expression of *rtxA* is predicted to be high, and the produced RtxA could contribute to the invasion of *V. vulnificus* from the small intestine to the bloodstream. In the later stage of infection, relatively low glucose levels in the ileum stimulate the synthesis of cAMP, resulting in the formation of active cAMP-CRP

complex (CRP^{cAMP}). Therefore, the expression of *rtxA* is decreased, and this decreased *rtxA* expression may be facilitated in response to other signals such as leucine at any rate (not shown). In contrast, the expression of *vvhA*, *vvpE*, and *plpA* is increased, causing further damage to host cells. This spatiotemporal and precise expression of the exotoxins will provide *V. vulnificus* with the benefit in the pathogenesis during infection.

Chapter III.

Identification of a Small-molecule Inhibitor of HlyU Attenuating Virulence of *Vibrio* Species

Part of this work in Chapter III was published in *Scientific Reports* in 2019, as an article entitled “Small-molecule inhibitor of HlyU attenuates virulence of *Vibrio* species”.

III-1. Introduction

Traditional strategies to combat bacterial infection largely depend on the use of antibiotics that inhibit bacterial viability. Unfortunately, inhibition of viability results in the inevitable emergence of strains resistant to antibiotics. The emergence and spread of antibiotic-resistant bacteria have become a threat to public health by reducing the effectiveness of present antibiotics, which is a major cause for the rising healthcare costs (Clatworthy et al., 2007; Rasko and Sperandio, 2010; Smith and Coast, 2002). This situation imminently requires the development of new strategies to impede the virulence, rather than viability, of bacterial pathogens (Cegelski et al., 2008; Davies and Davies, 2010). Anti-virulence strategies disarm the pathogens, thereby rendering them harmless and more susceptible to host immune clearance (Allen et al., 2014; Dickey et al., 2017; Johnson and Abramovitch, 2017). Compared to strategies that target viability, anti-virulence strategies may impose less selective pressure for the emergence of resistant strains (Rasko and Sperandio, 2010), and even further decrease the risk of commensal bacteria elimination (McFarland, 2008; Sekirov et al., 2010). Considerable works have been conducted to develop anti-virulence strategies, such as the inhibition of expression, secretion, or activity of virulence factors (Rasko and Sperandio, 2010; Johnson and Abramovitch, 2017).

Vibrio species generally inhabit diverse marine environments. As an emerging cause of bacterial infection, some pathogenic *Vibrio* species infect humans and lead to a

variety of clinical symptoms (Baker-Austin and Oliver, 2018; Newton et al., 2012). For example, *Vibrio vulnificus* can cause life-threatening septicemia and necrotizing fasciitis with high mortality rates in susceptible individuals (Baker-Austin and Oliver, 2018). *Vibrio parahaemolyticus* is a leading cause of seafood-borne gastroenteritis worldwide, resulting in diarrhea, nausea, fever, and chills (Getz and Thomas, 2018). *Vibrio cholerae*, a causative agent of watery diarrhea, is responsible for large outbreaks of cholera in various countries (Perez-Reytor et al., 2017), and *Vibrio alginolyticus* causes otitis and superficial wound infection in humans (Zhao et al., 2011). Although many antibiotics such as quinolones and tetracyclines have been applied for the treatment of *Vibrio* infection (Baker-Austin and Oliver, 2018; Wong et al., 2015), the recent reports of antibiotic resistant *Vibrios* threaten the efficacies of these antibiotics as treatment options (Scarano et al., 2014; Elmahdi et al., 2016). In an effort to develop anti-virulence strategies against pathogenic *Vibrio* species, small molecules targeting virulence of *Vibrio* species have been identified (Brackman et al., 2008; Imdad et al., 2018a; Imdad et al., 2018b; Kim et al., 2010a; Lee et al., 2016a; Packiavathy et al., 2013). However, very little is known about the molecular mechanisms of the compounds.

HlyU is a conserved transcriptional regulator required for the activation of various virulence genes in *Vibrio* species (Getz and Thomas, 2018; Li et al., 2011; Liu et al., 2007; Williams et al., 1993). For example, *V. vulnificus* HlyU induces the expression of *vvhA*, *rtxA*, and *plpA* encoding hemolysin, multifunctional-autoprocessing

repeats-in-toxin (MARTX) toxin, and phospholipase A_2, respectively, by directly binding to the promoter region (Choi et al., 2020; Jang et al., 2017; Liu et al., 2007). Similarly, *V. parahaemolyticus* HlyU directly induces the expression of *exsA*, which is essential for the type III secretion system 1 (T3SS1) (Getz and Thomas, 2018). The hemolysin VvhA lyses erythrocytes, damages endothelial cells, and induces inflammatory cell infiltration (Gray and Kreger, 1985; 1987). The MARTX toxin causes host cell rounding by dysregulating actin cytoskeleton and antagonizes phagocytic activity of host immune cells (Kim et al., 2015; Lo et al., 2011; Dolores et al., 2015; Zhou et al., 2017). The secretory phospholipase A_2 PlpA contributes to the lysis and necrotic death of host cells (Jang et al., 2017). T3SS1 directly delivers multiple cytopathic and cytotoxic effector proteins into the host cells (Broberg et al., 2011). Host tissue destruction and inflammation caused by these virulence factors promote the survival, dissemination, and pathogenesis of *V. vulnificus* and *V. parahaemolyticus* in mice (Jang et al., 2017; Jeong and Satchell, 2012; Pineyro et al., 2010). Accordingly, a deletion mutation of *hlyU* significantly attenuated virulence of the bacteria against human epithelial HeLa cells or mice (Getz and Thomas, 2018; Kim et al., 2003). Therefore, inhibition of the HlyU activity could be a plausible anti-virulence strategy against these *Vibrio* species.

In the present study, a high-throughput screening of 8,385 compounds was performed and identified a small-molecule inhibitor of HlyU, CM14, which significantly inhibited the HlyU activity in *V. vulnificus*. CM14 reduced the

expression of HlyU-regulated virulence genes, attenuating the virulence-related phenotypes of *V. vulnificus in vitro*, *ex vivo*, and in a mouse model. Biochemical analysis indicated that CM14 prevents HlyU binding to its target promoter DNA. Further mass spectrometric and mutational analyses revealed that a part of CM14 covalently modifies Cys30, a well-conserved residue of HlyU proteins in *Vibrio* species, both *in vitro* and *in vivo*. Remarkably, CM14 decreased the expression of virulence genes and showed anti-virulence effects against other pathogenic *Vibrio* species, without affecting the bacterial growth.

III-2. Materials and Methods

III-2-1. Strains, plasmids, and culture conditions

The strains and plasmids used in this study are listed in Table II-1. *Escherichia coli* and *V. vulnificus* strains were grown in Luria-Bertani (LB) medium and LB supplemented with 2% (w/v) NaCl (LBS) at 37°C and 30°C, respectively. *V. parahaemolyticus*, *V. alginolyticus*, and *V. cholerae* were grown in LBS, tryptic soy broth supplemented with 1% (w/v) NaCl, and LB, respectively, at 37°C. For T3SS1 inducing condition, *V. parahaemolyticus* was grown in DMEM supplemented with 1% fetal bovine serum (FBS) (Zhou et al., 2008). Bacterial growth was monitored spectrophotometrically at 600 nm (A_{600}). HeLa cells originated from the American Type Culture Collection were maintained at 37°C with 5% CO_2 in Dulbecco's modified Eagle's medium (DMEM) containing 10% FBS, 50 μg/ml penicillin and 50 μg/ml streptomycin. For infection experiments, the cells were washed with pre-warmed PBS and kept in fresh DMEM.

III-2-2. Transcriptome analyses

Total RNAs from the wild type and the *hlyU* mutant *V. vulnificus* MO6-24/O strains grown to A_{600} of 0.5 were isolated using RNAprotect® Bacteria Reagent and miRNeasy® Mini Kit (Qiagen, Valencia, CA) according to the manufacturer's procedure. The RNAs were further purified by removing genomic DNA using TURBO™ DNase (Ambion, Austin, TX) and then cleaned up using RNeasy® MinElute™ Cleanup Kit (Qiagen). The quality of total RNAs was verified using Agilent 2100 Bioanalyzer and Agilent RNA 6000 Nano reagents (Agilent Technologies, Santa Clara, CA) by Chunlab (Seoul, Republic of Korea). The procedures for a strand-specific cDNA library construction and RNA-sequencing were conducted by Chunlab (Seoul). Briefly, mRNA was selectively enriched by depleting ribosomal RNAs using Ribo-Zero™ rRNA Removal Kit (Epicentre, Madison, WI). Enriched mRNA was subjected to the cDNA library construction using TruSeq® Stranded mRNA Sample Preparation Kit (Illumina, San Diego, CA) following manufacturer's instruction. The quality of cDNA libraries was evaluated as described above for the quality verification of total RNA, except that Agilent DNA 1000 Reagents (Agilent Technologies) was used instead. To ensure biological replication, RNAs were isolated from two independent cultures of the *V. vulnificus* strains and two libraries were constructed per sample. Strand-specific paired-ended 100-nucleotide sequences from each cDNA library were obtained using HiSeq 2500 (Illumina). The raw sequencing reads were analyzed using CLC Genomics

Workbench 5.5.1 (CLC Bio, Aarhus, Denmark) and mapped to the *V. vulnificus* MO6-24/O reference genome (GenBank™ accession numbers: CP002469 and CP002470, www.ncbi.nlm.nih.gov). The expression level of each gene was defined using a RPKM (reads per kilobase of transcript per million mapped sequence reads) value, as described previously (Mortazavi et al., 2008). Quantile-normalized RPKM values were then statistically analyzed by *t*-tests to identify the differentially expressed genes (greater than 2-fold change with a p-value ≤ 0.05) from the *hlyU* mutant relative to the wild type.

Similarly, total RNAs from the wild type and the *hlyU* mutant *V. vulnificus* MO6-24/O strains grown to A_{600} of 0.5 in the presence of 20 μM of CM14 or 2% DMSO were isolated and subjected to the transcriptome analysis as described above. Heat maps were generated by the Gitools 2.3.1 (Perez-Llamas and Lopez-Bigas, 2011) using the RPKM-fold change for each gene in the test samples. CLC Genomics workbench 11.0.1 software (CLC Bio) was used for a principal-component analysis of the whole-gene expression profiles of the samples.

III-2-3. Construction of an *E. coli* reporter strain and HTS

The *hlyU* ORF, amplified by PCR using a pair of primers HLYUS-F and HLYUS-R (Table II-2), was subcloned into pBAD24 (Guzman et al., 1995) carrying an arabinose-inducible promoter to yield pKK1306 (Table II-1). The promoter region of VVMO6_00539, P_{VVMO6_00539}, was amplified by PCR using a pair of primers 00539S-F and 00539S-R (Table II-2) and then fused to the promoterless *lux* operon of pBBR_lux (Lenz et al., 2004) to create pZW1608, a HlyU-repressed reporter plasmid (Table II-1). A reporter strain was constructed by transforming *E. coli* DH5α with pKK1306 and pZW1608. The *E. coli* reporter strain was grown to A_{600} of 0.5 in LB containing 0.0002% (wt/vol) L-(+) arabinose, 20 μg/ml chloramphenicol and 100 μg/ml ampicillin. An aliquot (98 μl) of the culture was transferred to each well of a 96-well microtiter plate (Nunc™, Roskilde, Denmark) containing 2 μl of the small molecules to achieve 20 μM of each molecule or 2% DMSO (control) and incubated at 37°C with shaking. Luminescence and growth (A_{600}) of the reporter strain in each well were measured after 3 h incubation using a microplate reader (Infinite™ M200 microplate reader, Tecan, Männedorf, Switzerland), and relative luminescence units (RLUs) were calculated by dividing luminescence with A_{600}. The small-molecule library (each dissolved in 100% DMSO at 1 mM) was kindly provided by the Korea Chemical Bank (http://www.chembank.org). The library information and screening results are summarized in Table III-1. Hit molecules inhibiting more than 10% of the HlyU activity were selected for further verification.

Table III-1. Small molecule screening information

Category	Parameter	Description
Assay	Type of assay	Whole organism (*E. coli* cells)
	Target	HlyU protein
	Primary measurement	Detection of bioluminescence and absorbance at 600 nm (A_{600})
	Key reagents	L-(+)-arabinose for the induction of *hlyU* gene
	Assay protocol	Refer to the Materials and Methods
	Additional comments	*E. coli* cells contain the reporter plasmid with *lux* operon that is fused to a HlyU-repressed promoter
Library	Library size	Total of 8,385 molecules (8,364 used for initial screening, plus additional 21 structural homologues) Arrayed in 96-well plates as single compounds at 20 μM in DMSO (total 80 compounds per plate, leaving first and second columns empty for control samples)
	Library composition	Structure-representative library (contains diverse molecules from different PharmaCore structures (~1,000); considered for drug-likeness and solubility; all compounds confirmed as >85% pure by LC-MS analysis)
	Source	Korea Chemical Bank
	Additional comments	For more information about the library, refer to http://www.chembank.org/
Screen	Format	96-well optical bottom plate w/Lid Black (Thermo Fisher Scientific)
	Concentration(s) tested	20 μM compound, 2% DMSO
	Plate controls	Negative control: DMSO-treated *E. coli* cells plus L-(+)-arabinose; Positive control: DMSO-treated *E. coli* cells without L-(+)-arabinose
	Reagent/compound dispensing system	Manual
	Detection instrument and software	Infinite™ M200 microplate reader (Tecan, Männedorf, Switzerland); Tecan i-Control ver 1.4.9.0
	Assay validation/QC	For screening validation, every plate contained positive control samples that do not express HlyU protein Z-factor: 0.79; Z'-factor: 0.83; SD of positive control: 320.48; SD of negative control: 33.15
	Correction factors	Luminescence was normalized against *E. coli* cell growth (A_{600}) to obtain relative luminescence unit (RLU)
	Normalization	% HlyU-inhibition = 100×(y-z)/(y-x), where x is the average RLU of the positive control samples, y is the average RLU of the negative control samples, and z is the RLU of each molecule-treated sample
	Additional comments	Values were measured after 3 h of incubation at 37°C
Post-HTS analysis	Hit criteria	% HlyU-inhibition >10 (%)
	Hit rate	0.036% (3 of 8,385 molecules)
	Additional assay(s)	Verification of initial hits in the original (Fig. III-2B) and secondary assays (Fig. III-2C and D)
	Confirmation of hit purity and structure	A hit molecule was repurchased from Vitas-M Laboratory, and the structure of CM14 was confirmed by ^{1}H NMR, ^{13}C NMR, and mass spectrometric analyses
	Additional comments	

III-2-4. Verification, structural confirmation, and determination of half maximal effective concentration (EC_{50}) of CM14

The promoter region of *rtxA*, P_{rtxA}, was amplified by PCR using a pair of primers PrtxA-F and PrtxA-R (Table II-2) and then fused to the promoterless *lux* operon of pBBR_lux (Lenz et al., 2004) to create pZW1609, a HlyU-activated reporter plasmid (Table II-1). The reporter strain was constructed by conjugally transferring pZW1609 into the wild-type *V. vulnificus* MO6-24/O. The *V. vulnificus* reporter strains were constructed by conjugally transferring either pZW1608 or pZW1609 into the wild-type *V. vulnificus* MO6-24/O and the *hlyU* mutant ZW141, respectively. The reporter strains were grown to A_{600} of 0.2 in LBS containing 3 μg/ml chloramphenicol and transferred to each well of a 96-well microtiter plate to achieve 20 μM of each hit molecule or 2% DMSO (control) as describe above. RLUs of the reporter strains were determined as described above but after 1.5 h incubation, and then used to verify the HlyU-inhibiting activity of the hit molecules.

A molecule exhibiting the strongest HlyU-inhibiting activity was purchased from Vitas-M Laboratory (Moscow, Russian Federation) and named as CM14. The structure of CM14 was confirmed by ^{1}H NMR and ^{13}C NMR, using a Bruker AMX 500 spectrometer (Bruker, Karlsruhe, Germany), and by mass spectrometric analysis using Agilent 6530 Accurate-Mass Quadrupole Time-of-Flight (Q-TOF) mass spectrometer (Agilent Technologies) with a Jet Stream electrospray ionization source (ESI). The characteristics of CM14 were as follows: ^{1}H NMR (500 MHz, $CDCl_3$) δ

10.98 (s, 1 H), 7.78 (d with str, 1 H, J = 7.7 Hz), 7.65 (d with str, 2H, J = 7.2 Hz), 7.49-7.46 (m, 1H), 7.42-7.37 (m, 3 H), 7.31 (d with str, 1 H, 7.7 Hz), 7.27-7.25 (m, 1H), 7.19 (s, 1 H); ^{13}C NMR (125 MHz, $CDCl_3$) δ 159.93, 150.51, 149.67, 148.91, 133.01, 130.95, 130.89, 129.56, 128.67, 124.92, 123.45, 119.22, 117.63, 116.96, 107.72, 106.98, 89.96, 81.72; HRMS (ESI) Calcd for $C_{20}H_{11}NO_3S$ $(M+H)^+$ 346.0538, found 346.0545.

To determine EC_{50} (the concentration of CM14 inhibiting the HlyU activity by 50%), the wild-type *V. vulnificus* reporter strain containing pZW1609 was grown to A_{600} of 0.2 in LBS containing 3 μg/ml chloramphenicol. An aliquot (98 μl) of the culture was transferred to each well of a 96-well microtiter plate (Nunc) containing 2 μl of various concentrations (10^{-10} to 10^{-3} M) of CM14 and incubated at 30°C with shaking. RLUs of the reporter strain in each well were measured after 1.5 h incubation using a microplate reader. The HlyU activities were expressed using the RLU observed in the absence of CM14 (in the presence of 2% DMSO) as 100%. The EC_{50} was calculated by plotting the relative HlyU activities versus the CM14 concentrations using GraphPad Prism 7.0 (GraphPad Software, San Diego, CA).

III-2-5. Western blot and transcript analyses

To evaluate the activity of CM14 *in vitro*, CM14 or 2% DMSO (control) was added to the *V. vulnificus* strains at A_{600} of 0.2. The strains were further grown to A_{600} of 0.5 and then used to analyze either the HlyU protein or the transcript levels of virulence genes. Cellular proteins of the *V. vulnificus* strains grown along with various concentrations of CM14 were isolated using cOmplete™ Lysis-B EDTA-free buffer (Roche, Mannheim, Germany) and the total proteins in the clear cell lysates were quantitated using a Bradford method. HlyU and DnaK in the cell lysates equivalent to 100 μg and 10 μg of total proteins, respectively, were detected using rabbit anti-*V. vulnificus* HlyU antibody and mouse anti-*E. coli* DnaK antibody (Enzo lifescience, Farmingdale, NY) by Western blot analysis as described elsewhere (Jang et al., 2017; Lim and Choi, 2014).

Total RNAs from the *V. vulnificus* strains grown along with 20 μM of CM14 were isolated using RNeasy® Mini Kit (Qiagen) and quantified using a Nano-Vue Plus spectrophotometer (GE Healthcare, Menlo Park, CA). To evaluate expression of specific genes, cDNA was synthesized from 1 μg of the total RNA by using iScript™ cDNA Synthesis Kit (Bio-Rad, Hercules, CA) and amplified by using the Chromo 4 real-time PCR detection system (Bio-Rad) with a pair of specific primers (Table II-2). Relative expression levels of each gene were calculated by using the 16S rRNA expression level as the internal reference for normalization (Bang et al., 2016; Anthouard and DiRita, 2013; Burke et al., 2015; Rui et al., 2009).

III-2-6. Virulence assays

For hemolytic activity *in vitro*, the *V. vulnificus* strains grown to A_{600} of 1.0 along with CM14 or 2% DMSO (control) were harvested and fractionated into cells and supernatants by centrifugation. The culture supernatants were purified through Puradisc^{TM} 25 mm syringe filter (pore size 0.2 μm, GE healthcare, Menlo Park, CA) and concentrated using Amicon Ultra-15 (cut off 10 kDa, Millipore, Temecula, CA). An aliquot of the supernatants was mixed with an equal volume of human erythrocytes (10% in PBS; Innovative Research, Novi, MI) and incubated at 37°C for 3 h. The hemolytic activity was measured by spectrophotometry as described previously (Lim and Choi, 2014).

Two different assays were performed to determine cytopathicity and cytotoxicity of the *V. vulnificus* strains *ex vivo*. To examine the cytopathic changes, HeLa cells grown in a μ-slide 4-well plates (Ibidi, Germany) were infected with the *V. vulnificus* strains at a multiplicity of infection (MOI) of 2 along with 50 μM of CM14 or 1% DMSO (control). After 1 h incubation at 37°C, the cells were washed and fixed, and nuclei and actin of the cells were stained with Hoechst® 33342 (final 5 μg/ml; Thermo Fisher Scientific, Waltham, MA) and with rhodamine-phalloidin (one unit per microscope slide; Thermo Fisher Scientific), respectively. Cell morphological changes were photographed using a laser scanning confocal microscope (C2plus, Nikon, Japan), and analyzed using NIS-Elements software (Nikon). To examine cytotoxicity, the monolayers of INT-407 cells (HeLa cell-derived epithelial cells)

grown in a 96-well tissue culture plate (Nunc, Roskilde, Denmark) were infected with *V. vulnificus* strains at an MOI of 10 along with various concentrations of CM14 or 1% DMSO (control). After 2.5 h incubation at 37°C, the LDH activities in the supernatant were measured as described previously (Jang et al., 2017).

III-2-7. Mouse infection assays

All manipulations for mouse infection assay were performed following the National Institutes of Health Guidelines for Humane Treatment and approved by the Animal Care and Use Committee of Seoul National University (SNU-170417-26-2). Mouse mortality, blood biochemical parameters, pro-inflammatory cytokine production, and macrophage infiltration were evaluated to determine the virulence of *V. vulnificus in vivo*. For the mouse mortality test, the *V. vulnificus* strains grown to A_{600} of 0.5 were harvested and suspended in PBS to 7.5×10^6 colony forming unit (CFU)/ml. Groups of Institute of Cancer Research (ICR) female mice (7-week-old, specific-pathogen-free, Orient Bio, Seongnam, Republic of Korea) were injected with 100 μl of the bacterial suspension along with CM14 (to achieve 1.4 mg/kg body weight) or 10% DMSO subcutaneously under the dorsal skin. Survival of the mice was monitored for 36 h, as described previously (Jang et al., 2017).

To examine the levels of blood biochemical parameters, pro-inflammatory cytokine production, and macrophage infiltration to the injection sites, the mice injected as described above were sacrificed at 7 h post infection to obtain blood and skin tissue samples, respectively. For blood biochemical analysis, the blood samples were collected using cardiac puncture in heparin-coated tube (IDEXX Laboratories, Westbrook, ME) and analyzed as described previously (Jang et al., 2017). Breifly, the levels of TP, ALB, AST, ALT, BUN, and CREA in the blood plasma were measured by using a biochemistry autoanalyzer (Hitachi 7180 autoanalyzer, High-

Technologies Corp., Tokyo, Japan). The remaining blood samples were fractionated by centrifugation for 10 min at 1,000 × *g* to obtain the blood plasma. Cytokine levels of IL-1β and IL-6 in the blood plasma were determined by enzyme-linked immunosorbent assay (ELISA) using commercially available ELISA kits for IL-1β (R&D systems, Minneapolis, MN) and IL-6 (AbFrontier, Seoul, Republic of Korea). For immunohistochemical analysis, the mouse skin tissue samples around injection sites were embedded in optimum cutting temperature (O.C.T.) compound (Sakura Finetek, Torrance, CA) and stored at -80°C. Frozen tissue samples were cryo-sectioned to a 20-μm thickness and then mounted on silane-coated slides (Muto Pure Chemicals, Tokyo, Japan). Tissue samples on slides were fixed with 80% acetone for 10 min, washed twice with PBS, and blocked in 5% normal goat serum (Sigma-Aldrich, St. Louis, MO) for 20 min. Slides were incubated with F4/80 antibody (1:100 dilution, Santa Cruz, Paso Robles, CA) for 2 h at room temperature. After washing three times with PBS, the slides were incubated with Alexa Fluor 488®-conjugated goat anti-rabbit secondary antibody (1:200 dilution, Thermo Fisher Scientific) for 1 h. Subsequently, all slides were incubated with 4',6-diamidino-2-phenylindole (DAPI, Thermo Fisher Scientific) solution (5 μg/ml) in PBS for 5 min at room temperature. All immunofluorescence images were obtained by Eclipse Ts2® fluorescence microscopy (Nikon, Tokyo, Japan), and colocalization of F4/80 with DAPI was analyzed by MetaMorph software (Universal Imaging, West Chester, PA).

III-2-8. Protein purification, site-directed mutagenesis, and EMSA

The ORF of *hlyU* amplified by PCR using a pair of primers HLYUP-F and HLYUP-R (Table II-2) was digested with BamHI and XhoI and subcloned into pProEX-HTa (Invitrogen, Carlsbad, CA) to result in pZW1610 (Table II-1). Plasmids pZW1611 and pZW1612 encoding mutant HlyU proteins in which Cys30 or Cys96 was replaced with serine, respectively, were created from pZW1610 using QuikChange Site-Directed Mutagenesis Kit (Agilent Technologies). The complementary mutagenic primers were used as listed in Table II-2, and the mutations were confirmed by DNA sequencing. The His_6-tagged HlyU proteins were then expressed in BL21 (DE3) and purified by affinity chromatography (Qiagen). The His_6 tag was removed by treatment of recombinant tobacco etch virus (TEV) protease at room temperature, and the HlyU proteins were further purified by size exclusion chromatography using HiLoad Superdex 200 26/600 gel filtration column (GE Healthcare) equilibrated with buffer containing 300 mM NaCl, 20 mM Tris-HCl (pH 7.5), and 2 mM β-mercaptoethanol.

To express mutant HlyU proteins in which Cys30 or Cys96 was respectively replaced with serine, pZW1511 and pZW1512 were created in conjunction with the plasmid pZW1510 (Jang et al., 2017) as described above (Table II-1). *E. coli* S17-1 λ *pir* (Simon et al., 1983) harboring pZW1510, pZW1511, or pZW1512 was used as a conjugal donor to the *hlyU* mutant as described previously (Bang et al., 2016).

For EMSA, the 264-bp DNA fragment of P_{rtxA} was amplified by PCR using unlabeled PrtxA-EMSA-F and [γ-^{32}P]ATP-labeled PrtxA-EMSA-R as primers (Table II-2). The labeled P_{rtxA} DNA (5 nM) were incubated with the purified HlyU for 0.5 h at 25°C in a 20-μl reaction mixture containing 1× binding buffer (10 mM Tris-Cl, 50 mM KCl, 5 mM $MgCl_2$, and 5% glycerol) and 0.1 μg of poly(dI-dC) (Sigma-Aldrich, St. Louis, MO). Electrophoretic analysis of the DNA-protein complexes was performed on a 6% nondenaturing polyacrylamide gel as described previously (Jang et al., 2017). When necessary, either various concentrations of CM14 or DMSO was added to the reaction mixture before incubation. As a control, a chemical (20 μM) randomly chosen from libraries that had no HlyU-inhibiting activity was added to the reaction mixture instead of CM14.

III-2-9. Mass spectrometric analysis of the HlyU modification

For the *in vitro* reaction of HlyU and CM14, the purified HlyU protein was incubated with 10-fold excess amounts of CM14 for 0.5 h at 4°C. For the *in vivo* reaction, the HlyU protein was expressed in *E. coli* BL21 (DE3) cells in the presence of CM14 at 50 μM, and then purified as described above. The gel slices corresponding to HlyU protein treated with CM14 were destained in 50% acetonitrile (ACN) solution of 25 mM NH_4HCO_3 buffer for 10 min and then followed by in-gel reduction and alkylation of cysteine residues with dithiothreitol (DTT) and iodoacetamide (IAM). After washing out the excess reagents with 25 mM NH_4HCO_3 three times, the resulting samples were digested by sequencing-grade trypsin at ratio of 1:50 (wt/wt) for overnight at 37°C. The digested peptides were subjected to C18-SPE clean up using 10 μl of ZipTip (Millipore, Temecula, CA) and then reconstituted with 25 mM NH_4HCO_3 for LC-MS/MS analysis. LC-MS/MS experiment with higher energy collisional dissociation (HCD) fragmentation mode was performed on Orbitrap Fusion Lumos mass spectrometry (Thermo Fisher Scientific, Waltham, MA) coupled with nanoACQUITY UPLC (Waters, Milford, MA) carrying an in-house packed capillary trap column (150 μm inside diameter, 3 cm long) and analytical column (75 μm inside diameter, 100 cm long) of 3 μm Jupiter C18 particles (Phenomenex Terrance, CA). The acquired datasets were initially searched by MODification via alignment (MODa) (Na et al., 2012), which is a blind search tool to find the unknown cysteine modification. Next, the datasets were subjected to MS-GF+ analysis at 10

ppm of precursor ion mass tolerance against *V. vulnificus* proteome database (GCF_000009745.1_ASM974v1) to confirm the cysteine modification.

III-2-10. Crystallization, structure determination, and refinement

For crystallization, HlyU was expressed as described previously (Nishi et al., 2010), with the exception of using *E. coli* C43 (DE3) instead. The HlyU protein (1.2 mM) was incubated with CM14 (10 mM) for 0.5 h at 4°C (molar ratio, 1:8.3), and then the mixture was centrifuged at 18,000 × *g* for 7 min to remove materials made during incubation. The clear fraction was crystallized in a precipitation solution containing 0.1 M HEPES (pH 8.0), 20% (wt/vol) polyethylene glycol (PEG) 4K and 10% (vol/vol) 2-propanol by hanging-drop vapor diffusion method at 14°C. The HlyU-CM14 crystals were flash-frozen using 20% (wt/vol) sorbitol as a cryoprotectant in a nitrogen stream at -173°C. An X-ray diffraction dataset was collected at Pohang Accelerator Laboratory beamline 5C and processed with the HKL2000 package (Otwinowski and Minor, 1997). The structure was determined using the MOLREP program in the CCP4 package by the molecular replacement method and a search model taken from the HlyU from *V. vulnificus* CMCP6 (PDB code: 3JTH) (Nishi et al., 2010). The final structure of the HlyU-CM14 was refined at a 2.1 Å resolution with an R factor of 23.8% and an R_{free} of 26.8% using the Coot and PHENIX refinement program (Adams et al., 2010). Further details on the structure determination and refinement are given in Table III-2.

Table III-2. Statistics for X-ray data collection and refinement

	HlyU-CM14
Data collection	
Beamline	PAL 5C
Wavelength (Å)	0.97960
Space group	$P4_12_12$
Cell dimensions	
a, b, c (Å)	35.1, 35.1, 180.4
α, β, γ (˚)	90, 90, 90
Resolution (Å)	50-2.1 (2.14-2.10)[a]
R_{merge}[b]	0.208 (0.114)
$I/\sigma I$	24.12 (5.64)
Completeness (%)	97.2 (92.2)
Redundancy	19.7 (9.5)
Refinement	
Resolution (Å)	32.74-2.1
No. of reflections	6758
R_{work}/R_{free}[c]	0.238/0.268
No. of total atoms	789
Wilson B-factor (Å)	22.60
RMSD	
Bond lengths (Å)	0.004
Bond angles (˚)	0.81
Ramachandran plot	
Favored (%)	94.6
Allowed (%)	5.4
Outliers (%)	0

[a] Values in parentheses are for the highest-resolution shell.

[b] $R_{merge} = \Sigma_{hkl}\Sigma_i|I_i(hkl) - [I(hkl)]|/\Sigma_{hkl}\Sigma_i I_i(hkl)$, where $I_i(hkl)$ is the intensity of the *i*th observation of reflection *hkl* and [I(*hkl*)] is the average intensity of the *i* observations.

[c] R_{free} calculated for a random set of 10% of reflections not used in the refinement.

III-2-11. Data analyses

Averages and standard deviations (SD) were calculated from at least three independent experiments. Statistical analyses were performed as indicated in figure legends using GraphPad Prism 7.0 (GraphPad Software). For mouse lethality, mouse infection experiments were repeated twice to ensure reproducibility.

III-2-12. Data availability

The RNA-sequencing data for the transcriptome analyses were deposited in NCBI Sequence Read Archive (SRA) database under accession numbers SRP128085 and PRJNA505764, respectively. The atomic coordinates and structure factors have been deposited in the Protein Data Bank (http://www.pdb.org) under PDB ID code 5ZNX.

III-3. Results

III-3-1. Identification of CM14 as an inhibitor of HlyU activity

To identify a specific inhibitor of HlyU, an *E. coli* reporter strain containing pKK1306 (carrying an arabinose-inducible *hlyU* of *V. vulnificus*) and pZW1608 (carrying a promoterless *lux* operon fused to a promoter P_{VVMO6_00539}) was constructed (Kim et al., 2018a). Because the VVMO6_00539 gene is directly repressed by HlyU (Fig. III-1A and B), the resulting *E. coli* strain remains non-luminescent in an arabinose-containing media unless a potential hit molecule inhibits either the expression or activity of HlyU (Fig. III-2A). Using this HlyU-repressed *lux* reporter system instead of the HlyU-activated system could prevent the false identification of luciferase-inhibiting and/or luminescence-absorbing molecules as hits. Due to the lack of a previously discovered ligand or a putative ligand-binding site in HlyU, a random chemical library containing 8,385 small molecules was screened using the *E. coli* reporter strain. From the screening, three hit molecules (1025E12, 1030B04, and 1040E12) were identified as putative HlyU inhibitors (Fig. III-2B). These hit molecules were reexamined using the *V. vulnificus* reporter strains containing the same reporter plasmid pZW1608 (Fig. III-2C) or pZW1609 (Fig. III-2D), respectively. In contrast to pZW1608, pZW1609 carries the promoterless *lux* operon fused to a promoter of the *rtxA* gene, P_{rtxA}, which is directly induced by HlyU (Liu et al., 2007). With each of the hit molecules, the wild-type *V. vulnificus* containing

pZW1608 was more luminescent than the negative control (DMSO) (Fig. III-2C), while *V. vulnificus* containing pZW1609 was less luminescent than the negative control (Fig. III-2D). The use of these two distinct *V. vulnificus* reporter strains verified that the hit inhibitor molecules function directly on HlyU, not other components such as a luciferase enzyme.

Among the hit molecules, 1025E12, *N*-(4-oxo-4H-thieno[3,4-c]chromen-3-yl)-3-phenylprop-2-ynamide ($C_{20}H_{11}NO_3S$, MW of 345.37) was most effective in the inhibition of HlyU, and thus selected as a HlyU inhibitor and renamed 'CM14' (Fig. III-3A). The structure of CM14 was confirmed by ^{1}H NMR, ^{13}C NMR, and mass spectrometric analyses (see Materials and Methods). The HlyU activities were assessed using the wild-type *V. vulnificus* containing pZW1609 in the presence of various concentrations of CM14, and the half maximal effective concentration (EC_{50}) of the molecule was determined as 30.97 μM (Fig. III-3B). It is noteworthy that CM14 in the range of 20 to 200 μM did not affect the HlyU levels in *V. vulnificus* cells (Fig. III-3C), suggesting that CM14 inhibits the activity rather than the cellular levels of HlyU. In addition, CM14 did not affect the growth of *V. vulnificus* (up to 2 mM) and was not toxic to the human epithelial INT-407 cells (up to 500 μM) (Fig. III-3D and E). Therefore, these results suggested that CM14 is a small-molecule inhibitor of the HlyU activity having a potential to be developed as an anti-virulence agent against *V. vulnificus*.

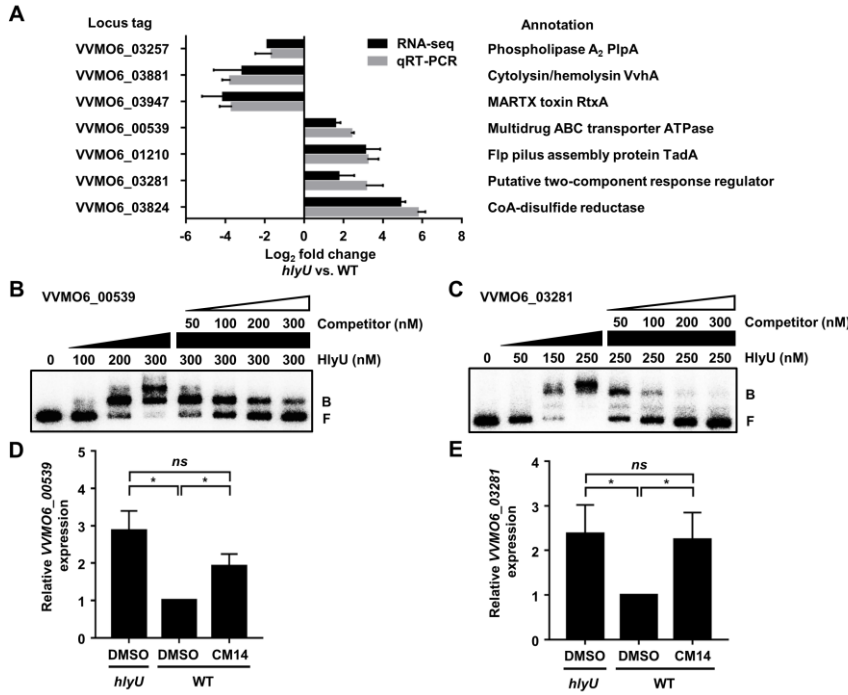

Figure III-1. Genes regulated by HlyU. Genes expressed differentially in the isogenic *hlyU* mutant (fold change ≥ 2; $p \leq 0.05$) were identified by transcriptome analyses and considered as a HlyU regulon. (A) Among them, 7 genes whose expressions were confirmed by qRT-PCR are presented. Each column represents the mRNA expression level in the *hlyU* mutant relative to that in the wild type. Means and SD were calculated from at least three independent experiments. Locus tags are based on the database of the *V. vulnificus* MO6-24/O genome (GenBank™ accession numbers: CP002469 and CP002470), and the products of the 7 genes are presented on the right. (B and C) EMSA for the HlyU binding to the upstream regions of VVMO6_00539 (B) and VVMO6_03281 (C). Each radioactively-labeled probe DNA (5 nM) was incubated with increasing amounts of HlyU as indicated. For competition analysis, the same but unlabeled each DNA fragment was used as a self-

competitor and added to the reaction mixture containing the 5 nM labeled DNA before the addition of 300 nM (B) and 250 nM (C) HlyU as indicated. The DNA-HlyU complexes were separated by electrophoresis. B, bound DNA; F, free DNA. (D and E) Effects of CM14 on the expression of the HlyU-repressed genes. The *V. vulnificus* strains were grown in the presence of CM14 (20 μM) or 2% DMSO (control) to A_{600} of 0.5. The transcript levels of VVMO6_00539 (D) and VVMO6_03281 (E) in the total RNA of the cells were quantified by qRT-PCR and expressed using each transcript level of the wild type in the presence of DMSO as 1. Error bars represent the SD. Statistical significance was determined by the Student's *t*-test (*, $p < 0.05$; *ns*, not significant). WT, wild type; *hlyU*, *hlyU* mutant.

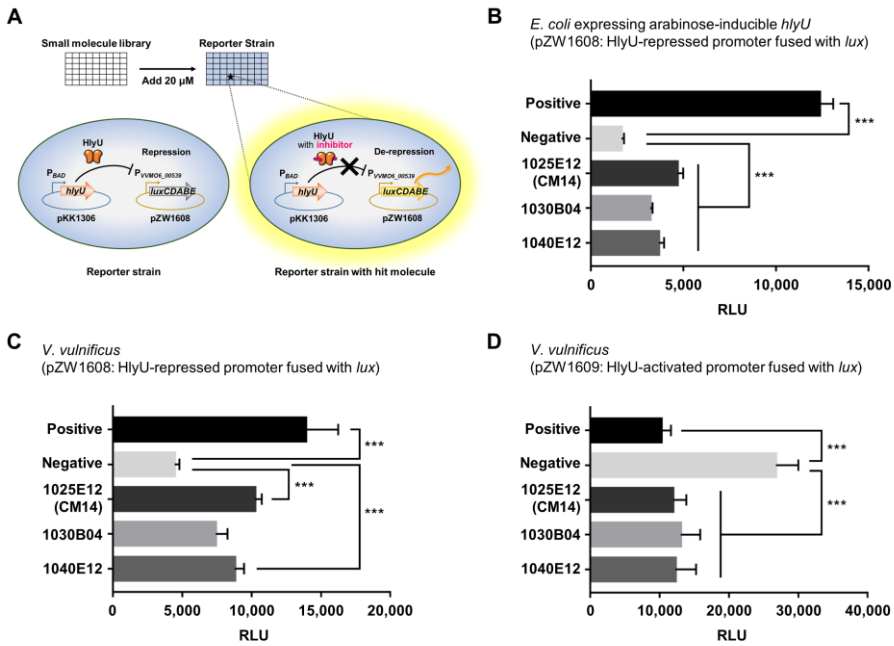

Figure III-2. High-throughput screening for HlyU inhibitors. (A) Schematic demonstration of high-throughput screening of small molecules. An *E. coli* reporter strain contains pKK1306 expressing HlyU under arabinose inducible promoter P_{BAD} and pZW1608 carrying the *luxCDABE* genes under HlyU-repressed promoter P_{VVMO6_00539}. (B to D) Each bar represents RLU of the *E. coli* reporter strain (B) and *V. vulnificus* reporter strains carrying pZW1608 (C) or pZW1609 (D) in the presence of hit molecules as indicated. Error bars represent the SD. Statistical significance was determined by multiple comparisons after one-way analysis of variance (ANOVA) (***, $p < 0.0005$). 1025E12, 1030B04, and 1040E12, hit molecules; Positive, RLUs from *E. coli* without arabinose (B) or *V. vulnificus hlyU* mutant (C and D); Negative, RLUs from *E. coli* with arabinose (B) or *V. vulnificus* wild type (C and D); RLU, relative luminescence unit.

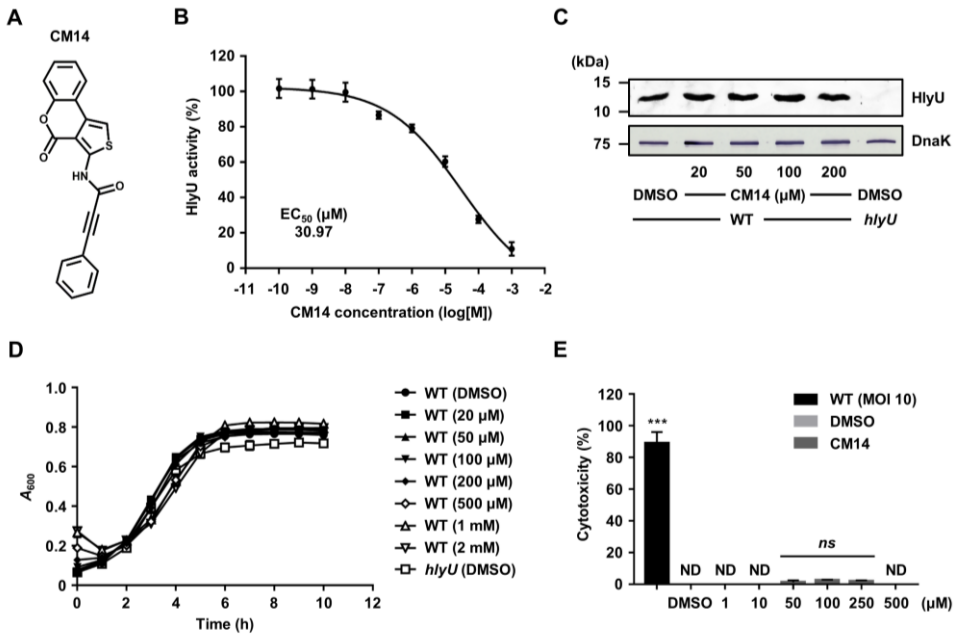

Figure III-3. CM14 inhibits the HlyU activity without affecting *V. vulnificus* growth. (A) The chemical structure of CM14, *N*-(4-oxo-4H-thieno[3,4-c]chromen-3-yl)-3-phenylprop-2-ynamide. (B) The EC_{50} of CM14 inhibiting the HlyU activity was calculated as described in the Materials and Methods. (C) Cellular HlyU and DnaK (as an internal control) levels of the wild-type and *hlyU* mutant cells grown along with various concentrations of CM14 or DMSO (control) were determined by Western blot analysis. Molecular size markers (Bio-Rad) are shown in kDa. (D) Growth of the *V. vulnificus* strains along with various concentrations of CM14 or 2% DMSO (control) was monitored at 1 h intervals using a microplate reader. (E) Cytotoxicity was determined using LDH activities released from INT-407 cells incubated at 37°C for 3 h with various concentration of CM14, the wild-type *V. vulnificus* (at an MOI of 10), or 2% DMSO (control). The cytotoxicity was expressed using the LDH activity from the cells completely lysed by 5% Triton X-100 as 100%.

Error bars represent the SD. Statistical significance was determined by one-way ANOVA (E) (***, $p < 0.0005$; *ns*, not significant; ND, not detected). WT, wild type; *hlyU*, *hlyU* mutant.

III-3-2. CM14 reduces the HlyU-dependent virulence gene expression *in vitro*

Next, to examine if CM14 affects the expression of *vvhA*, *rtxA*, and *plpA* in *V. vulnificus*, the transcript levels of *vvhA*, *rtxA*, and *plpA* of the wild-type *V. vulnificus* strain were investigated in the presence or absence of CM14. Consistent with the previous result that CM14 inhibits HlyU activity, the transcript levels of *vvhA*, *rtxA*, and *plpA* of the wild-type *V. vulnificus* strain were significantly reduced in the presence of the molecule at 20 μM (Fig. III-4A; WT+DMSO vs. WT+CM14). The reduced expression levels of the genes were close to those of the *hlyU* mutant strain ZW141 (Fig. III-4A; WT+CM14 vs. *hlyU*+DMSO). To further investigate whether the reduced expression of the virulence genes is reflected in the virulence-related phenotypes, the hemolytic activities were compared in the culture supernatants of the *V. vulnificus* strains grown in the presence or absence of CM14. When incubated with human erythrocytes, the culture supernatant of the wild-type *V. vulnificus* grown in the presence of DMSO control showed robust hemolytic activity (Fig. III-4B). In contrast, the culture supernatant of the wild-type *V. vulnificus* grown in the presence of CM14 exhibited significantly reduced (at 20 μM) or nearly no hemolytic activities (at 50 μM) similar to that of the *hlyU* mutant (Fig. III-4B). Collectively, these results indicated that the effect of CM14 on the decreased expression of virulence genes is also represented as a reduced virulence-related phenotype of *V. vulnificus in vitro*.

III-3-3. CM14 attenuates the virulence of *V. vulnificus ex vivo*

The effects of CM14 on the *V. vulnificus*-mediated cytopathic changes of the host cells were assessed *ex vivo*. Because CM14 significantly decreased the *rtxA* transcript level in *V. vulnificus* (Fig. III-4A), it was first examined whether the molecule prevents the actin cytoskeleton dysregulation primarily caused by the MARTX toxin (Dolores et al., 2015; Zhou et al., 2017). To this end, a rapid rounding phenotype of the HeLa cells infected with the *V. vulnificus* strains was monitored in the presence or absence of CM14. HeLa cells became round at 1 h post infection of the wild type (Satchell, 2015) (Fig. III-4C; WT+DMSO). However, the rounding of HeLa cells was significantly attenuated in the presence of CM14 at 50 μM (Fig. III-4C; WT+CM14), and thus the morphology of the cells was comparable to that of the cells with phosphate buffered saline (PBS, vehicle control) or the *hlyU* mutant (Fig. III-4C; PBS+DMSO or *hlyU*+DMSO). Furthermore, the effects of CM14 on the cytotoxicity of *V. vulnificus* were evaluated. For this purpose, lactate dehydrogenase (LDH) release from the INT-407 cells infected with the bacteria was determined. As shown in Fig. III-4D, CM14 reduced the LDH release from the cells infected with the wild-type *V. vulnificus* in a dose-dependent manner. Notably, CM14 at 100 μM almost abolished the LDH-releasing activity of *V. vulnificus* (Fig. III-4D). Taken together, these results revealed that CM14 successfully attenuates the cytopathicity and cytotoxicity of *V. vulnificus ex vivo*.

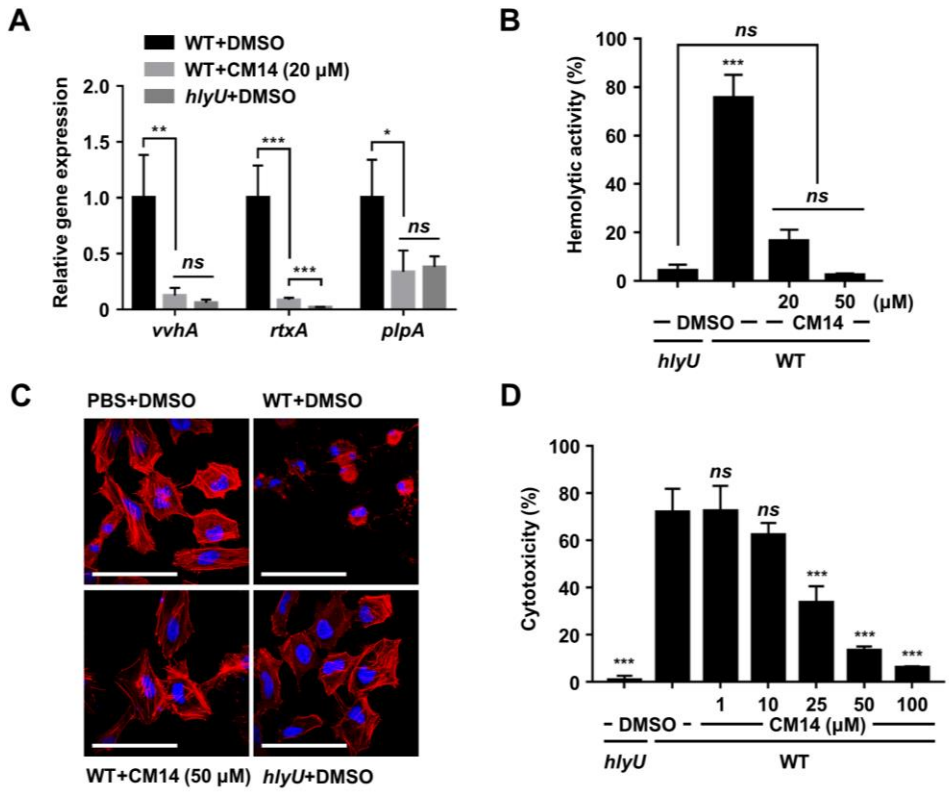

Figure III-4. Effects of CM14 on virulence-related phenotypes of *V. vulnificus*. (A and B) The *V. vulnificus* strains grown along with CM14 as indicated or DMSO (control) were harvested and fractionated for further analyses. (A) The transcript levels of *vvhA*, *rtxA*, and *plpA* in the total RNA of the cells were quantitated by qRT-PCR and expressed using each transcript level of the wild type in the presence of DMSO as 1. (B) Hemolytic activities of the culture supernatants were determined against human erythrocytes and expressed using complete hemolysis by 5% Triton X-100 as 100%. (C) Morphological changes of HeLa cells infected with the *V. vulnificus* strains along with CM14 (50 μM) or DMSO (control) were photographed. Scale bars, 100 μm. (D) Cytotoxicity was determined using LDH activities released

from INT-407 cells infected with the *V. vulnificus* strains along with CM14 as indicated and expressed using the LDH activity from the cells completely lysed by 5% Triton X-100 as 100%. Error bars represent the SD. Statistical significance was determined by the Student's *t*-test (A) and by one-way ANOVA (B and D) (***, $p < 0.0005$; **, $p < 0.005$; *, $p < 0.05$; *ns*, not significant). WT, wild type; *hlyU*, *hlyU* mutant.

III-3-4. CM14 impedes the pathogenesis of *V. vulnificus* in mice

To investigate the *in vivo* efficacy of CM14, mortality of mice infected with *V. vulnificus* was evaluated with or without co-administration of the molecule (Fig. III-5A). All of the mice infected subcutaneously with the wild-type strain were succumbed within 15 h post infection (Fig. III-5A; WT+DMSO). In contrast, 80% of the mice survived until the end of experiment (36 h post infection) when CM14 was co-administered at 1.125 mM concentration (1.4 mg/kg body weight) (Fig. III-5A; WT+CM14). These results revealed that co-administration of CM14 significantly prolonged the survival of mice infected with *V. vulnificus* ($p < 0.0001$, log rank test). Markedly, the survival rate of the mice infected with the wild type in the presence of CM14 was not statistically different from that of mice infected with the *hlyU* mutant (Fig. III-5A; *hlyU*+DMSO). The combined results indicated that CM14 effectively inhibits the pathogenesis of *V. vulnificus* during mouse infection.

To examine not only survival but also pathophysiological changes, especially in the degree of hepatic and renal dysfunction, the biochemical parameters in the blood of the mice infected with *V. vulnificus* were analyzed in the presence or absence of CM14. When mice were infected with the wild type (WT+DMSO), the blood plasma levels of total protein (TP) and albumin (ALB) decreased, while the levels of aspartate aminotransferase (AST) and blood urea nitrogen (BUN) increased, compared to the uninfected control mice injected with the vehicle (Fig. III-5B; PBS+DMSO). However, the levels of biochemical parameters in mice infected with

wild type in the presence of CM14 (WT+CM14) were comparable to those in the control groups such as mice injected with the vehicle or *hlyU* mutant (Fig. III-5B; PBS+DMSO or *hlyU*+DMSO). The levels of alanine aminotransferase (ALT) and creatine (CREA) did not show any significant differences among the groups in the conditions tested (Fig. III-5B).

Because severe inflammation is accompanied with *V. vulnificus* infection (Shin et al., 2002; Jeong and Satchell, 2012), the immune responses were assessed in the *V. vulnificus*-infected mice either co-administered with or without CM14. The pro-inflammatory cytokines interleukin (IL)-1β and IL-6 levels in mouse blood plasma were significantly elevated upon infection of the wild type (Fig. III-5C and D; PBS+DMSO vs. WT+DMSO). However, co-administration of CM14 alleviated the secretion of these pro-inflammatory cytokines (Fig. III-5C and D; WT+CM14). Consistent with this, the recruitment of $F4/80^+$ macrophages to the infection site was also reduced by the administration of CM14 (Fig. III-5E). Remarkably, the percentage of $F4/80^+$ cells over $DAPI^+$ cells at the site infected with the wild type in the presence of CM14 was not significantly different from that with the *hlyU* mutant (Fig. III-5E). Meanwhile, CM14 did not appear to be toxic to mice, as the levels of blood parameters and macrophage infiltration of the mice injected with CM14 were comparable to those of the mice injected with the vehicle (Fig. III-5B to E; CM14 vs. PBS+DMSO). Furthermore, none of the mice injected with CM14 died (Fig. III-

5A). Taken together, these results indicated that CM14 attenuates the virulence of *V. vulnificus in vivo* and is not toxic toward mice.

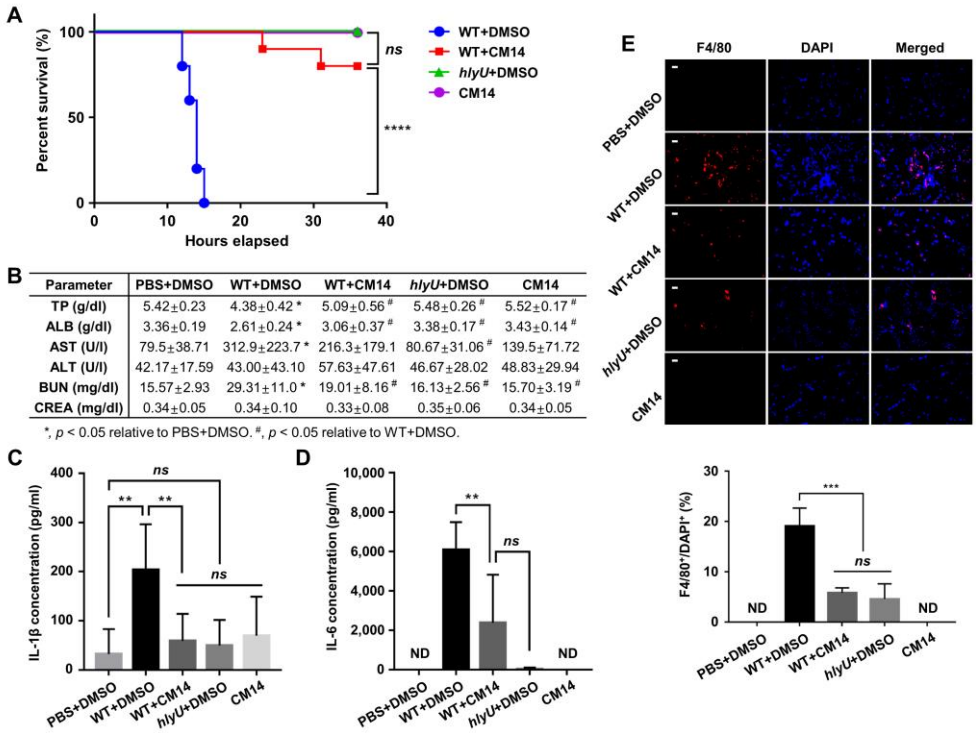

Figure III-5. Effects of CM14 on the survival, pathophysiological changes, and inflammatory responses of mice infected with *V. vulnificus*. (A) Survival of the mice anesthetized with isoflurane and subcutaneously injected with wild type (n = 10), wild type with CM14 (n = 10), *hlyU* mutant (n = 5) at doses of 7.5×10^5 CFU, or CM14 alone (n = 5, control). (B to E) The mice, injected as described in (A), were sacrificed at 7 h post infection to obtain blood and skin tissue samples. (B) The levels of TP, ALB, AST, ALT, BUN, and CREA in the blood plasma of each group [WT+DMSO (n = 10), WT+CM14 (n = 8), *hlyU*+DMSO (n = 6), DMSO (n = 6, control), and CM14 (n = 6, control)] were determined by blood biochemical analysis. The data represent the mean ± SD. Statistical significance was determined by multiple comparisons after one-way ANOVA (*, $p < 0.05$ relative to PBS+DMSO; #,

$p < 0.05$ relative to WT+DMSO). (C and D) The cytokine levels of IL-1β (c) and IL-6 (d) in the blood plasma of each group ($n = 7$) were quantified by ELISA. (E) Infiltration of macrophages at the injection sites was determined using skin tissue samples that were immune-stained with F4/80 antibody (for macrophages, red) and DAPI (for nucleus, blue) for counter staining. The percentage of $F4/80^+$ cells in $DAPI^+$ cells was analyzed by using MetaMorph software. Scale bars, 10 μm ($n = 4$). Error bars represent the SD. Statistical significance was determined by log rank test (A) and by multiple comparisons after one-way ANOVA (C to E) (****, $p < 0.0001$; ***, $p < 0.0005$; **, $p < 0.005$; *, $p < 0.05$; *ns*, not significant; ND, not detected). WT, wild type; *hlyU*, *hlyU* mutant.

III-3-5. CM14 inhibits the HlyU binding to its target promoter DNA

As a transcriptional regulator, HlyU functions by directly binding to its target DNA (Jang et al., 2017; Mukherjee et al., 2015; Liu et al., 2007; Getz and Thomas, 2018). Thus, it was examined whether CM14 inhibits the activity of HlyU by altering the DNA-binding of HlyU. EMSAs revealed that HlyU bound to the target P_{rtxA} DNA and resulted in a retarded band of the DNA-HlyU complex in a HlyU concentration-dependent manner (Fig. III-6A, DMSO). When 20 μM of CM14 was added, however, the HlyU binding to DNA decreased, as less amount of retarded bands were detected compared to the DMSO-added control (Fig. III-6A; CM14). In contrast, a random molecule that showed no HlyU-inhibiting activity in the screening did not alter the HlyU binding to DNA (Fig. III-6A; Control). To determine the effect of CM14 on the dissociation constant (K_d) for HlyU, additional EMSA experiments were performed (Fig. III-6B and C). Based on the concentration of HlyU required to bind 50% of the DNA probe, the K_d for HlyU without CM14 was estimated as 25.16 nM, while that with 2.5 μM of CM14 was estimated as 54.83 nM (Fig. III-6D), indicating that the molecule significantly affects the equilibrium between free and DNA-bound HlyU proteins in the binding reaction. Indeed, the addition of increasing amounts of CM14 resulted in a concentration-dependent inhibition of HlyU binding to DNA, and 50 μM of CM14 completely abolished the formation of the DNA-HlyU complex (Fig. III-6E). Together, the results suggested that inhibition of the HlyU binding to its target DNA is a possible mechanism of CM14.

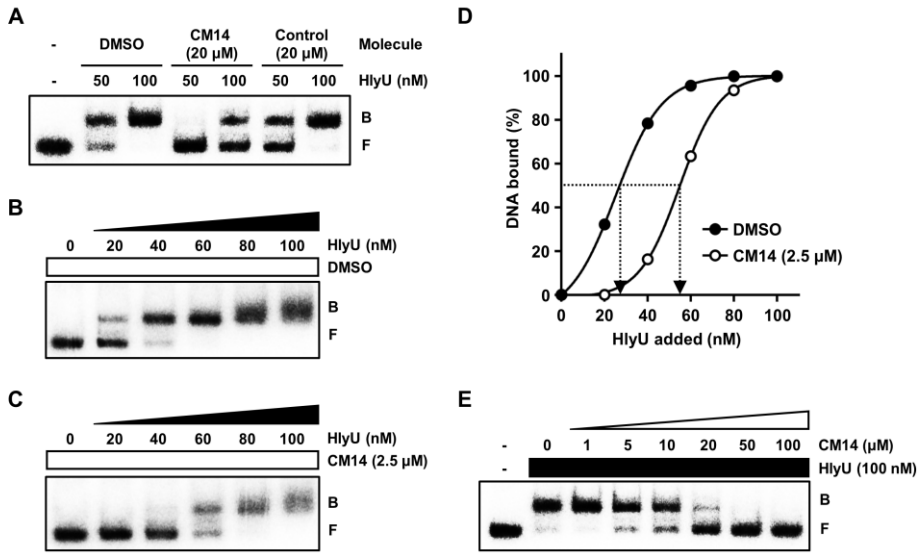

Figure III-6. EMSA of HlyU and the *rtxA* regulatory DNA complexes. (A) HlyU protein (50 or 100 nM) was added to the radioactively-labeled P_{rtxA} DNA (5 nM) along with either DMSO (10%), CM14 (20 μM), or a random chemical (20 μM, control), and the complexes were separated by electrophoresis. (B and C) The labeled probe DNA were mixed with increasing amounts of HlyU as indicated, and then the complexes were separated as described above. (D) The relative affinities of HlyU in the presence or absence of CM14 were compared using the data from (B) and (C). The concentration of bound DNA was calculated and plotted against the concentration of HlyU added. Each arrow points to the position of half-maximal binding corresponding to the K_d. (E) HlyU protein (100 nM) was added to the labeled probe DNA along with increasing concentrations of CM14 as indicated, and then the complexes were separated as described above. B, bound DNA; F, free DNA.

III-3-6. CM14 leads to chemical modification of HlyU

The possible mechanism of CM14 to inhibit the DNA-binding activity of HlyU was further investigated at a molecular level. To this end, tandem mass spectrometric analysis was performed for the CM14-treated HlyU sample. Fig. III-7A clearly showed that the Cys30 residue (C#) in the HlyU peptide, RLQILC#MLHNQELSVGELCAK, was covalently modified by the moiety with molecular mass of 130.042 Da, indicating that a certain part of CM14, probably consisting of C_9H_7O, is attached to Cys30 of HlyU. Importantly, this modification seems to occur *in vivo* as well, because the freshly purified HlyU protein from the CM14 (50 μM)-treated *E. coli* cells also revealed the same result (Fig. III-7B). To verify this modification on the Cys30, a mutant HlyU protein with Cys to Ser substitution at Cys30 ($HlyU_{C30S}$) was prepared and reacted with CM14. When the resulting mixture was analyzed by tandem mass spectrometry, a spectrum corresponding to the HlyU peptide containing a substituted serine, but not containing the covalently modified moiety, was detected (Fig. III-7C), indicating that the thiol group of Cys30 is important for the covalent modification. Consistent with this, the mutant $HlyU_{C30S}$ became resistant to CM14, as supported by the observations that the DNA-binding activity of $HlyU_{C30S}$ was less affected by the molecule *in vitro* (Fig. III-8A) and that the expression of *rtxA* was not attenuated by the molecule *in vivo* (Fig. III-8B).

According to the previously determined crystal structure of HlyU, there is another Cys residue, Cys96, near the Cys30 (Fig. III-8C, PDB code: 3JTH). To examine the role of Cys96 on the CM14-mediated modification of Cys30, this residue was also substituted with Ser. The resulting $HlyU_{C96S}$ was also resistant to CM14 *in vitro* and *in vivo*, as was $HlyU_{C30S}$ (Fig. III-8A and B; $HlyU_{C96S}$). Notably, however, Cys96 residue was detected unmodified in the above tandem mass spectrometric analysis of CM14-treated HlyU sample. Taken together, the results indicated that CM14 reacts with the thiol group of Cys30 of HlyU via a putative chemical reaction involving Cys96, and consequently inhibits the DNA-binding activity of HlyU.

To gain insights into the structural influence of CM14 on HlyU, the crystal structure of CM14-treated HlyU protein at 2.1 Å resolution was determined and compared with the previously determined apo-HlyU structure (Nishi et al., 2010) (PDB code: 3JTH) (Fig. III-8D and E). The overall structure of the CM14-treated HlyU is similar to that of apo-HlyU (Fig. III-8D). However, there is an extra electron density map around Cys30 of the CM14-treated HlyU suggesting a potential chemical modification of Cys30 (Fig. III-8E). Although the moiety attached to Cys30 is partially visible presumably due to the high flexibility, this observation is consistent with the above result that CM14 modifies the Cys30 of HlyU (Fig. III-7A and B). Notably, further comparison revealed that CM14 induces a conformational change in HlyU, thereby substantially decreasing the distance between Cys30 and Cys96 from 8.4 Å to 4.1 Å (Fig. III-8F and G). In addition, the distance between two DNA-

binding α-helices (α4) in HlyU dimer was decreased by 2.9 Å (Fig. III-8D), which may account for the impaired DNA-binding activity of HlyU (Fig. III-6).

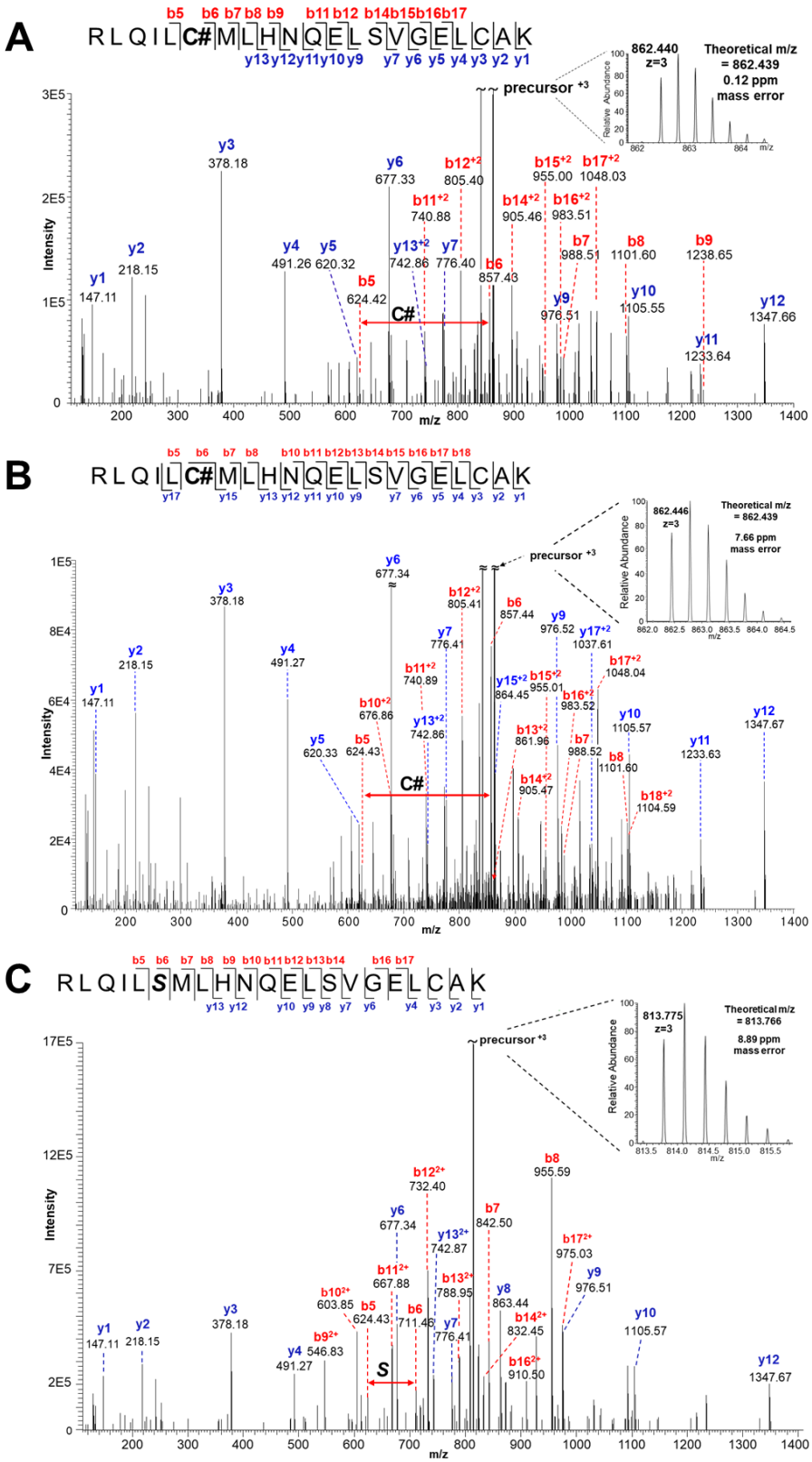
A
RLQILC#MLHNQELSVGELCAK
b5 b6 b7 b8 b9 b11 b12 b14 b15 b16 b17
y13 y12 y11 y10 y9 y7 y6 y5 y4 y3 y2 y1
precursor +3
862.440 z=3
Theoretical m/z = 862.439
0.12 ppm mass error
Relative Abundance
Intensity
m/z
C#
B
RLQILC#MLHNQELSVGELCAK
b5 b6 b7 b8 b10 b11 b12 b13 b14 b15 b16 b17 b18
y17 y15 y13 y12 y11 y10 y9 y7 y6 y5 y4 y3 y2 y1
precursor +3
862.446 z=3
Theoretical m/z = 862.439
7.66 ppm mass error
Relative Abundance
Intensity
m/z
C#
C
RLQILSMLHNQELSVGELCAK
b5 b6 b7 b8 b9 b10 b11 b12 b13 b14 b16 b17
y13 y12 y10 y9 y8 y7 y6 y4 y3 y2 y1
precursor +3
813.775 z=3
Theoretical m/z = 813.766
8.89 ppm mass error
Relative Abundance
Intensity
m/z
S

Figure III-7. Mass spectrum of HlyU and HlyU$_{C30S}$ in the presence of CM14. (A and B) MS/MS spectrum of Cys30-modified peptide (RLQIL**C#**MLHNQELSVGELCAK) from the CM14-treated HlyU protein (A) or the freshly purified HlyU protein expressed in the *E. coli* cells treated with 50 μM of CM14 (B). C# indicates the mass shift of C_9H_6O (# = + 130.042 Da) by the cysteine modification. Both N- and C-terminal fragment ion series are represented as b and y series, respectively (e.g. b5, b6, b7… and y1, y2, y3…), and the annotated fragment ions are marked in the inserted peptide sequence. The observed precursor ion [monoisotopic m/z 862.440 in (A) and 862.446 in (B)] in the inserted high resolution MS spectrum matched exactly with a theoretical m/z (862.439). (C) MS/MS spectrum of RLQIL***S***MLHNQELSVGELCAK from the CM14-treated HlyU$_{C30S}$ mutant protein. ***S*** indicates the Ser30 that replaced the Cys30. Both N- and C-terminal fragment ion series are represented as b and y series, respectively (e.g. b5, b6, b7… and y1, y2, y3…), and the annotated fragment ions are marked in the inserted peptide sequence. The observed precursor ion (monoisotopic m/z 813.775) in the inserted high resolution MS spectrum matched exactly with a theoretical m/z (813.766).

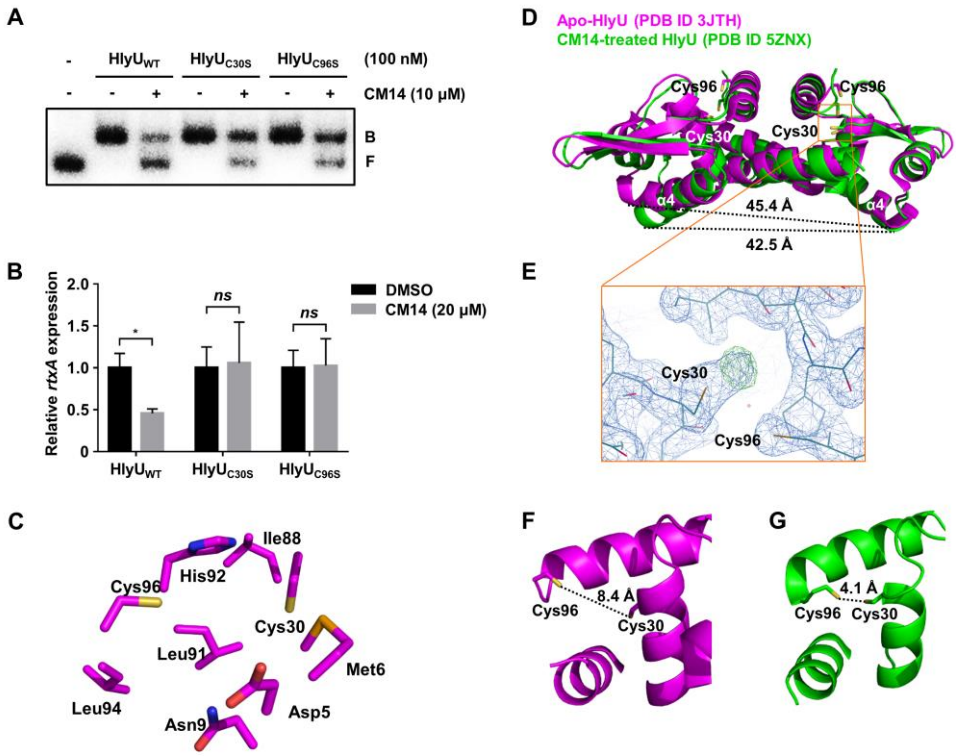

Figure III-8. Chemical modification of the Cys30 residue of HlyU by CM14. (A) EMSA of wild-type (WT), C30S mutant, or C96S mutant HlyU proteins and the radioactively-labeled P_{rtxA} DNA complexes. The HlyU proteins (100 nM) were added to the probe DNA (5 nM) along with either 10% DMSO (control) or CM14 (10 μM) as indicated, and then the complexes were separated by electrophoresis. B, bound DNA; F, free DNA. (B) The *hlyU* mutant strains containing plasmids expressing wild-type or mutant HlyU proteins as indicated were grown along with CM14 (20 μM) or DMSO (control). The *rtxA* transcript levels in the total RNA of the cells were quantitated by qRT-PCR and expressed using the transcript level of each group in the presence of DMSO as 1. Error bars represent the SD. Statistical significance was determined by the Student's *t*-test (*, $p < 0.05$; *ns*, not significant). (C) Close-up view

around the Cys30 residue in the HlyU structure (PDB code: 3JTH). Sulfur, oxygen, and nitrogen atoms of the residues are shown as yellow, red, and blue, respectively. (D) Structural comparison of the CM14-treated HlyU (green, PDB code: 5ZNX) and the apo-HlyU (magenta, PDB code: 3JTH). The distances between the DNA-binding helices (α4) are indicated. (E) Electron density map around Cys30 of the CM14-treated HlyU structure. The $2F_o$ - F_c (blue mesh) and the F_o - F_c (green mesh) maps are contoured at 1.5 σ and 4.4 σ, respectively. (F and G) Close-up views around Cys30 and Cys96 of the apo-HlyU (F) and the CM14-treated HlyU (G). The distances between sulfur atoms of the two cysteine residues are indicated.

III-3-7. CM14 exhibits anti-virulence effects against other *Vibrio* species

HlyU proteins are well conserved in *Vibrio* species and show high degree of sequence similarity. Especially, the residues corresponding to Cys30 and Cys96 of *V. vulnificus* HlyU are present in HlyU homologues of pathogenic *Vibrios*, including *V. parahaemolyticus*, *V. alginolyticus*, and *V. cholerae* (Mukherjee et al., 2015) (Fig. III-9). Thus, it was hypothesized that CM14 would be effective against other *Vibrio* species harboring the HlyU homologue. Unfortunately, the homologues of *rtxA* and *vvhA* are absent in *V. parahaemolyticus* and *V. alginolyticus*, while the *plpA* homologue is present. However, the *plpA* homologues have not been reported to be regulated by HlyU. Accordingly, the expression of *V. parahaemolyticus exsA* which is directly induced by HlyU (Getz and Thomas, 2018) was examined. As expected, CM14 significantly reduced the *exsA* expression in *V. parahaemolyticus* (Fig. III-10A). Because ExsA positively regulates multiple T3SS1-associated genes (Getz and Thomas, 2018), the expressions of T3SS1 genes were further examined in the presence or absence of CM14 (Zhou et al., 2008; Broberg et al., 2011). Again, the expressions of tested T3SS1 genes, such as *vp1668, vopQ, vopS,* and *vopR*, were significantly attenuated by CM14 (Fig. III-10A). Moreover, this molecule reduced the cytotoxicity of *V. parahaemolyticus* against the INT-407 cells in a dose-dependent manner (Fig. III-10B).

Next, the effects of CM14 on *V. alginolyticus* and *V. cholerae* were investigated. Because *V. alginolyticus* possesses T3SS which is particularly similar to that of *V.*

parahaemolyticus (Zhao et al., 2011), it was assumed that HlyU may also regulate T3SS genes in *V. alginolyticus*. In *V. cholerae,* HlyU activates the expression of *hlyA* by directly binding to the promoter region (Mukherjee et al., 2015). As shown in Fig. III-10C to F, CM14 markedly inhibited the expressions of *exsA* and T3SS genes (*val1668*, *vopQ*, *vopS*, and *vopR*) in *V. alginolyticus* and two divergently transcribed hemolysin genes (*hlyA* and *tlh*) in *V. cholerae*, thereby attenuating cytotoxicity or hemolytic activity of the *Vibrios*. Notably, CM14 did not suppress the growth of *V. parahaemolyticus*, *V. alginolyticus*, and *V. cholerae* (Fig. III-11), as in the case of *V. vulnificus* (Fig. III-3D).

Figure III-9. Sequence alignment of HlyU from different *Vibrio* species. The amino acid sequences of HlyU retrieved from NCBI protein database (accession numbers: WP_011078600.1 for *V. vulnificus* HlyU, WP_005461077.1 for *V. parahaemolyticus* HlyU, WP_001888967.1 for *V. cholerae* HlyU, WP_005381940.1 for *V. alginolyticus* HlyU, WP_011261241.1 for *V. fischeri* HlyU, WP_005447923.1 for *V. harveyi* HlyU, WP_026028082.1 for *V. anguillarum* HlyU, WP_001053147.1 for *V. mimicus* HlyU, WP_006075375.1 for *V. shilonii* HlyU, WP_004397917.1 for *V. nigripulchritudo* HlyU, WP_001888967.1 for *V. albensis* HlyU, WP_004735028.1 for *V. splendidus* HlyU, and WP_004744856.1 for *V. tubiashii* HlyU) were aligned using the Clustal Omega program. Identical (asterisks), highly conserved (double dots), and conserved (dots) sequences are indicated. The positions of Cys30 and Cys96 of *V. vulnificus* HlyU are highlighted as red and blue, respectively.

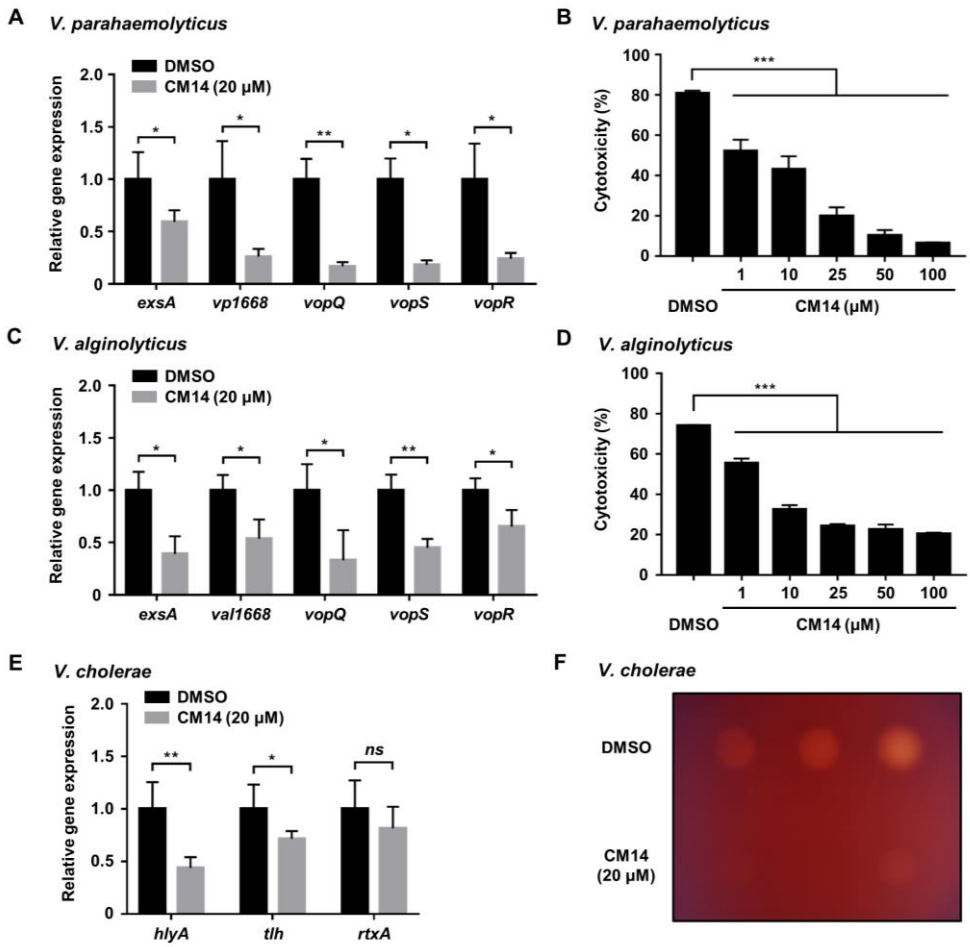

Figure III-10. CM14 is effective in attenuating virulence of other *Vibrio* species.

(A) *V. parahaemolyticus* was grown in T3SS1 inducing condition for 3 h along with CM14 (20 μM) or DMSO (control). The transcript levels of *exsA*, *vp1668*, *vopQ*, *vopS*, and *vopR* in the total RNA of the cells were quantitated by qRT-PCR and expressed using each transcript level in the presence of DMSO as 1. (B) Cytotoxicity was determined using LDH activities released from INT-407 cells infected with *V. parahaemolyticus* at an MOI of 10 along with CM14 as indicated for 2 h, and expressed using the LDH activity from the cells completely lysed by 5% Triton X-

100 as 100%. (C) *V. alginolyticus* was grown to A_{600} of 0.5 along with CM14 (20 μM) or 2% DMSO (control). The transcript levels of each gene in the total RNA of the cells were quantified by qRT-PCR and expressed using each transcript level in the presence of DMSO as 1. (D) Cytotoxicity of *V. alginolyticus* was determined as described in (B), except that *V. alginolyticus* infection was performed for 4 h. (E and F) *V. cholerae* grown to A_{600} of 0.5 along with CM14 (20 μM) or 2% DMSO (control) were harvested and fractionated for further analyses. (E) The transcript levels of *hlyA*, *tlh*, and *rtxA* in the total RNA of the cells were quantified by qRT-PCR and expressed using each transcript level in the presence of DMSO as 1. (F) Hemolytic activities of the culture supernatants of *V. cholerae*. Ten microliters of the concentrated supernatants were spotted on 7% horse blood agar plate. Three different culture supernatants were spotted and monitored after incubation at 37°C for 24 h. Error bars represent the SD. Statistical significance was determined by the Student's *t*-test (A, C, and E) and by one-way ANOVA (B and D) (***, $p < 0.0005$; **, $p < 0.005$; *, $p < 0.05$; *ns*, not significant).

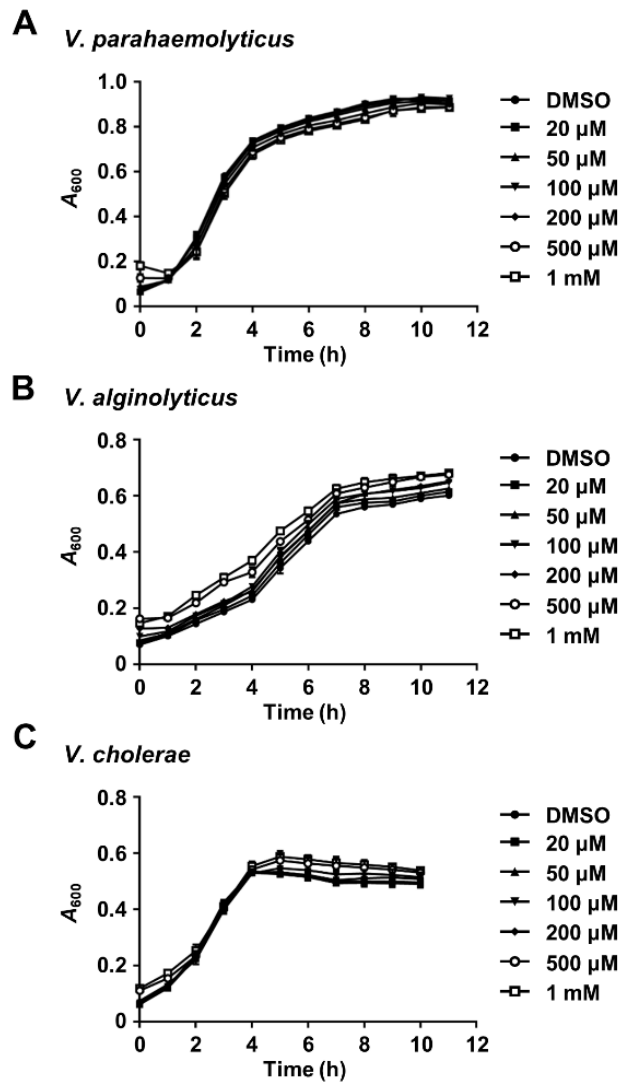

Figure III-11. Effects of CM14 on the growth of other *Vibrio* species. *V. parahaemolyticus* (A), *V. alginolyticus* (B), and *V. cholerae* (C) were grown at 37°C in LBS, tryptic soy broth supplemented with 1% (w/v) NaCl, and LB, respectively, along with various concentrations of CM14 or 2% DMSO (control). Their growth was monitored at 1 h intervals using a microplate reader.

III-4. Discussion

Numerous bacterial genes encoding virulence factors required for the successful pathogenesis have been identified (Finlay and Falkow, 1997; Wu et al., 2008). Many of these genes are coordinately regulated by a global regulatory system(s) to obtain their effective cooperation during infection (Cotter and DiRita, 2000; Miller et al., 1989). Therefore, inhibiting the activity of global regulatory proteins is a promising strategy that can prevent the production of virulence factors simultaneously and impede bacterial pathogenesis efficiently (Clatworthy et al., 2007; Dickey et al., 2017; Rasko and Sperandio, 2010). HlyU homologue in *Vibrio* species is a key regulatory protein that induces the expression of various virulence genes, suggesting that it could be an attractive target to develop the anti-virulence strategies against the pathogenic *Vibrios*. In the present study, a small molecule CM14 has been identified and characterized to specifically inhibit HlyU activity and thus attenuate the pathogenesis of *V. vulnificus* without suppressing its growth. As expected, it also attenuated virulence phenotypes of other pathogenic *Vibrios.*

Among the genes regulated by HlyU in *V. vulnificus*, the expressions of VVMO6_00539 and VVMO6_03281, which are directly repressed by the protein, were significantly induced in the presence of CM14 (Fig. III-1). These results indicated that CM14 inhibits the HlyU activity regardless of its regulatory mode and further suggested that the molecule functions at a stage of HlyU binding to the target

promoter DNA rather than other stages such as interaction of the protein with RNA polymerase. Indeed, the EMSA results revealed that CM14 directly inhibits the DNA-HlyU interaction (Fig. III-6). This inhibitory mode of action has the advantage of controlling bacterial pathogenesis by blocking the production of virulence factors at the earliest step (Cegelski et al., 2008; Rasko and Sperandio, 2010).

To the best of knowledge, CM14 is the first compound that covalently modifies HlyU and inhibits the virulence of *V. vulnificus* in a mammalian infection model. Although two compounds, fursultiamine hydrochloride and 2',4'-dihydroxychalcone, have been identified as HlyU inhibitors, their mode of action was barely demonstrated (Imdad et al., 2018a; Imdad et al., 2018b). Moreover, both of them failed to show *in vivo* efficacy in an animal model, and the latter even impeded bacterial growth at the low concentration of 15 μM. From a structural point of view, compared to the two compounds, CM14 is endowed with a novel keto-alkyne moiety that is required for the covalent modification of Cys30 in HlyU (discussed later).

Acute failures of liver and kidney in *V. vulnificus*-infected patients are the key pathophysiological features associated with fatal outcome (Chou et al., 2010; Huang et al., 2015). This study revealed that the inhibition of HlyU activity by CM14 suppressed the hepatic and renal dysfunction (Fig. III-5B) and subsequently increased the survival rate of mice infected with *V. vulnificus* (Fig. III-5A). In addition, these data showed that CM14 reduces both the production of pro-inflammatory cytokines in the blood plasma (Fig. III-5C and D) and the massive

recruitment of macrophages to the infection site (Fig. III-5E). Because the MARTX toxin and VvhA induce pro-inflammatory cytokine production in mice (Jeong and Satchell, 2012) and these cytokines trigger the recruitment of immune cells such as macrophages (Akira et al., 2006; Kumar et al., 2011), the *in vivo* results indicate that CM14 alleviates the clinical manifestations related to the *V. vulnificus*-induced septicemia by down-regulating the virulence factors. Because these virulence factors are also crucial for the invading pathogen to combat against residing immune cells and thus to proliferate/disseminate in the host (Jang et al., 2017; Jeong and Satchell, 2012; Lo et al., 2011), *V. vulnificus* cells attenuated by the molecule might be readily cleared out of the mice.

From the clear mass spectrometric evidence and biochemical data (Figs. III-7 and 8), it was concluded that the Cys30 residue of HlyU was covalently modified with a certain part of CM14 consisting of C_9H_7O, and the Cys96 residue participated in this modification reaction. Based on these findings, a possible chemical reaction mechanism is proposed for the covalent modification of HlyU by CM14 (Fig. III-12; see the blue dashed box on the right). In the proposed reaction, the sulfur atom of Cys96 may first attack a carbon atom of the carbon-carbon triple bond of CM14. The second attack by the sulfur atom of Cys30 would release the amine group with the bulky rings, leaving a part with the phenyl group of CM14. Subsequently, a nucleophile (e.g. His92; Fig. III-8C) around the reaction site would cleave the sulfur-carbon bond between Cys96 and the remaining part of CM14, and the carbon would

be protonated. The series of these reactions could result in the C_9H_7O moiety attached to Cys30 of HlyU.

One of the remarkable features of CM14 is that this molecule seems specific for HlyU among various thiol-dependent transcriptional regulators, because only the HlyU regulon was differentially regulated by CM14 in the whole transcriptome sequencing analysis (Fig. III-13A). Indeed, samples of WT+CM14, *hlyU*+DMSO, *hlyU*+CM14 were clustered into a certain group that is distinct from the WT+DMSO samples in a principal component analysis (Fig. III-13B). Hence, it was hypothesized that the bulky rings of CM14 may be involved in the specific interaction with HlyU at the early steps of binding, but the details of interactions including binding constant remain to be studied in the future. The effects of CM14 on thiol groups of other proteins such as those in the host should also be clarified by future studies.

Nonetheless, how does this modification affect the DNA-binding activity of HlyU protein? Intriguingly, a previous simulation study on the *V. cholerae* HlyU protein revealed that a distance between Cys38 and Cys104, which correspond to the Cys30 and Cys96 of *V. vulnificus* HlyU, respectively, has a correlation with the target DNA binding of HlyU. Specifically, the distance between Cys38 and Cys104 in *V. cholerae* HlyU is 8.67 Å, when it is expected to bind to a target DNA (Mukherjee et al., 2015). This is close to 8.4 Å, the distance between Cys30 and Cys96 in *V. vulnificus* HlyU (Fig. III-8D). From the comparison of the crystal structure of CM14-treated HlyU with that of apo-HlyU (Fig. III-8D), the distance between Cys30 and Cys96 residues

was found to be significantly shortened from 8.4 Å to 4.1 Å upon CM14 treatment (Fig. III-8F and G). Furthermore, the distance between two DNA-binding α-helices (α4) in HlyU dimer was also decreased by 2.9 Å (Fig. III-8D). Altogether, the results indicate that CM14-mediated Cys30 modification substantially changes the HlyU conformation, and thus inhibits the HlyU binding to target DNA (Figs. III-6 to 8).

Many studies have reported small molecules that can inhibit the activity or expression of virulence factors without affecting bacterial growth. For instance, Virstatin precludes dimerization of *V. cholerae* ToxT and prevents the expression of cholera toxin and toxin coregulated pilus (Hung et al., 2005; Shakhnovich et al., 2007). Similarly, LED209 inhibits QseC activity, reducing the QseC-dependent virulence gene expression and virulence of multiple Gram-negative pathogens (Curtis et al., 2014; Rasko et al., 2008). ITC-12 covalently modifies a cysteine residue of LasR, inhibits quorum sensing-mediated gene expression, and attenuates virulence of *Pseudomonas aeruginosa* (Amara et al., 2009). Ebselen binds to an active cysteine residue in the cysteine protease domain and thereby inhibits the autoproteolytic cleavage of TcdA and TcdB, the *Clostridium difficile* major toxins (Bender et al., 2015). Interestingly, CM14, in addition to ITC-12 and Ebselen, also covalently modifies Cys30 of *V. vulnificus* HlyU (Fig. III-7). This supports the present idea that targeting cysteine residues could be promising for the development of selective inhibitors of target proteins due to the scarcity and high reactivity (Lagoutte et al., 2017).

CM14 successfully inhibited the expressions of various virulence genes in *Vibrio* species, including *vvhA*, *rtxA*, and *plpA* of *V. vulnificus* (Fig. III-4A), T3SS1 genes of *V. parahaemolyticus* (Fig. III-10A), T3SS genes of *V. alginolyticus* (Fig. III-10C), and *hlyA* and *tlh* of *V. cholerae* (Fig. III-10E). Consistent with the previous report that the promoter region of *rtxA* in *V. cholerae* is not directly bound by the HlyU protein (Wang et al., 2015), the expression of *rtxA* in *V. cholera*e was not affected by CM14 (Fig. III-10E). This is noteworthy because it further supports that CM14 specifically affects the HlyU protein. Nevertheless, these results suggest that CM14 has a broad-spectrum anti-virulence effect against pathogenic *Vibrio* species harboring HlyU homologue to regulate the expression of diverse virulence genes.

In conclusion, a small molecule CM14 was identified and found to inhibit HlyU activity by covalently modifying Cys30 and attenuate the virulence of *Vibrio* species. CM14 exhibited its anti-virulence effect even at the post-infection treatment, although it was *ex vivo* case (Fig. III-14). Further studies are needed to explore the potential of CM14 as a therapeutic agent against *V. vulnificus* infection, including the evaluation of CM14 analogues with improved bioavailability. Because CM14 does not suppress the bacterial growth, it would present no or low selective pressure for resistance.

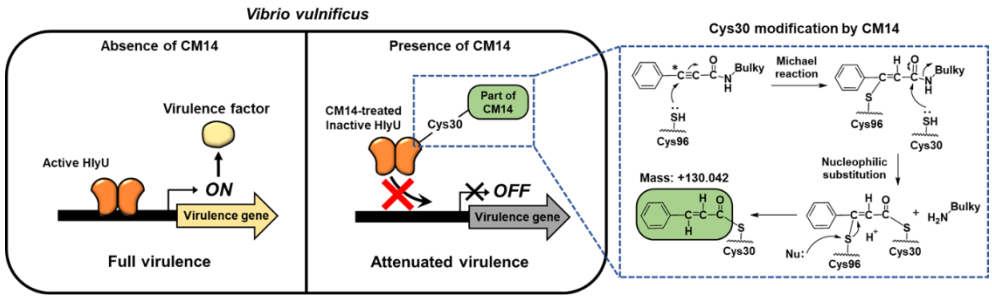

Figure III-12. Proposed molecular mechanism underlying the CM14-mediated inhibition of HlyU binding to target DNA. A possible reaction mechanism for the Cys30 modification of HlyU by CM14 is shown in a blue dashed box on the right. First, the sulfur atom of Cys96 of HlyU reacts with a carbon atom (asterisk) of CM14, a Michael reaction acceptor site. Then, a sulfur atom of Cys30 of HlyU attacks a carbonyl carbon of CM14 and releases an amine group with bulky rings. Subsequently, a nucleophile (Nu, e.g. His92) around the reaction site cleaves the sulfur-carbon bond between Cys96 and the remaining part of CM14, protonating the carbon to create the carbon-carbon double bond. The remaining part of CM14 (represented by a green rounded box) is covalently linked to the sulfur atom of Cys30. Active HlyU can bind to target promoter DNA, leading to the production of virulence factors and rendering *V. vulnificus* fully virulent. In contrast, inactivation of HlyU by CM14 inhibits the DNA binding of HlyU, resulting in reduced expressions of HlyU-regulated virulence genes. These events eventually attenuate the virulence of *V. vulnificus*.

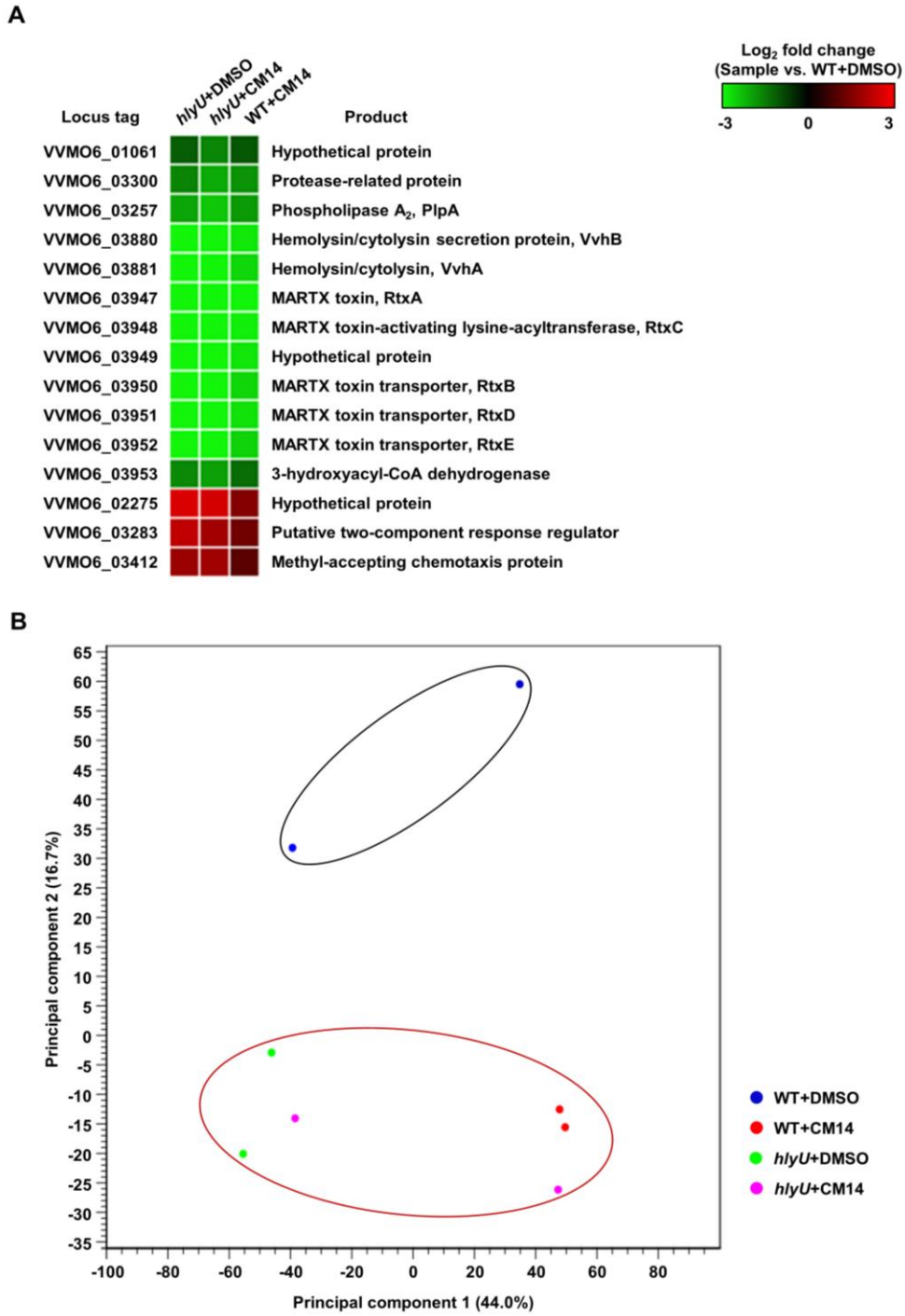
A
Log2 fold change
(Sample vs. WT+DMSO)
-3
0
3
hlyU+DMSO
hlyU+CM14
WT+CM14
Locus tag
Product
VVMO6_01061 Hypothetical protein
VVMO6_03300 Protease-related protein
VVMO6_03257 Phospholipase A2, PlpA
VVMO6_03880 Hemolysin/cytolysin secretion protein, VvhB
VVMO6_03881 Hemolysin/cytolysin, VvhA
VVMO6_03947 MARTX toxin, RtxA
VVMO6_03948 MARTX toxin-activating lysine-acyltransferase, RtxC
VVMO6_03949 Hypothetical protein
VVMO6_03950 MARTX toxin transporter, RtxB
VVMO6_03951 MARTX toxin transporter, RtxD
VVMO6_03952 MARTX toxin transporter, RtxE
VVMO6_03953 3-hydroxyacyl-CoA dehydrogenase
VVMO6_02275 Hypothetical protein
VVMO6_03283 Putative two-component response regulator
VVMO6_03412 Methyl-accepting chemotaxis protein
B
Principal component 2 (16.7%)
Principal component 1 (44.0%)
WT+DMSO
WT+CM14
hlyU+DMSO
hlyU+CM14

Figure III-13. Effects of CM14 on HlyU regulon expression. (A) Genes differentially expressed in DMSO-treated *hlyU* mutant, CM14-treated *hlyU* mutant, and CM14-treated wild type relative to those expressed in DMSO-treated wild type (fold change ≥ 2; $p \leq 0.05$) were identified by transcriptome sequencing analyses, and the fold changes of the expression of these genes are shown in the heat map with colors representing the $\log_2$ RPKM ratio. Locus tags are based on the database of the *V. vulnificus* MO6-24/O genome (GenBank™ accession numbers: CP002469 and CP002470) and the products of the genes are presented on the right. (B) Principal-component analysis of the whole-gene expression profiles of the samples. Each symbol represents the transcriptome of a single sample from two biological replicates per sample group. WT, wild type; *hlyU*, *hlyU* mutant.

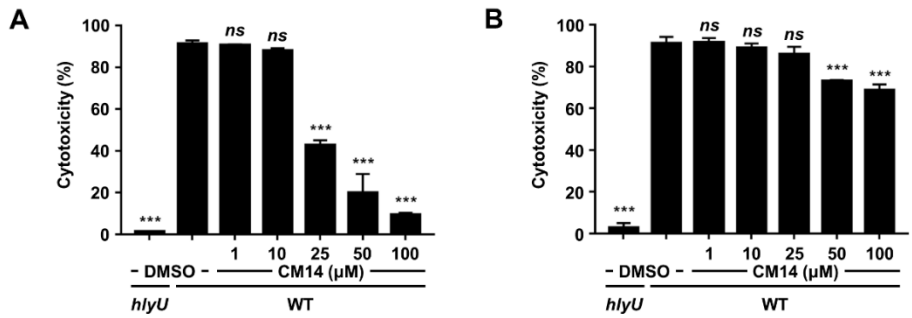

Figure III-14. Effects of CM14 treatment after infection of *V. vulnificus* to host cells. INT-407 cells were infected with the *V. vulnificus* strains at a multiplicity of infection of 10 and then treated with various concentrations of CM14 as indicated after 0.5 h (A) or 1 h (B) of infection. Cytotoxicity was determined using LDH activities released from the cells after 2.5 h incubation and expressed using the LDH activity from the cells completely lysed by 5% Triton X-100 as 100%. Error bars represent the SD. Statistical significance was determined by one-way ANOVA (***, $p < 0.0005$; *ns*, not significant). WT, wild type; *hlyU*, *hlyU* mutant.

Chapter IV.

Conclusion

For a successful infection, the opportunistic human pathogen *V. vulnificus* must recognize environmental changes and produce appropriate virulence factors to survive and cause disease in the host. The MARTX toxin RtxA of *V. vulnificus* is an essential virulence factor that exhibits cytopathic and cytotoxic activities to host cells and enables the pathogen to invade the host bloodstream. RtxA further contributes to the pathogenicity of *V. vulnificus* by protecting the bacteria from phagocytosis of host immune cells. H-NS and HlyU directly repress and derepress the expression of *rtxA* encoding RtxA, respectively. In addition, Lrp activates the *rtxA* expression by binding directly and specifically to P_{rtxA} in an independent manner with H-NS and HlyU. Leucine act as an antagonist of the Lrp-mediated *rtxA* activation by inhibiting the binding of Lrp to P_{rtxA}. On the other hand, CRP directly represses the *rtxA* expression, which is derepressed upon addition of exogenous glucose. It is noteworthy that CRP binds to upstream regions of P_{rtxA} and represses the *rtxA* transcription, as shown in biochemical and mutational analyses. CRP also directly represses the expressions of *lrp* and *hlyU*, forming coherent feedforward loops in the *rtxA* regulation. As a result, the *rtxA* regulatory network consists of global regulators CRP and Lrp, in addition to H-NS and HlyU, providing the fine-tuning of *rtxA* expression in response to environmental and metabolic stimuli during infection.

From the combined results, HlyU is proposed as a plausible target to control the virulence of *V. vulnificus*, because it activates multiple virulence genes including *rtxA*, *vvhA*, and *plpA*. The HlyU inhibitor CM14 was identified from the high-

throughput screening of 8,385 compounds. CM14 inhibits the activity rather than the cellular level of HlyU, without affecting bacterial growth or host cell viability. Treatment of CM14 decreases the HlyU-dependent virulence gene expression and thus attenuates the hemolytic activity and cytotoxicity of *V. vulnificus* against human erythrocytes and epithelial cells. In a mouse model, co-administration of CM14 enhances the survival of mice infected by *V. vulnificus* and suppresses the hepatic and renal dysfunction. At the same time, CM14 reduces the production of pro-inflammatory cytokines and the recruitment of macrophages to the infection site. These results suggested that CM14 can alleviate the clinical manifestations associated with the primary septicemia due to the *V. vulnificus* infection. To explain the mechanism underlying the CM14-mediated inhibition of HlyU, biochemical, mass spectrometric, and crystallographic analyses were conducted. According to the results, CM14 prevents HlyU from binding to the target promoter DNA through covalent modification of Cys30 followed by the conformational change in HlyU. Interestingly, the amino acid sequences of HlyU proteins, including the Cys30 residue, are well conserved in HlyU of pathogenic *Vibrio* species. Accordingly, CM14 reveals the broad-spectrum anti-virulence effects against other pathogenic *Vibrios* such as *V. parahaemolyticus*, *V. alginolyticus*, and *V. cholerae*.

In conclusion, the findings of this study provide an extended understanding of the regulatory mechanisms by which *V. vulnificus* coordinates the expression of *rtxA* within host environments. This understanding further enables the development of a

small-molecule CM14 inhibiting the activity of the transcriptional regulator HlyU to control the virulence of *V. vulnificus*. The small-molecule inhibitor of HlyU identified and characterized in this study has the potential to be exploited as an anti-virulence agent against HlyU-harboring *Vibrio* species.

References

Adams, P. D., Afonine, P. V., Bunkoczi, G., Chen, V. B., Davis, I. W., Echols, N., Headd, J. J., Hung, L. W., Kapral, G. J., Grosse-Kunstleve, R. W., Mccoy, A. J., Moriarty, N. W., Oeffner, R., Read, R. J., Richardson, D. C., Richardson, J. S., Terwilliger, T. C., and Zwart, P. H. 2010. PHENIX: A comprehensive Python-based system for macromolecular structure solution. *Acta Crystallogr D Biol Crystallogr* **66,** 213-221.

Akira, S., Uematsu, S., and Takeuchi, O. 2006. Pathogen recognition and innate immunity. *Cell* **124,** 783-801.

Alice, A. F., and Crosa, J. H. 2012. The TonB3 system in the human pathogen *Vibrio vulnificus* is under the control of the global regulators Lrp and cyclic AMP receptor protein. *J Bacteriol* **194,** 1897-1911.

Alice, A. F., Naka, H., and Crosa, J. H. 2008. Global gene expression as a function of the iron status of the bacterial cell: Influence of differentially expressed genes in the virulence of the human pathogen *Vibrio vulnificus*. *Infect Immun* **76,** 4019-4037.

Allen, R. C., Popat, R., Diggle, S. P., and Brown, S. P. 2014. Targeting virulence: Can we make evolution-proof drugs? *Nat Rev Microbiol* **12,** 300-308.

Alon, U. 2007. Network motifs: Theory and experimental approaches. *Nat Rev Genet* **8,** 450-461.

Amara, N., Mashiach, R., Amar, D., Krief, P., Spieser, S. a. H., Bottomley, M. J., Aharoni, A., and Meijler, M. M. 2009. Covalent inhibition of bacterial quorum sensing. *J Am Chem Soc* **131,** 10610-10619.

Anthouard, R., and Dirita, V. J. 2013. Small-molecule inhibitors of *toxT* expression in *Vibrio cholerae*. *mBio* **4,** e00403-00413.

Antunes, L. C. M., Ferreira, R. B. R., Buckner, M. M. C., and Finlay, B. B. 2010. Quorum sensing in bacterial virulence. *Microbiol-Sgm* **156,** 2271-2282.

Aslund, F., Zheng, M., Beckwith, J., and Storz, G. 1999. Regulation of the OxyR transcription factor by hydrogen peroxide and the cellular thiol-disulfide status. *Proc Natl Acad Sci U S A* **96,** 6161-6165.

Baek, C. H., and Kim, K. S. 2003. *lacZ*- and *aph*-based reporter vectors for *in vivo* expression technology. *J Microbiol Biotechnol* **13,** 872-880.

Baek, C. H., Wang, S. F., Roland, K. L., and Curtiss, R. 2009a. Leucine-responsive regulatory protein (Lrp) acts as a virulence repressor in *Salmonella enterica* serovar Typhimurium. *J Bacteriol* **191,** 1278-1292.

Baek, W. K., Lee, H. S., Oh, M. H., Koh, M. J., Kim, K. S., and Choi, S. H. 2009b. Identification of the *Vibrio vulnificus ahpCl* gene and its influence on survival under oxidative stress and virulence. *J Microbiol* **47,** 624-632.

Baker-Austin, C., and Oliver, J. D. 2018. *Vibrio vulnificus*: New insights into a deadly opportunistic pathogen. *Environ Microbiol* **20,** 423-430.

Bang, Y. J., Lee, Z. W., Kim, D., Jo, I., Ha, N. C., and Choi, S. H. 2016. OxyR2 functions as a three-state redox switch to tightly regulate production of Prx2, a peroxiredoxin of *Vibrio vulnificus*. *J Biol Chem* **291,** 16038-16047.

Bang, Y. J., Oh, M. H., and Choi, S. H. 2012. Distinct characteristics of two 2-Cys peroxiredoxins of *Vibrio vulnificus* suggesting differential roles in detoxifying oxidative stress. *J Biol Chem* **287,** 42516-42524.

Baumman, P., Baumman, L., and Hall, B. G. 1981. Lactose utilization by *Vibrio vulnificus*. *Curr Microbiol* **6,** 131-135.

Bender, K. O., Garland, M., Ferreyra, J. A., Hryckowian, A. J., Child, M. A., Puri, A. W., Solow-Cordero, D. E., Higginbottom, S. K., Segal, E., Banaei, N., Shen, A., Sonnenburg, J. L., and Bogyo, M. 2015. A small-molecule antivirulence agent for treating *Clostridium difficile* infection. *Sci Transl Med* **7,** 1-12.

Bisharat, N., Bronstein, M., Korner, M., Schnitzer, T., and Koton, Y. 2013. Transcriptome profiling analysis of *Vibrio vulnificus* during human infection. *Microbiol-Sgm* **159,** 1878-1887.

Boardman, B. K., and Satchell, K. J. F. 2004. *Vibrio cholerae* strains with mutations in an atypical type I secretion system accumulate RTX toxin intracellularly. *J Bacteriol* **186,** 8137-8143.

Bodero, M. D., and Munson, G. P. 2009. Cyclic AMP receptor protein-dependent repression of heat-labile enterotoxin. *Infect Immun* **77,** 791-798.

Brackman, G., Defoirdt, T., Miyamoto, C., Bossier, P., Van Calenbergh, S., Nelis, H., and Coenye, T. 2008. Cinnamaldehyde and cinnamaldehyde derivatives reduce virulence in *Vibrio* spp. by decreasing the DNA-binding activity of the quorum sensing response regulator LuxR. *BMC Microbiol* **8,** 1-14.

Brinkman, A. B., Ettema, T. J. G., De Vos, W. M., and Van Der Oost, J. 2003. The Lrp family of transcriptional regulators. *Mol Microbiol* **48,** 287-294.

Broberg, C. A., Calder, T. J., and Orth, K. 2011. *Vibrio parahaemolyticus* cell biology and pathogenicity determinants. *Microbes Infect* **13,** 992-1001.

Burke, A. K., Guthrie, L. T. C., Modise, T., Cormier, G., Jensen, R. V., Mccarter, L. L., and Stevens, A. M. 2015. OpaR controls a network of downstream transcription factors in *Vibrio parahaemolyticus* BB22OP. *PLoS One* **10,** e0121863.

Cassat, J. E., and Skaar, E. P. 2013. Iron in infection and immunity. *Cell Host Microbe* **13,** 510-520.

Cegelski, L., Marshall, G. R., Eldridge, G. R., and Hultgren, S. J. 2008. The biology and future prospects of antivirulence therapies. *Nat Rev Microbiol* **6,** 17-27.

Chang, A. K., Kim, H. Y., Park, J. E., Acharya, P., Park, I. S., Yoon, S. M., You, H. J., Hahm, K. S., Park, J. K., and Lee, J. S. 2005. *Vibrio vulnificus* secretes a broad-specificity metalloprotease capable of interfering with blood homeostasis through prothrombin activation and fibrinolysis. *J Bacteriol* **187,** 6909-6916.

Chatzidaki-Livanis, M., Jones, M. K., and Wright, A. C. 2006. Genetic variation in the *Vibrio vulnificus* group 1 capsular polysaccharide operon. *J Bacteriol* **188,** 1987-1998.

Chen, C. L., Chien, S. C., Leu, T. H., Harn, H. I. C., Tang, M. J., and Hor, L. I. 2017. *Vibrio vulnificus* MARTX cytotoxin causes inactivation of phagocytosis-related signaling molecules in macrophages. *J Biomed Sci* **24,** 1-14.

Cho, B. K., Barrett, C. L., Knight, E. M., Park, Y. S., and Palsson, B. O. 2008. Genome-scale reconstruction of the Lrp regulatory network in *Escherichia coli*. *Proc Natl Acad Sci U S A* **105,** 19462-19467.

Choi, G., Jang, K. K., Lim, J. G., Lee, Z. W., Im, H., and Choi, S. H. 2020. The transcriptional regulator IscR integrates host-derived nitrosative stress and iron starvation in activation of the *vvhBA* operon in *Vibrio vulnificus*. *J Biol Chem* **295,** 5350-5361.

Choi, H. K., Park, N. Y., Kim, D. I., Chung, H. J., Ryu, S., and Choi, S. H. 2002. Promoter analysis and regulatory characteristics of *vvhBA* encoding cytolytic hemolysin of *Vibrio vulnificus*. *J Biol Chem* **277,** 47292-47299.

Chou, T. N. K., Chao, W. N., Yang, C., Wong, R. H., Ueng, K. C., and Chen, S. C. 2010. Predictors of mortality in skin and soft-tissue infections caused by *Vibrio vulnificus*. *World J Surg* **34,** 1669-1675.

Chung, K. J., Cho, E. J., Kim, M. K., Kim, Y. R., Kim, S. H., Yang, H. Y., Chung, K. C., Lee, S. E., Rhee, J. H., Choy, H. E., and Lee, T. H. 2010. RtxA1-induced

expression of the small GTPase Rac2 plays a key role in the pathogenicity of *Vibrio vulnificus*. *Journal of Infectious Diseases* **201,** 97-105.

Clatworthy, A. E., Pierson, E., and Hung, D. T. 2007. Targeting virulence: A new paradigm for antimicrobial therapy. *Nat Chem Biol* **3,** 541-548.

Cotter, P. A., and Dirita, V. J. 2000. Bacterial virulence gene regulation: An evolutionary perspective. *Annual Review of Microbiology* **54,** 519-565.

Cowles, K. N., Cowles, C. E., Richards, G. R., Martens, E. C., and Goodrich-Blair, H. 2007. The global regulator Lrp contributes to mutualism, pathogenesis and phenotypic variation in the bacterium *Xenorhabdus nematophila*. *Cell Microbiol* **9,** 1311-1323.

Curtis, M. M., Russell, R., Moreira, C. G., Adebesin, A. M., Wang, C. G., Williams, N. S., Taussig, R., Stewart, D., Zimmern, P., Lu, B. A., Prasad, R. N., Zhu, C., Rasko, D. A., Huntley, J. F., Falck, J. R., and Sperandio, V. 2014. QseC inhibitors as an antivirulence approach for Gram-negative pathogens. *mBio* **5,** e02165-02114.

Davies, J., and Davies, D. 2010. Origins and evolution of antibiotic resistance. *Microbiol Mol Biol Rev* **74,** 417-433.

Deng, W. Y., Wang, H. H., and Xie, J. P. 2011. Regulatory and pathogenesis roles of *Mycobacterium* Lrp/AsnC family transcriptional factors. *J Cell Biochem* **112,** 2655-2662.

Depaola, A., Capers, G. M., and Alexander, D. 1994. Densities of *Vibrio vulnificus* in the intestines of fish from the U.S. Gulf Coast. *Appl Environ Microbiol* **60,** 984-988.

Dickey, S. W., Cheung, G. Y. C., and Otto, M. 2017. Different drugs for bad bugs: antivirulence strategies in the age of antibiotic resistance. *Nat Rev Drug Discov* **16,** 457-471.

Dolores, J. S., Agarwal, S., Egerer, M., and Satchell, K. J. F. 2015. *Vibrio cholerae* MARTX toxin heterologous translocation of beta-lactamase and roles of individual effector domains on cytoskeleton dynamics. *Mol Microbiol* **95,** 590-604.

Dumon-Seignovert, L., Cariot, G., and Vuillard, L. 2004. The toxicity of recombinant proteins in *Escherichia coli*: A comparison of overexpression in BL21(DE3), C41(DE3), and C43(DE3). *Protein Expr Purif* **37,** 203-206.

Duong-Nu, T. M., Jeong, K., Hong, S. H., Puth, S., Kim, S. Y., Tan, W., Lee, K. H., Lee, S. E., and Rhee, J. H. 2019. A stealth adhesion factor contributes to *Vibrio*

vulnificus pathogenicity: Flp pili play roles in host invasion, survival in the blood stream and resistance to complement activation. *PLoS Pathog* **15,** e1007767.

Egerer, M., and Satchell, K. J. F. 2010. Inositol hexakisphosphate-induced autoprocessing of large bacterial protein toxins. *PLoS Pathog* **6,** e1000942.

Elmahdi, S., Dasilva, L. V., and Parveen, S. 2016. Antibiotic resistance of *Vibrio parahaemolyticus* and *Vibrio vulnificus* in various countries: A review. *Food Microbiol* **57,** 128-134.

Evans, L. D. B., Hughes, C., and Fraser, G. M. 2014. Building a flagellum outside the bacterial cell. *Trends Microbiol* **22,** 566-572.

Fan, J. J., Shao, C. P., Ho, Y. C., Yu, C. K., and Hor, L. I. 2001. Isolation and characterization of a *Vibrio vulnificus* mutant deficient in both extracellular metalloprotease and cytolysin. *Infect Immun* **69,** 5943-5948.

Fang, F. C., Frawley, E. R., Tapscott, T., and Vazquez-Torres, A. 2016. Bacterial stress responses during host infection. *Cell Host Microbe* **20,** 133-143.

Finlay, B. B., and Falkow, S. 1997. Common themes in microbial pathogenicity revisited. *Microbiol Mol Biol Rev* **61,** 136-169.

Fullner, K. J., and Mekalanos, J. J. 1999. Genetic characterization of a new type IV-A pilus gene cluster found in both classical and El Tor biotypes of *Vibrio cholerae*. *Infect Immun* **67,** 1393-1404.

Gander, R. M., and Larocco, M. T. 1989. Detection of piluslike structures on clinical and environmental isolates of *Vibrio vulnificus*. *J Clin Microbiol* **27,** 1015-1021.

Gavin, H. E., Beubier, N. T., and Satchell, K. J. F. 2017. The effector domain region of the *Vibrio vulnificus* MARTX toxin confers biphasic epithelial barrier disruption and is essential for systemic spread from the intestine. *PLoS Pathog* **13,** e1006119.

Gavin, H. E., and Satchell, K. J. F. 2015. MARTX toxins as effector delivery platforms. *Pathog Dis* **73,** 1-9.

Gavin, H. E., and Satchell, K. J. F. 2019. RRSP and RID effector domains dominate the virulence impact of *Vibrio vulnificus* MARTX toxin. *Journal of Infectious Diseases* **219,** 889-897.

Getz, L. J., and Thomas, N. A. 2018. The transcriptional regulator HlyU positively regulates expression of *exsA*, leading to type III secretion system 1 activation in

Vibrio parahaemolyticus. *J Bacteriol* **200,** 1-14.

Ghannoum, M. A. 2000. Potential role of phospholipases in virulence and fungal pathogenesis. *Clin Microbiol Rev* **13,** 122-143.

Giel, J. L., Nesbit, A. D., Mettert, E. L., Fleischhacker, A. S., Wanta, B. T., and Kiley, P. J. 2013. Regulation of iron-sulphur cluster homeostasis through transcriptional control of the Isc pathway by [2Fe-2S]-IscR in *Escherichia coli*. *Mol Microbiol* **87,** 478-492.

Goo, S. Y., Han, Y. S., Kim, W. H., Lee, K. H., and Park, S. J. 2007. *Vibrio vulnificus* IlpA-induced cytokine production is mediated by toll-like receptor 2. *J Biol Chem* **282,** 27647-27658.

Goo, S. Y., Lee, H. J., Kim, W. H., Han, K. L., Park, D. K., Lee, H. J., Kim, S. M., Kim, K. S., Lee, K. H., and Park, S. J. 2006. Identification of OmpU of *Vibrio vulnificus* as a fibronectin-binding protein and its role in bacterial pathogenesis. *Infect Immun* **74,** 5586-5594.

Gray, L. D., and Kreger, A. S. 1985. Purification and characterization of an extracellular cytolysin produced by *Vibrio vulnificus*. *Infect Immun* **48,** 62-72.

Gray, L. D., and Kreger, A. S. 1987. Mouse skin damage caused by cytolysin from *Vibrio vulnificus* and by *V. vulnificus* infection. *J Infect Dis* **155,** 236-241.

Green, J., Stapleton, M. R., Smith, L. J., Artymiuk, P. J., Kahramanoglou, C., Hunt, D. M., and Buxton, R. S. 2014. Cyclic-AMP and bacterial cyclic-AMP receptor proteins revisited: Adaptation for different ecological niches. *Curr Opin Microbiol* **18,** 1-7.

Gulig, P. A., Bourdage, K. L., and Starks, A. M. 2005. Molecular pathogenesis of *Vibrio vulnificus*. *J Microbiol* **43,** 118-131.

Guzman, L. M., Belin, D., Carson, M. J., and Beckwith, J. 1995. Tight regulation, modulation, and high-level expression by vectors containing the arabinose P_{BAD} promoter. *J Bacteriol* **177,** 4121-4130.

Ha, C., Kim, S. K., Lee, M. N., and Lee, J. H. 2014. Quorum sensing-dependent metalloprotease VvpE is important in the virulence of *Vibrio vulnificus* to invertebrates. *Microb Pathog* **71-72,** 8-14.

Herrera, A., Muroski, J., Sengupta, R., Nguyen, H. H., Agarwal, S., Loo, R. R. O., Mattoo, S., Loo, J. A., and Satchell, K. J. F. 2020. N-terminal autoprocessing and acetylation of multifunctional-autoprocessing repeats-in-toxins (MARTX) Makes Caterpillars Floppy-like effector is stimulated by adenosine diphosphate

(ADP)-Ribosylation Factor 1 in advance of Golgi fragmentation. *Cell Microbiol* **22,** 1-14.

Ho, Y. C., Hung, F. R., Weng, C. H., Li, W. T., Chuang, T. H., Liu, T. L., Lin, C. Y., Lo, C. J., Chen, C. L., Chen, J. W., Hashimoto, M., and Hor, L. I. 2017. Lrp, a global regulator, regulates the virulence of *Vibrio vulnificus*. *J Biomed Sci* **24,** 1-16.

Horseman, M. A., and Surani, S. 2011. A comprehensive review of *Vibrio vulnificus*: An important cause of severe sepsis and skin and soft-tissue infection. *Int J Infect Dis* **15,** e157-e166.

Huang, K. C., Tsai, Y. H., Huang, K. C., and Lee, M. S. 2015. Model for end-stage liver disease (MELD) score as a predictor and monitor of mortality in patients with *Vibrio vulnificus* necrotizing skin and soft tissue infections. *PLoS Neglect Trop D* **9,** e0003720.

Hung, D. T., Shakhnovich, E. A., Pierson, E., and Mekalanos, J. J. 2005. Small-molecule inhibitor of *Vibrio cholerae* virulence and intestinal colonization. *Science* **310,** 670-674.

Hwang, S. H., Park, J. H., Lee, B., and Choi, S. H. 2019. A regulatory network controls *cabABC* expression leading to biofilm and rugose colony development in *Vibrio vulnificus*. *Front Microbiol* **10,** 3063.

Imdad, S., Batool, N., Pradhan, S., Chaurasia, A. K., and Kim, K. K. 2018a. Identification of 2',4'-dihydroxychalcone as an antivirulence agent targeting HlyU, a master virulence regulator in *Vibrio vulnificus*. *Molecules* **23,** 1-13.

Imdad, S., Chaurasia, A. K., and Kim, K. K. 2018b. Identification and validation of an antivirulence agent targeting HlyU-regulated virulence in *Vibrio vulnificus*. *Front Cell Infect Microbiol* **8,** 1-13.

Imlay, J. A. 2006. Iron-sulphur clusters and the problem with oxygen. *Mol Microbiol* **59,** 1073-1082.

Jang, K. K., Gil, S. Y., Lim, J. G., and Choi, S. H. 2016. Regulatory characteristics of *Vibrio vulnificus gbpA* gene encoding a mucin-binding protein essential for pathogenesis. *J Biol Chem* **291,** 5774-5787.

Jang, K. K., Lee, Z. W., Kim, B., Jung, Y. H., Han, H. J., Kim, M. H., Kim, B. S., and Choi, S. H. 2017. Identification and characterization of *Vibrio vulnificus plpA* encoding a phospholipase A_2 essential for pathogenesis. *J Biol Chem* **292,** 17129-17143.

Jeong, H. G., and Choi, S. H. 2008. Evidence that AphB, essential for the virulence of *Vibrio vulnificus*, is a global regulator. *J Bacteriol* **190,** 3768-3773.

Jeong, H. G., and Satchell, K. J. F. 2012. Additive function of *Vibrio vulnificus* MARTX(Vv) and VvhA cytolysins promotes rapid growth and epithelial tissue necrosis during intestinal infection. *PLoS Pathog* **8,** e1002581.

Jeong, H. S., Lee, M. H., Lee, K. H., Park, S. J., and Choi, S. H. 2003a. SmcR and cyclic AMP receptor protein coactivate *Vibrio vulnificus vvpE* encoding elastase through the RpoS-dependent promoter in a synergistic manner. *J Biol Chem* **278,** 45072-45081.

Jeong, H. S., Rhee, J. E., Lee, J. H., Choi, H. K., Kim, D., Lee, M. H., Park, S., and Choi, S. H. 2003b. Identification of *Vibrio vulnificus lrp* and its influence on survival under various stresses. *J Microbiol Biotechnol* **13,** 159-163.

Jeong, K. C., Jeong, H. S., Rhee, J. H., Lee, S. E., Chung, S. S., Starks, A. M., Escudero, G. M., Gulig, P. A., and Choi, S. H. 2000. Construction and phenotypic evaluation of a *Vibrio vulnificus vvpE* mutant for elastolytic protease. *Infect Immun* **68,** 5096-5106.

Jo, I., Kim, D., Bang, Y. J., Ahn, J., Choi, S. H., and Ha, N. C. 2017. The hydrogen peroxide hypersensitivity of OxyR2 in *Vibrio vulnificus* depends on conformational constraints. *J Biol Chem* **292,** 7223-7232.

Johnson, B. K., and Abramovitch, R. B. 2017. Small molecules that sabotage bacterial virulence. *Trends Pharmacol Sci* **38,** 339-362.

Jones, M. K., and Oliver, J. D. 2009. *Vibrio vulnificus*: Disease and pathogenesis. *Infect Immun* **77,** 1723-1733.

Jung, Y. C., Lee, M. A., and Lee, K. H. 2019. Role of flagellin-homologous proteins in biofilm formation by pathogenic *Vibrio* species. *mBio* **10,** e01793-01719.

Kang, M. K., Jhee, E. C., Koo, B. S., Yang, J. Y., Park, B. H., Kim, J. S., Rho, H. W., Kim, H. R., and Park, J. W. 2002. Induction of nitric oxide synthase expression by *Vibrio vulnificus* cytolysin. *Biochem Biophys Res Commun* **290,** 1090-1095.

Kaus, K., Lary, J. W., Cole, J. L., and Olson, R. 2014. Glycan specificity of the *Vibrio vulnificus* hemolysin lectin outlines evolutionary history of membrane targeting by a toxin family. *J Mol Biol* **426,** 2800-2812.

Kim, B. S. 2018. The modes of action of MARTX toxin effector domains. *Toxins* **10,** 1-16.

Kim, B. S., Gavin, H. E., and Satchell, K. J. F. 2015. Distinct roles of the repeat-containing regions and effector domains of the *Vibrio vulnificus* multifunctional-autoprocessing repeats-in-toxin (MARTX) toxin. *mBio* **6,** e00324-00315.

Kim, B. S., Hwang, J., Kim, M. H., and Choi, S. H. 2011a. Cooperative regulation of the *Vibrio vulnificus nan* gene cluster by NanR protein, cAMP receptor protein, and *N*-acetylmannosamine 6-phosphate. *J Biol Chem* **286,** 40889-40899.

Kim, B. S., Jang, S. Y., Bang, Y. J., Hwang, J., Koo, Y., Jang, K. K., Lim, D., Kim, M. H., and Choi, S. H. 2018a. QStatin, a selective inhibitor of quorum sensing in *Vibrio* species. *mBio* **9,** e02262-02217.

Kim, B. S., and Kim, J. S. 2002a. Cholesterol induce oligomerization of *Vibrio vulnificus* cytolysin specifically. *Exp Mol Med* **34,** 239-242.

Kim, B. S., and Kim, J. S. 2002b. *Vibrio vulnificus* cytolysin induces hyperadhesiveness of pulmonary endothelial cells for neutrophils through endothelial P-selectin: a mechanism for pulmonary damage by *Vibrio vulnificus* cytolysin. *Exp Mol Med* **34,** 308-312.

Kim, C. M., Park, R. Y., Chun, H. J., Kim, S. Y., Rhee, J. H., and Shin, S. H. 2007a. *Vibrio vulnificus* metalloprotease VvpE is essentially required for swarming. *FEMS Microbiol Lett* **269,** 170-179.

Kim, C. M., Park, R. Y., Park, J. H., Sun, H. Y., Bai, Y. H., Ryu, P. Y., Kim, S. Y., Rhee, J. H., and Shin, S. H. 2006. *Vibrio vulnificus* vulnibactin, but not metalloprotease VvpE, is essentially required for iron-uptake from human holotransferrin. *Biol Pharm Bull* **29,** 911-918.

Kim, C. M., Park, Y. J., and Shin, S. H. 2007b. A widespread deferoxamine-mediated iron-uptake system in *Vibrio vulnificus*. *Journal of Infectious Diseases* **196,** 1537-1545.

Kim, H. R., Rho, H. W., Jeong, M. H., Park, J. W., Kim, J. S., Park, B. H., Kim, U. H., and Park, S. D. 1993. Hemolytic mechanism of cytolysin produced from *V. vulnificus*. *Life Sci* **53,** 571-577.

Kim, H. Y., Chang, A. K., Park', J. E., Park, I. S., Yoon, S. M., and Lee, J. S. 2007c. Procaspase-3 activation by a metalloprotease secreted from *Vibrio vulnificus*. *Int J Mol Med* **20,** 591-595.

Kim, I. H., Kim, B. S., Lee, K. S., Kim, I. J., Son, J. S., and Kim, K. S. 2011b. Identification of virulence factors in *Vibrio vulnificus* by comparative transcriptomic analyses between clinical and environmental isolates using cDNA microarray. *J*

Microbiol Biotechnol **21,** 1228-1235.

Kim, I. H., Shim, J. I., Lee, K. E., Hwang, W., Kim, I. J., Choi, S. H., and Kim, K. S. 2008a. Nonribosomal peptide synthase is responsible for the biosynthesis of siderophore in *Vibrio vulnificus* MO6-24/O. *J Microbiol Biotechnol* **18,** 35-42.

Kim, J. A., Lee, M. A., Jung, Y. C., Jang, B. R., and Lee, K. H. 2018b. Repression of VvpM protease expression by quorum sensing and the cAMP-cAMP receptor protein complex in *Vibrio vulnificus*. *J Bacteriol* **200,** 1-14.

Kim, J. R., Cha, M. H., Oh, D. R., Oh, W. K., Rhee, J. H., and Kim, Y. R. 2010a. Resveratrol modulates RTX toxin-induced cytotoxicity through interference in adhesion and toxin production. *Eur J Pharmacol* **642,** 163-168.

Kim, J. S., Chae, M. R., Chang, K., Park, K. H., Rho, H. W., Park, B. H., Park, J. W., and Kim, H. R. 1998. Cytotoxicity of *Vibrio vulnificus* cytolysin on rat peritoneal mast cells. *Microbiol Immunol* **42,** 837-843.

Kim, S., Bang, Y. J., Kim, D., Lim, J. G., Oh, M. H., and Choi, S. H. 2014a. Distinct characteristics of OxyR2, a new OxyR-type regulator, ensuring expression of Peroxiredoxin 2 detoxifying low levels of hydrogen peroxide in *Vibrio vulnificus*. *Mol Microbiol* **93,** 992-1009.

Kim, S., Chung, H. Y., Lee, D. H., Lim, J. G., Kim, S. K., Ku, H. J., Kim, Y. T., Kim, H., Ryu, S., Lee, J. H., and Choi, S. H. 2016. Complete genome sequence of *Vibrio parahaemolyticus* strain FORC_008, a foodborne pathogen from a flounder fish in South Korea. *Pathog Dis* **74,** 1-5.

Kim, S. M., Lee, D. H., and Choi, S. H. 2012. Evidence that the *Vibrio vulnificus* flagellar regulator FlhF is regulated by a quorum sensing master regulator SmcR. *Microbiol-Sgm* **158,** 2017-2025.

Kim, S. M., Park, J. H., Lee, H. S., Kim, W. B., Ryu, J. M., Han, H. J., and Choi, S. H. 2013a. LuxR homologue SmcR is essential for *Vibrio vulnificus* pathogenesis and biofilm detachment, and its expression is induced by host cells. *Infect Immun* **81,** 3721-3730.

Kim, S. Y., Thanh, X. T. T., Jeong, K., Kim, S. B., Pan, S. O., Jung, C. H., Hong, S. H., Lee, S. E., and Rhee, J. H. 2014b. Contribution of six flagellin genes to the flagellum biogenesis of *Vibrio vulnificus* and *in vivo* invasion. *Infect Immun* **82,** 29-42.

Kim, T. J., Chauhan, S., Motin, V. L., Goh, E. B., Igo, M. M., and Young, G. M. 2007d. Direct transcriptional control of the plasminogen activator gene of *Yersinia*

pestis by the cyclic AMP receptor protein. *J Bacteriol* **189,** 8890-8900.

Kim, Y. R., Kim, B. U., Kim, S. Y., Kim, C. M., Na, H. S., Koh, J. T., Choy, H. E., Rhee, J. H., and Lee, S. E. 2010b. Outer membrane vesicles of *Vibrio vulnificus* deliver cytolysin-hemolysin VvhA into epithelial cells to induce cytotoxicity. *Biochem Biophys Res Commun* **399,** 607-612.

Kim, Y. R., Lee, S. E., Kang, I. C., Nam, K. I., Choy, H. E., and Rhee, J. H. 2013b. A bacterial RTX toxin causes programmed necrotic cell death through calcium-mediated mitochondrial dysfunction. *Journal of Infectious Diseases* **207,** 1406-1415.

Kim, Y. R., Lee, S. E., Kim, C. M., Kim, S. Y., Shin, E. K., Shin, D. H., Chung, S. S., Choy, H. E., Progulske-Fox, A., Hillman, J. D., Handfield, M., and Rhee, J. H. 2003. Characterization and pathogenic significance of *Vibrio vulnificus* antigens preferentially expressed in septicemic patients. *Infect Immun* **71,** 5461-5471.

Kim, Y. R., Lee, S. E., Kook, H., Yeom, J. A., Na, H. S., Kim, S. Y., Chung, S. S., Choy, H. E., and Rhee, J. H. 2008b. *Vibrio vulnificus* RTX toxin kills host cells only after contact of the bacteria with host cells. *Cell Microbiol* **10,** 848-862.

Kim, Y. R., and Rhee, J. H. 2003. Flagellar basal body flg operon as a virulence determinant of *Vibrio vulnificus*. *Biochem Biophys Res Commun* **304,** 405-410.

Kirn, T. J., Jude, B. A., and Taylor, R. K. 2005. A colonization factor links *Vibrio cholerae* environmental survival and human infection. *Nature* **438,** 863-866.

Koo, B. S., Lee, J. H., Kim, S. C., Yoon, H. Y., Kim, K. A., Kwon, K. B., Kim, H. R., Park, J. W., and Park, B. H. 2007. Phospholipase A as a potent virulence factor of *Vibrio vulnificus*. *Int J Mol Med* **20,** 913-918.

Kothary, M. H., and Kreger, A. S. 1987. Purification and characterization of an elastolytic protease of *Vibrio vulnificus*. *J Gen Microbiol* **133,** 1783-1791.

Kühn, J., Finger, F., Bertuzzo, E., Borgeaud, S., Gatto, M., Rinaldo, A., and Blokesch, M. 2014. Glucose- but not rice-based oral rehydration therapy enhances the production of virulence determinants in the human pathogen *Vibrio cholerae*. *PLoS Neglect Trop D* **8,** e3347.

Kumar, H., Kawai, T., and Akira, S. 2011. Pathogen Recognition by the Innate Immune System. *Int Rev Immunol* **30,** 16-34.

Kwon, J. Y., Chang, A. K., Park, J. E., Shin, S. Y., Yoon, S. M., and Lee, J. S. 2007. Vibrio extracellular protease with prothrombin activation and fibrinolytic activities. *Int J Mol Med* **19,** 157-163.

Kwon, K. B., Yang, J. Y., Ryu, D. G., Rho, H. W., Kim, J. S., Park, J. W., Kim, H. R., and Park, B. H. 2001. *Vibrio vulnificus* cytolysin induces superoxide anion-initiated apoptotic signaling pathway in human ECV304 cells. *J Biol Chem* **276,** 47518-47523.

Lagoutte, R., Patouret, R., and Winssinger, N. 2017. Covalent inhibitors: an opportunity for rational target selectivity. *Curr Opin Chem Biol* **39,** 54-63.

Lee, A., Kim, M. S., Cho, D., Jang, K. K., Choi, S. H., and Kim, T. S. 2018. *Vibrio vulnificus* RtxA is a major factor driving inflammatory T helper type 17 cell responses *in vitro* and *in vivo*. *Front Immunol* **9,** 1-11.

Lee, B. C., Choi, S. H., and Kim, T. S. 2008a. *Vibrio vulnificus* RTX toxin plays an important role in the apoptotic death of human intestinal epithelial cells exposed to *Vibrio vulnificus*. *Microbes Infect* **10,** 1504-1513.

Lee, B. C., Lee, A., Jung, J. H., Choi, S. H., and Kim, T. S. 2016a. *In vitro* and *in vivo* anti-*Vibrio vulnificus* activity of psammaplin A, a natural marine compound. *Mol Med Rep* **14,** 2691-2696.

Lee, B. C., Lee, J. H., Kim, M. W., Kim, B. S., Oh, M. H., Kim, K. S., Kim, T. S., and Choi, S. H. 2008b. *Vibrio Vulnificus rtxE* is important for virulence, and its expression is induced by exposure to host cells. *Infect Immun* **76,** 1509-1517.

Lee, D. H., Jeong, H. S., Jeong, H. G., Kim, K. M., Kim, H., and Choi, S. H. 2008c. A consensus sequence for binding of SmcR, a *Vibrio vulnificus* LuxR homologue, and genome-wide identification of the SmcR regulon. *J Biol Chem* **283,** 23610-23618.

Lee, D. J., and Busby, S. J. W. 2012. Repression by cyclic AMP receptor protein at a distance. *mBio* **3,** e00289-00212.

Lee, J. H., Kim, M. W., Kim, B. S., Kim, S. M., Lee, B. C., Kim, T. S., and Choi, S. H. 2007a. Identification and characterization of the *Vibrio vulnificus rtxA* essential for cytotoxicity *in vitro* and virulence in mice. *J Microbiol* **45,** 146-152.

Lee, J. H., Rhee, J. E., Park, U., Ju, H. M., Lee, B. C., Kim, T. S., Jeong, H. S., and Choi, S. H. 2007b. Identification and functional analysis of *Vibrio vulnificus* SmcR, a novel global regulator. *J Microbiol Biotechnol* **17,** 325-334.

Lee, J. H., Rho, J. B., Park, K. J., Kim, C. B., Han, Y. S., Choi, S. H., Lee, K. H., and Park, S. J. 2004. Role of flagellum and motility in pathogenesis of *Vibrio vulnificus*. *Infect Immun* **72,** 4905-4910.

Lee, K. E., Bang, J. S., Baek, C. H., Park, D. K., Hwang, W., Choi, S. H., and

Kim, K. S. 2007c. IVET-based identification of virulence factors in *Vibrio vulnificus* MO6-24/O. *J Microbiol Biotechnol* **17,** 234-243.

Lee, K. J., Lee, N. Y., Han, Y. S., Kim, J., Lee, K. H., and Park, S. J. 2010. Functional characterization of the IlpA protein of *Vibrio vulnificus* as an adhesin and its role in bacterial pathogenesis. *Infect Immun* **78,** 2408-2417.

Lee, N. Y., Lee, H. Y., Lee, K. H., Han, S. H., and Park, S. J. 2011. *Vibrio vulnificus* IlpA induces MAPK-mediated cytokine production via TLR1/2 activation in THP-1 cells, a human monocytic cell line. *Mol Immunol* **49,** 143-154.

Lee, S. E., Shin, S. H., Kim, S. Y., Kim, Y. R., Shin, D. H., Chung, S. S., Lee, Z. H., Lee, J. Y., Jeong, K. C., Choi, S. H., and Rhee, J. H. 2000. *Vibrio vulnificus* has the transmembrane transcription activator ToxRS stimulating the expression of the hemolysin gene *vvhA*. *J Bacteriol* **182,** 3405-3415.

Lee, S. J., Jung, Y. H., Oh, S. Y., Jang, K. K., Lee, H. S., Choi, S. H., and Han, H. J. 2015a. *Vibrio vulnificus* VvpE inhibits mucin 2 expression by hypermethylation via lipid raft-mediated ROS signaling in intestinal epithelial cells. *Cell Death & Disease* **6,** 1-11.

Lee, S. J., Jung, Y. H., Oh, S. Y., Song, E. J., Choi, S. H., and Han, H. J. 2015b. *Vibrio vulnificus* VvhA induces NF-κB-dependent mitochondrial cell death via lipid raft-mediated ROS production in intestinal epithelial cells. *Cell Death Dis* **6,** 1-11.

Lee, S. J., Jung, Y. H., Ryu, J. M., Jang, K. K., Choi, S. H., and Han, H. J. 2016b. VvpE mediates the intestinal colonization of *Vibrio vulnificus* by the disruption of tight junctions. *Int J Med Microbiol* **306,** 10-19.

Lee, S. J., Jung, Y. H., Song, E. J., Jang, K. K., Choi, S. H., and Han, H. J. 2015c. *Vibrio vulnificus* VvpE stimulates IL-1 beta production by the hypomethylation of the IL-1 beta promoter and NF-κB activation via lipid raft-dependent ANXA2 recruitment and reactive oxygen species signaling in intestinal epithelial cells. *J Immunol* **195,** 2282-2293.

Lee, T. H., Cha, S. S., Lee, C. S., Rhee, J. H., and Chung, K. M. 2014. Monoclonal antibodies against *Vibrio vulnificus* RtxA1 elicit protective immunity through distinct mechanisms. *Infect Immun* **82,** 4813-4823.

Lee, Y., Kim, B. S., Choi, S., Lee, E. Y., Park, S., Hwang, J., Kwon, Y., Hyun, J., Lee, C., Kim, J. F., Eom, S. H., and Kim, M. H. 2019a. Makes caterpillars floppy-like effector-containing MARTX toxins require host ADP-ribosylation factor (ARF) proteins for systemic pathogenicity. *Proc Natl Acad Sci U S A* **116,** 18031-18040.

Lee, Z. W., Kim, B. S., Jang, K. K., Bang, Y. J., Kim, S., Ha, N. C., Jung, Y. H., Lee, H. J., Han, H. J., Kim, J. S., Kim, J., Sahu, P. K., Jeong, L. S., Kim, M. H., and Cho, S. H. 2019b. Small-molecule inhibitor of HIyU attenuates virulence of *Vibrio* species. *Sci Rep* **9,** 4346.

Lenz, D. H., Mok, K. C., Lilley, B. N., Kulkarni, R. V., Wingreen, N. S., and Bassler, B. L. 2004. The small RNA chaperone Hfq and multiple small RNAs control quorum sensing in *Vibrio harveyi* and *Vibrio cholerae*. *Cell* **118,** 69-82.

Li, L., Mou, X. Y., and Nelson, D. R. 2011. HlyU is a positive regulator of hemolysin expression in *Vibrio anguillarum*. *J Bacteriol* **193,** 4779-4789.

Lim, J. G., Bang, Y. J., and Choi, S. H. 2014a. Characterization of the *Vibrio vulnificus* 1-Cys peroxiredoxin Prx3 and regulation of its expression by the Fe-S cluster regulator IscR in response to oxidative stress and iron starvation. *J Biol Chem* **289,** 36263-36274.

Lim, J. G., and Choi, S. H. 2014. IscR Is a global regulator essential for pathogenesis of *Vibrio vulnificus* and induced by host cells. *Infect Immun* **82,** 569-578.

Lim, J. G., Park, J. H., and Choi, S. H. 2014b. Low cell density regulator AphA upregulates the expression of *Vibrio vulnificus iscR* gene encoding the Fe-S cluster regulator IscR. *J Microbiol* **52,** 413-421.

Lin, C. T., Lin, T. H., Wu, C. C., Wan, L., Huang, C. F., and Peng, H. L. 2016. CRP-cyclic AMP regulates the expression of type 3 fimbriae via cyclic di-GMP in *Klebsiella pneumoniae*. *PLoS One* **11,** e0162884.

Lin, W., Kovacikova, G., and Skorupski, K. 2007. The quorum sensing regulator HapR downregulates the expression of the virulence gene transcription factor AphA in *Vibrio cholerae* by antagonizing Lrp- and VpsR-mediated activation. *Mol Microbiol* **64,** 953-967.

Litwin, C. M., Rayback, T. W., and Skinner, J. 1996. Role of catechol siderophore synthesis in *Vibrio vulnificus* virulence. *Infect Immun* **64,** 2834-2838.

Liu, M., Alice, A. F., Naka, H., and Crosa, J. H. 2007. HlyU protein is a positive regulator of *rtxA1*, a gene responsible for cytotoxicity and virulence in the human pathogen *Vibrio vulnificus*. *Infect Immun* **75,** 3282-3289.

Liu, M. Q., Naka, H., and Crosa, J. H. 2009. HlyU acts as an H-NS antirepressor in the regulation of the RTX toxin gene essential for the virulence of the human pathogen *Vibrio vulnificus* CMCP6. *Mol Microbiol* **72,** 491-505.

Lo, H. R., Lin, J. H., Chen, Y. H., Chen, C. L., Shao, C. P., Lai, Y. C., and Hor, L. I. 2011. RTX toxin enhances the survival of *Vibrio vulnificus* during infection by protecting the organism from phagocytosis. *Journal of Infectious Diseases* **203,** 1866-1874.

Manneh-Roussel, J., Haycocks, J. R. J., Magan, A., Perez-Soto, N., Voelz, K., Camilli, A., Krachler, A. M., and Grainger, D. C. 2018. cAMP receptor protein controls *Vibrio cholerae* gene expression in response to host colonization. *mBio* **9,** e00966-00918.

Maruo, K., Akaike, T., Ono, T., and Maeda, H. 1998. Involvement of bradykinin generation in intravascular dissemination of *Vibrio vulnificus* and prevention of invasion by a bradykinin antagonist. *Infect Immun* **66,** 866-869.

Mcfarland, L. V. 2008. Antibiotic-associated diarrhea: Epidemiology, trends and treatment. *Future Microbiol* **3,** 563-578.

Mcguckin, M. A., Linden, S. K., Sutton, P., and Florin, T. H. 2011. Mucin dynamics and enteric pathogens. *Nat Rev Microbiol* **9,** 265-278.

Mekalanos, J. J. 1992. Environmental signals controlling expression of virulence determinants in bacteria. *J Bacteriol* **174,** 1-7.

Miller, J. F., Mekalanos, J. J., and Falkow, S. 1989. Coordinate regulation and sensory transduction in the control of bacterial virulence. *Science* **243,** 916-922.

Miller, J. H. 1972. *Experiments in molecular genetics.* Cold Spring Harbor, N.Y.: Cold Spring Harbor Laboratory.

Milton, D. L., Otoole, R., Horstedt, P., and Wolfwatz, H. 1996. Flagellin A is essential for the virulence of *Vibrio anguillarum*. *J Bacteriol* **178,** 1310-1319.

Miyoshi, S. 2006. *Vibrio vulnificus* infection and metalloprotease. *J Dermatol* **33,** 589-595.

Miyoshi, S., Nakazawa, H., Kawata, K., Tomochika, K., Tobe, K., and Shinoda, S. 1998. Characterization of the hemorrhagic reaction caused by *Vibrio vulnificus* metalloprotease, a member of the thermolysin family. *Infect Immun* **66,** 4851-4855.

Miyoshi, S., and Shinoda, S. 1988. Role of the protease in the permeability enhancement by *Vibrio vulnificus*. *Microbiol Immunol* **32,** 1025-1032.

Miyoshi, S., and Shinoda, S. 1992. Activation mechanism of human Hageman-factor plasma kallikrein kinin system by *Vibrio vulnificus* metalloprotease. *FEBS Lett* **308,** 315-319.

Miyoshi, S., and Shinoda, S. 1997. Bacterial metalloprotease as the toxic factor in infection. *J Toxicol-Toxin Rev* **16,** 177-194.

Miyoshi, S., Wakae, H., Tomochika, K., and Shinoda, S. 1997. Functional domains of a zinc metalloprotease from *Vibrio vulnificus*. *J Bacteriol* **179,** 7606-7609.

Mortazavi, A., Williams, B. A., Mccue, K., Schaeffer, L., and Wold, B. 2008. Mapping and quantifying mammalian transcriptomes by RNA-Seq. *Nat Methods* **5,** 621-628.

Motes, M. L., Depaola, A., Cook, D. W., Veazey, J. E., Hunsucker, J. C., Garthright, W. E., Blodgett, R. J., and Chirtel, S. J. 1998. Influence of water temperature and salinity on *Vibrio vulnificus* in northern Gulf and Atlantic Coast oysters (*Crassostrea virginica*). *Appl Environ Microbiol* **64,** 1459-1465.

Mukherjee, D., Pal, A., Chakravarty, D., and Chakrabarti, P. 2015. Identification of the target DNA sequence and characterization of DNA binding features of HlyU, and suggestion of a redox switch for *hlyA* expression in the human pathogen *Vibrio cholerae* from in silico studies. *Nucleic Acids Res* **43,** 1407-1417.

Na, S., Bandeira, N., and Paek, E. 2012. Fast multi-blind modification search through tandem mass spectrometry. *Mol Cell Proteomics* **11,** 1-13.

Newton, A., Kendall, M., Vugia, D. J., Henao, O. L., and Mahon, B. E. 2012. Increasing rates of Vibriosis in the United States, 1996-2010: Review of surveillance data from 2 systems. *Clin Infect Dis* **54,** S391-S395.

Ng, W. L., and Bassler, B. L. 2009. Bacterial quorum-sensing network architectures. *Annu Rev Genet* **43,** 197-222.

Nishi, K., Lee, H. J., Park, S. Y., Bae, S. J., Lee, S. E., Adams, P. D., Rhee, J. H., and Kim, J. S. 2010. Crystal structure of the transcriptional activator HlyU from *Vibrio vulnificus* CMCP6. *FEBS Lett* **584,** 1097-1102.

Oh, M. H., Jeong, H. G., and Choi, S. H. 2008. Proteomic identification and characterization of *Vibrio vulnificus* proteins induced upon exposure to INT-407 intestinal epithelial cells. *J Microbiol Biotechnol* **18,** 968-974.

Oh, M. H., Lee, S. M., Lee, D. H., and Choi, S. H. 2009. Regulation of the *Vibrio vulnificus hupA* gene by temperature alteration and cyclic AMP receptor protein and evaluation of its role in virulence. *Infect Immun* **77,** 1208-1215.

Oliver, J. D. 2005a. The viable but nonculturable state in bacteria. *J Microbiol* **43,** 93-100.

Oliver, J. D. 2005b. Wound infections caused by *Vibrio vulnificus* and other marine bacteria. *Epidemiol Infect* **133,** 383-391.

Oliver, J. D. 2015. The Biology of *Vibrio vulnificus*. *Microbiol Spectr* **3,** 1-10.

Otwinowski, Z., and Minor, W. 1997. Processing of X-ray diffraction data collected in oscillation mode. *Methods Enzymol* **276,** 307-326.

Outten, F. W., Djaman, O., and Storz, G. 2004. A *suf* operon requirement for Fe-S cluster assembly during iron starvation in *Escherichia coli*. *Mol Microbiol* **52,** 861-872.

Packiavathy, I., Sasikumar, P., Pandian, S., and Veera Ravi, A. 2013. Prevention of quorum-sensing-mediated biofilm development and virulence factors production in *Vibrio* spp. by curcumin. *Appl Microbiol Biotechnol* **97,** 10177-10187.

Paranjpye, R. N., Lara, J. C., Pepe, J. C., Pepe, C. M., and Strom, M. S. 1998. The type IV leader peptidase/*N*-methyltransferase of *Vibrio vulnificus* controls factors required for adherence to HEp-2 cells and virulence in iron-overloaded mice. *Infect Immun* **66,** 5659-5668.

Paranjpye, R. N., and Strom, M. S. 2005. A *Vibrio vulnificus* type IV pilin contributes to biofilm formation, adherence to epithelial cells, and virulence. *Infect Immun* **73,** 1411-1422.

Park, D. K., Lee, K. E., Baek, C. H., Kim, I. H., Kwon, J. H., Lee, W. K., Lee, K. H., Kim, B. S., Choi, S. H., and Kim, K. S. 2006a. Cyclo(Phe-Pro) modulates the expression of *ompU* in *Vibrio* spp. *J Bacteriol* **188,** 2214-2221.

Park, J., Kim, S. M., Jeong, H. G., and Choi, S. H. 2012. Regulatory characteristics of the *Vibrio vulnificus rtxHCA* operon encoding a MARTX toxin. *J Microbiol* **50,** 878-881.

Park, J. E., Park, J. W., Lee, W., and Lee, J. S. 2014. Pleiotropic effects of a vibrio extracellular protease on the activation of contact system. *Biochem Biophys Res Commun* **450,** 1099-1103.

Park, J. W., Ma, S. N., Song, E. S., Song, C. H., Chae, M. R., Park, B. H., Rho, R. W., Park, S. D., and Kim, H. R. 1996. Pulmonary damage by *Vibrio vulnificus* cytolysin. *Infect Immun* **64,** 2873-2876.

Park, K. H., Lee, Y. R., Hur, H., Yu, H. N., Rah, S. Y., Kim, U. H., Yu, K. Y., Jin, C. M., Han, M. K., and Kim, J. S. 2009. Role of calcium/calmodulin signaling pathway in *Vibrio vulnificus* cytolysin-induced hyperpermeability. *Microb Pathog* **47,** 47-51.

Park, K. H., Yang, H. B., Kim, H. G., Lee, Y. R., Hur, H., Kim, J. S., Koo, B. S., Han, M. K., Kim, J. H., Jeong, Y. J., and Kim, J. S. 2005. Low density lipoprotein inactivates *Vibrio vulnificus* cytolysin through the oligomerization of toxin monomer. *Med Microbiol Immunol* **194,** 137-141.

Park, N. Y., Lee, J. H., Kim, M. W., Jeong, H. G., Lee, B. C., Kim, T. S., and Choi, S. H. 2006b. Identification of the *Vibrio vulnificus wbpP* gene and evaluation of its role in virulence. *Infect Immun* **74,** 721-728.

Peeters, E., Le Minh, P. N., Foulquie-Moreno, M., and Charlier, D. 2009. Competitive activation of the *Escherichia coli argO* gene coding for an arginine exporter by the transcriptional regulators Lrp and ArgP. *Mol Microbiol* **74,** 1513-1526.

Perez-Llamas, C., and Lopez-Bigas, N. 2011. Gitools: Analysis and visualisation of genomic data using interactive heat-maps. *PLoS One* **6,** e19541.

Perez-Reytor, D., Plaza, N., Espejo, R. T., Navarrete, P., Bastias, R., and Garcia, K. 2017. Role of non-coding regulatory RNA in the virulence of human pathogenic *Vibrios*. *Front Microbiol* **7**.

Phillips, K. E., and Satchell, K. J. F. 2017. *Vibrio vulnificus*: From oyster colonist to human pathogen. *PLoS Pathog* **13,** e1006053.

Pineyro, P., Zhou, X. H., Orfe, L. H., Friel, P. J., Lahmers, K., and Call, D. R. 2010. Development of two animal models to study the function of *Vibrio parahaemolyticus* type III secretion systems. *Infect Immun* **78,** 4551-4559.

Pizarro-Cerda, J., and Cossart, P. 2006. Bacterial adhesion and entry into host cells. *Cell* **124,** 715-727.

Prochazkova, K., and Satchell, K. J. F. 2008. Structure-function analysis of inositol hexakisphosphate-induced autoprocessing of the *Vibrio cholerae* multifunctional autoprocessing RTX toxin. *J Biol Chem* **283,** 23656-23664.

Pul, U., Wurm, R., and Wagner, R. 2007. The role of LRP and H-NS in transcription regulation: Involvement of synergism, allostery and macromolecular crowding. *J Mol Biol* **366,** 900-915.

Qin, K. W., Fu, K. F., Liu, J. F., Wu, C. L., Wang, Y. X., and Zhou, L. J. 2019. *Vibrio vulnificus* cytolysin induces inflammatory responses in RAW264.7 macrophages through calcium signaling and causes inflammation *in vivo*. *Microb Pathog* **137,** 1-9.

Rasko, D. A., Moreira, C. G., Li, D. R., Reading, N. C., Ritchie, J. M., Waldor,

M. K., Williams, N., Taussig, R., Wei, S. G., Roth, M., Hughes, D. T., Huntley, J. F., Fina, M. W., Falck, J. R., and Sperandio, V. 2008. Targeting QseC signaling and virulence for antibiotic development. *Science* **321,** 1078-1080.

Rasko, D. A., and Sperandio, V. 2010. Anti-virulence strategies to combat bacteria-mediated disease. *Nat Rev Drug Discov* **9,** 117-128.

Rhee, J. E., Kim, K. S., and Choi, S. H. 2005. CadC activates pH-dependent expression of the *Vibrio vulnificus cadBA* operon at a distance through direct binding to an upstream region. *J Bacteriol* **187,** 7870-7875.

Rhee, J. E., Kim, K. S., and Choi, S. H. 2008a. Activation of the *Vibrio vulnificus cadBA* operon by leucine-responsive regulatory protein is mediated by CadC. *J Microbiol Biotechnol* **18,** 1755-1761.

Rhee, J. E., Kim, K. S., and Choi, S. H. 2008b. Activation of the *Vibrio vulnificus cadBA* operon by leucine-responsive regulatory protein is mediated by CadC. *J Microbiol Biotechnol* **18,** 1755-1761.

Rho, H. W., Choi, M. J., Lee, J. N., Park, J. W., Kim, J. S., Park, B. H., Sohn, H. S., and Kim, H. R. 2002. Cytotoxic mechanism of *Vibrio vulnificus* cytolysin in CPAE cells. *Life Sci* **70,** 1923-1934.

Rui, H. P., Liu, Q., Wang, Q. Y., Ma, Y., Liu, H., Shi, C. B., and Zhang, Y. X. 2009. Role of alkaline serine protease, Asp, in *Vibrio alginolyticus* virulence and regulation of its expression by LuxO-LuxR regulatory system. *J Microbiol Biotechnol* **19,** 431-438.

Rutherford, S. T., and Bassler, B. L. 2012. Bacterial quorum sensing: Its role in virulence and possibilities for its control. *Cold Spring Harb Perspect Med* **2,** 1-26.

Satchell, K. J. F. 2007. MARTX, multifunctional autoprocessing repeats-in-toxin toxins. *Infect Immun* **75,** 5079-5084.

Satchell, K. J. F. 2011. Structure and function of MARTX toxins and other large repetitive RTX proteins. *Annu Rev Microbiol* **65,** 71-90.

Satchell, K. J. F. 2015. Multifunctional-autoprocessing repeats-in-toxin (MARTX) Toxins of *Vibrios*. *Microbiol Spectr* **3,** 1-22.

Scarano, C., Spanu, C., Ziino, G., Pedonese, F., Dalmasso, A., Spanu, V., Virdis, S., and De Santis, E. P. L. 2014. Antibiotic resistance of *Vibrio* species isolated from Sparus aurata reared in Italian mariculture. *New Microbiol* **37,** 329-337.

Schmiel, D. H., and Miller, V. L. 1999. Bacterial phospholipases and pathogenesis.

Microbes Infect **1,** 1103-1112.

Schwartz, C. J., Giel, J. L., Patschkowski, T., Luther, C., Ruzicka, F. J., Beinert, H., and Kiley, P. J. 2001. IscR, an Fe-S cluster-containing transcription factor, represses expression of *Escherichia coli* genes encoding Fe-S cluster assembly proteins. *Proc Natl Acad Sci U S A* **98,** 14895-14900.

Sekirov, I., Russell, S. L., Antunes, L. C. M., and Finlay, B. B. 2010. Gut microbiota in health and disease. *Physiol Rev* **90,** 859-904.

Shakhnovich, E. A., Hung, D. T., Pierson, E., Lee, K., and Mekalanos, J. J. 2007. Virstatin inhibits dimerization of the transcriptional activator ToxT. *Proc Natl Acad Sci U S A* **104,** 2372-2377.

Shao, C. P., and Hor, L. I. 2000. Metalloprotease is not essential for *Vibrio vulnificus* virulence in mice. *Infect Immun* **68,** 3569-3573.

Shin, S. H., Shin, D. H., Ryu, P. Y., Chung, S. S., and Rhee, J. H. 2002. Proinflammatory cytokine profile in *Vibrio vulnificus* septicemic patients' sera. *FEMS Immunol Med Microbiol* **33,** 133-138.

Simon, R., Priefer, U., and Puhler, A. 1983. A broad host range mobilization system for *in vivo* genetic engineering: Transposon mutagenesis in Gram-negative bacteria. *Nat Biotechnol* **1,** 784-791.

Simpson, L. M., and Oliver, J. D. 1983. Siderophore production by *Vibrio vulnificus*. *Infect Immun* **41,** 644-649.

Simpson, L. M., and Oliver, J. D. 1987. Ability of *Vibrio vulnificus* to obtain iron from transferrin and other iron-binding proteins. *Curr Microbiol* **15,** 155-157.

Simpson, L. M., White, V. K., Zane, S. F., and Oliver, J. D. 1987. Correlation between virulence and colony morphology in *Vibrio vulnificus*. *Infect Immun* **55,** 269-272.

Skorupski, K., and Taylor, R. K. 1997a. Control of the ToxR virulence regulon in *Vibrio cholerae* by environmental stimuli. *Mol Microbiol* **25,** 1003-1009.

Skorupski, K., and Taylor, R. K. 1997b. Cyclic AMP and its receptor protein negatively regulate the coordinate expression of cholera toxin and toxin-coregulated pilus in *Vibrio cholerae*. *Proc Natl Acad Sci U S A* **94,** 265-270.

Smith, R. D., and Coast, J. 2002. Antimicrobial resistance: A global response. *B World Health Organ* **80,** 126-133.

Song, E. J., Lee, S. J., Lim, H. S., Kim, J. S., Jang, K. K., Choi, S. H., and Han,

H. J. 2016. *Vibrio vulnificus* VvhA induces autophagy-related cell death through the lipid raft-dependent c-Src/NOX signaling pathway. *Sci Rep* **6,** 27080.

Srivastava, M., Tucker, M. S., Gulig, P. A., and Wright, A. C. 2009. Phase variation, capsular polysaccharide, pilus and flagella contribute to uptake of *Vibrio vulnificus* by the Eastern oyster (Crassostrea virginica). *Environ Microbiol* **11,** 1934-1944.

Strom, M. S., and Paranjpye, R. N. 2000. Epidemiology and pathogenesis of *Vibrio vulnificus*. *Microbes Infect* **2,** 177-188.

Tanabe, T., Naka, A., Aso, H., Nakao, H., Narimatsu, S., Inoue, Y., Ono, T., and Yamamoto, S. 2005. A novel aerobactin utilization cluster in *Vibrio vulnificus* with a gene involved in the transcription regulation of the *iutA* homologue. *Microbiol Immunol* **49,** 823-834.

Testa, J., Daniel, L. W., and Kreger, A. S. 1984. Extracellular phospholipase A_2 and lysophospholipase produced by *Vibrio vulnificus*. *Infect Immun* **45,** 458-463.

Toma, C., Higa, N., Koizumi, Y., Nakasone, N., Ogura, Y., Mccoy, A. J., Franchi, L., Uematsu, S., Sagara, J., Taniguchi, S., Tsutsui, H., Akira, S., Tschopp, J., Nunez, G., and Suzuki, T. 2010. Pathogenic *Vibrio* activate NLRP3 inflammasome via cytotoxins and TLR/nucleotide-binding oligomerization domain-mediated NF-κB signaling. *J Immunol* **184,** 5287-5297.

Wan, Y., Liu, C. S., and Ma, Q. J. 2019. Structural analysis of a *Vibrio* phospholipase reveals an unusual Ser-His-chloride catalytic triad. *J Biol Chem* **294,** 11391-11401.

Wang, H. X., Ayala, J. C., Benitez, J. A., and Silva, A. J. 2015. RNA-Seq analysis identifies new genes regulated by the histone-like nucleoid structuring protein (H-NS) affecting *Vibrio cholerae* virulence, stress response and chemotaxis. *PLoS One* **10,** e0118295.

Wang, Q., and Calvo, J. M. 1993. Lrp, a major regulatory protein in *Escherichia coli*, bends DNA and can organize the assembly of a higher-order nucleoprotein structure. *EMBO J* **12,** 2495-2501.

Webster, A. C. D., and Litwin, C. M. 2000. Cloning and characterization of *vuuA*, a gene encoding the *Vibrio vulnificus* ferric vulnibactin receptor. *Infect Immun* **68,** 526-534.

Weinberg, E. D. 1978. Iron and Infection. *Microbiol Rev* **42,** 45-66.

Williams, S. G., Attridge, S. R., and Manning, P. A. 1993. The transcriptional

activator HlyU of *Vibrio cholerae* - Nucleotide sequence and role in virulence gene expression. *Mol Microbiol* **9,** 751-760.

Williams, T. C., Ayrapetyan, M., Ryan, H., and Oliver, J. D. 2014. Serum survival of *Vibrio vulnificus*: Role of genotype, capsule, complement, clinical origin, and *in situ* incubation. *Pathogens* **3,** 822-832.

Wong, E., Vaaje-Kolstad, G., Ghosh, A., Hurtado-Guerrero, R., Konarev, P. V., Ibrahim, A. F. M., Svergun, D. I., Eijsink, V. G. H., Chatterjee, N. S., and Van Aalten, D. M. F. 2012. The *Vibrio cholerae* colonization factor GbpA possesses a modular structure that governs binding to different host surfaces. *PLoS Pathog* **8,** e1002373.

Wong, K. C., Brown, A. M., Luscombe, G. M., Wong, S. J., and Mendis, K. 2015. Antibiotic use for *Vibrio* infections: Important insights from surveillance data. *BMC Infect Dis* **15,** 1-9.

Wright, A. C., and Morris, J. G. 1991. The extracellular cytolysin of *Vibrio vulnificus*: Inactivation and relationship to virulence in mice. *Infect Immun* **59,** 192-197.

Wright, A. C., Powell, J. L., Kaper, J. B., and Morris, J. G., Jr. 2001. Identification of a group 1-like capsular polysaccharide operon for *Vibrio vulnificus*. *Infect Immun* **69,** 6893-6901.

Wright, A. C., Powell, J. L., Tanner, M. K., Ensor, L. A., Karpas, A. B., Morris, J. G., and Sztein, M. B. 1999. Differential expression of *Vibrio vulnificus* capsular polysaccharide. *Infect Immun* **67,** 2250-2257.

Wright, E. M., Martin, M. G., and Turk, E. 2003. Intestinal absorption in health and disease-sugars. *Best Pract Res Clin Gastroenterol* **17,** 943-956.

Wu, H. J., Wang, A. H. J., and Jennings, M. P. 2008. Discovery of virulence factors of pathogenic bacteria. *Curr Opin Chem Biol* **12,** 93-101.

Yamamoto, K., Wright, A. C., Kaper, J. B., and Morris, J. G. 1990. The cytolysin gene of *Vibrio vulnificus*: Sequence and relationship to the *Vibrio cholerae* El Tor hemolysin gene. *Infect Immun* **58,** 2706-2709.

Yamamoto, M., Kashimoto, T., Tong, P., Xiao, J., Sugiyama, M., Inoue, M., Matsunaga, R., Hosohara, K., Nakata, K., Yokota, K., Oguma, K., and Yamamoto, K. 2015. Signature-tagged mutagenesis of *Vibrio vulnificus*. *J Vet Med Sci* **77,** 823-828.

Yamazaki, K., Kashimoto, T., Morita, M., Kado, T., Matsuda, K., Yamasaki, M.,

and Ueno, S. 2019. Identification of *in vivo* essential genes of *Vibrio vulnificus* for establishment of wound infection by signature-tagged mutagenesis. *Front Microbiol* **10,** 1-12.

Yoshida, S. I., Ogawa, M., and Mizuguchi, Y. 1985. Relation of capsular materials and colony opacity to virulence of *Vibrio vulnificus*. *Infect Immun* **47,** 446-451.

Yu, H. N., Lee, Y. R., Park, K. H., Rah, S. Y., Noh, E. M., Song, E. K., Han, M. K., Kim, B. S., Lee, S. H., and Kim, J. S. 2007. Membrane cholesterol is required for activity of *Vibrio vulnificus* cytolysin. *Arch Microbiol* **187,** 467-473.

Zhao, J. F., Sun, A. H., Ruan, P., Zhao, X. H., Lu, M. Q., and Yan, J. 2009. *Vibrio vulnificus* cytolysin induces apoptosis in HUVEC, SGC-7901 and SMMC-7721 cells via caspase-9/3-dependent pathway. *Microb Pathog* **46,** 194-200.

Zhao, Z., Zhang, L. P., Ren, C. H., Zhao, J. J., Chen, C., Jiang, X. A., Luo, P., and Hu, C. Q. 2011. Autophagy is induced by the type III secretion system of *Vibrio alginolyticus* in several mammalian cell lines. *Arch Microbiol* **193,** 53-61.

Zheng, M., Wang, X., Templeton, L. J., Smulski, D. R., Larossa, R. A., and Storz, G. 2001. DNA microarray-mediated transcriptional profiling of the *Escherichia coli* response to hydrogen peroxide. *J Bacteriol* **183,** 4562-4570.

Zhou, X. H., Shah, D. H., Konkel, M. E., and Call, D. R. 2008. Type III secretion system 1 genes in *Vibrio parahaemolyticus* are positively regulated by ExsA and negatively regulated by ExsD. *Mol Microbiol* **69,** 747-764.

Zhou, Y., Huang, C. F., Yin, L., Wan, M. Y., Wang, X. F., Li, L., Liu, Y. H., Wang, Z., Fu, P. H., Zhang, N., Chen, S., Liu, X. Y., Shao, F., and Zhu, Y. Q. 2017. N-epsilon-Fatty acylation of Rho GTPases by a MARTX toxin effector. *Science* **358,** 528-530.

국문초록

세균성 병원균은 여러 다른 환경에서 생존 및 증식하며 숙주 내에서 질병을 일으키는 능력을 진화시켜 왔다. 이러한 능력은 환경 변화에 따라 조절 시스템에 의해 공동으로 발현이 조절되는 다양한 독성 인자의 생산을 필요로 한다. 기회감염균인 인간 병원균 패혈증 비브리오균은 식중독을 유발함으로써 위장염과 생명을 위협하는 패혈증을 야기할 수 있다. 패혈증 비브리오균이 생성하는 다양한 독성 인자들 중, *rtxA* 유전자에 의해 발현되는 Multifunctional-autoprocessing repeat-in-toxin (MARTX) toxin RtxA 는 이 병원균의 독성에 있어 필수적인 역할을 한다. 기존 연구에 따르면, 패혈증 비브리오균의 전사 조절자 H-NS 와 HlyU 만이 *rtxA* 발현을 각각 음성적으로 또는 양성적으로 조절한다고 알려져 있다. 본 연구에서는, *rtxA* 발현에 관여하는 추가적인 조절 단백질과 환경 신호를 조사하고, 패혈증 비브리오균의 독성을 제어하는 소분자 저해 물질(small-molecule inhibitor)을 발굴하였다. 그 결과, Leucine-responsive regulatory protein (Lrp)이 *rtxA* 의 양성 조절자로 발견되었다. Electrophoretic mobility shift assay (EMSA) 및 DNase I 보호 분석 (DNase I protection assay) 결과, Lrp 가 P_{rtxA} 에 직접적이고 특이적으로 결합하여 *rtxA* 발현을 활성화시킴을 확인하였다. 특히, P_{rtxA} 조절 영역의 DNase I cleavage 는 phased hypersensitivity 를 보였는데, 이는 Lrp 가 아마도 P_{rtxA} 의 DNA 굽힘(DNA bending)을 유도함을 시사한다. Lrp 는 H-NS, HlyU 와

독립적인 방식으로 *rtxA* 를 활성화시키며, 류신은 Lrp 가 P_{rtxA} 에 결합하는 것을 저해하고 Lrp 에 의해 매개되는 *rtxA* 발현을 감소시켰다. 또한, cAMP receptor protein (CRP)은 *rtxA* 발현의 음성 조절자로 작용하며, 외인성 포도당은 CRP 에 의해 매개되는 *rtxA* 억제를 완화하였다. 흥미롭게도, 생화학 및 돌연변이 분석은 CRP 가 P_{rtxA} 의 upstream region 에 직접적이고 특이적으로 결합하여 P_{rtxA} 의 DNA 형태를 변화시키고 *rtxA* 를 억제할 수 있음을 입증하였다. 더불어, CRP 는 *lrp* 와 *hlyU* 의 upstream region 에 직접 결합함으로써 Lrp 와 HlyU 의 발현을 억제하고, 동 단백질들과 coherent feedforward loop 를 형성함으로써 *rtxA* 발현을 간접적으로 억제하였다. 결론적으로, CRP, Lrp, H-NS, HlyU 로 구성된 조절 네트워크는 패혈증 비브리오균의 감염 동안 류신과 포도당 등의 숙주 환경 신호의 변화에 반응하여 *rtxA* 발현을 공동으로 조절한다. 이러한 공동 조절은 패혈증 비브리오균의 발병 동안 *rtxA* 의 정확한 발현에 기여할 것이다.

패혈증 비브리오균의 독성을 제어하려는 시도에서, 세균성 병원균의 독성을 표적으로 하는 항독성 전략이라는 새로운 방식이 개발되어 본 연구에 적용되었다. 항독성 전략은 생존 능력(viability)을 표적으로 하는 기존의 전략보다 내성을 유도하는 선택적 압력이 낮다는 장점이 있다. 따라서, 패혈증 비브리오균의 독성에 필수적인 전사 조절자 HlyU 를 저해하기 위해 8,385 개의 화합물을 포함하는 small molecule library 의 대량 발굴 탐색(high-throughput screening)을 수행하였다. 그 결과, [*N*-(4-oxo-4H-

thieno[3,4-c]chromen-3-yl)-3-phenylprop-2-ynamide]의 소분자가 HlyU 활성의 저해제로서 발견되었고, CM14 으로 명명되었다. CM14 은 패혈증 비브리오균의 HlyU 에 의해 활성화되는 독성 유전자 발현을 감소시키지만, 균의 생장을 저해하거나 숙주 세포 사멸을 일으키지 않았다. CM14 의 처리는 패혈증 비브리오균이 야기하는 인간 적혈구의 용혈을 감소시키고 숙주 세포의 rounding 및 용해를 저지하였다. CM14 의 투여는 패혈증 비브리오균에 감염된 쥐의 간 및 신장 기능 장애와 전신성 염증을 완화시킴으로써 쥐의 생존에 기여하였다. 생화학적, 질량 분석, 돌연변이 분석에서 밝혀진 바와 같이, CM14 은 HlyU 의 Cys30 잔기를 공유 변형(covalent modification)시키고 동 단백질이 표적 DNA 에 결합하는 것을 막는다. 이러한 결과를 바탕으로, CM14 에 의한 HlyU 의 covalent modification 에 대해 가능한 분자 메커니즘이 제안되었다. HlyU 는 다양한 비브리오 종 내 보존된 독성 유전자 전사 활성화 인자이기 때문에, CM14 은 다른 비브리오 종의 여러 독성 유전자 발현을 감소시키고 이들의 독성을 약화시켰다. 종합적으로, 본 연구는 CM14 이 저항성을 발생시킬 가능성이 낮으며, HlyU 를 보유하는 다양한 독성 비브리오 종에 대한 항독성 물질이 될 수 있음을 제시한다.

핵심어: 패혈증 비브리오균, MARTX 독소, RtxA, 독성 유전자 조절, CRP, Lrp, HlyU, 소분자 독성 발현 저해 물질

학번: 2016-30488